INTERACTION AND COALESCENCE OF BUBBLES IN QUIESCENT LIQUID

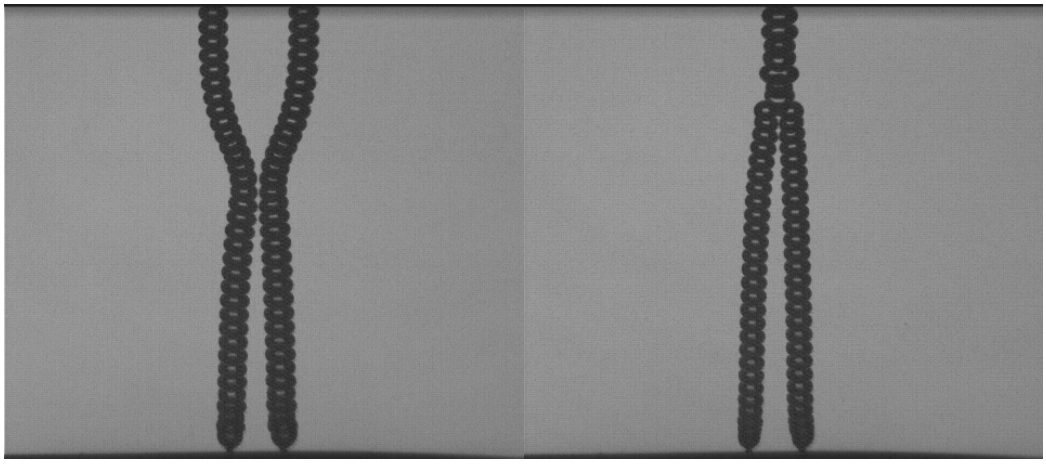

INTERACTION AND COALESCENCE OF BUBBLES IN QUIESCENT LIQUID

Toshiyuki SANADA

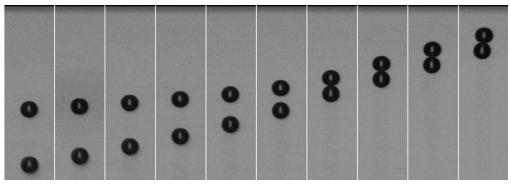

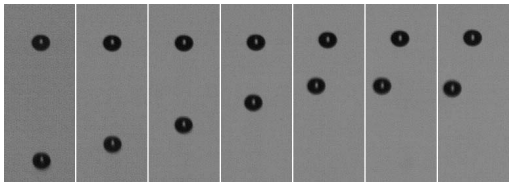

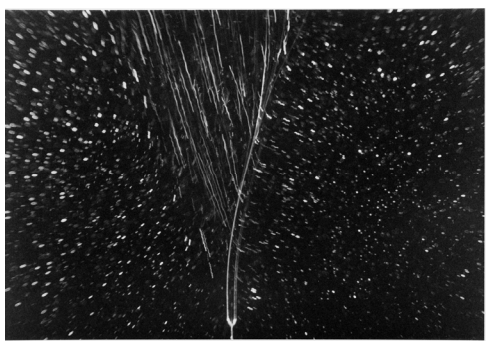

Interaction and Coalescence of Bubbles in Quiescent Liquid

by

Toshiyuki Sanada

Assosiate Bachelor (Oita National College of Technology) 1998
Bachelor (Kyushu University) 2000
Master of Engineering (Kyushu University) 2002

A thesis submitted in partial fulfillment of the requirements for the
Degree of Doctor of Engineering

in

Mechanical Engineering Science

Graduate School of Engineering
Kyushu University

Thesis Committee:

Professor Yasuyuki Takata (Kyushu University: Chairman)
Professor Tohru Fukano (Kurume Institute of Technology)
Professor Akinori Furukawa (Kyushu University)
Associate Professor Masao Watanabe (Kyushu University)

Fukuoka, Japan
January, 2005

TABLE OF CONTENTS

Nomenclatures

a	minor axis of bubble	mm
A_m	volume of amplifier	
b	major axis of bubble	mm
C_D	drag coefficient	$(=4gd/3u^2)$
d	bubble diameter	mm
d_n	diameter of nozzle or orifice	mm
d_u	duty ratio ((ON time of the signal) / (one period of the signal))	
Eo	Eotvos number	$(=2\rho d^2 g/\sigma)$
$\boldsymbol{f}$	external force	N
f	generation frequency of bubbles	Hz
F_{AM}	added mass force	N
F_B	buoyancy force	N
F_{BC}	bubble chain force	N
F_H	historical force	N
F_L	lift force	N
F_{QS}	drag force	N
Fr	Froude number	$(=u^2/gd)$
g	gravitational acceleration	N/m^2
Ga	Galileo number	$(=g^{1/2}r^{3/2}/\nu)$
l	bubble distance	mm
L_e	dimensionless equilibrium distance	
L_i	dimensionless initial distance	
M	momentum flux	N
m	mass	kg
Mo	Morton number	$(=g\nu^4\rho^3/\sigma^3)$
N	time step	
N	bubble order	
N	number of terms of Fourier Descriptors	
n	bouncing number	
n	number of bubbles	
P	function of bubble existence	
p	pressure	Pa
P	constant of re-initialization of mass	
p_∞	liquid pressure of a quiescent point	Pa
p_B	pressure in the bubble	Pa

p_C	pressure of chamber	Pa
p_t	pressure inside the pressure tank	Pa
Q	gas flow rate	kg/m^3
r	bubble radius	mm
r	coordinate	mm
Re	Reynolds number	(=ud/ν)
r_F	Fritz radius	mm
r_n	radius of nozzle or orifice	mm
s	shutter speed	sec
S	sign function	
s	distance from orifice to bubble center	mm
T	characteristic time of liquid jet	sec
T	coalescence time	sec
t	time	sec
u	bubble velocity	mm/s
w	bubble velocity	mm/s
We	Weber number	(=$\rho u^2 d/\sigma$)
x	coordinate	mm
y	coordinate	mm
z	coordinate	mm
Δr	distance from the nozzle (r-direction)	mm
Δt	time interval	sec or msec
Δx	distance from the nozzle (x-direction)	mm
Δx	relative distance of bubbles	mm
Δy	distance from the nozzle (y-direction)	mm
$\Delta\eta$	length of control volume (η-direction)	mm
$\Delta\xi$	length of control volume (ξ-direction)	mm
$\Delta\zeta$	length of control volume (ζ-direction)	mm
α	thickness of interface	
χ	aspect ratio	(=b/a)
ϕ	angle between liquid jet and bubble trajectory	^{o}
ϕ	Level Set function	
η	coordinate	mm
κ	curvature	1/mm

ν	kinematic viscosity	mm^2/s
θ	angle between bubble trajectories and vertical axis	^{o}
ρ	density	kg/m^3
σ	surface tension	mN/m
σ^2	variance of Δr	mm^2
ξ	coordinate	mm
ζ	coordinate	mm

subscript

e	equilibrium condition
G	Gas
i	initial condition
L	Liquid

Chapter I INTRODUCTION

1.1 Motivation

Fluid mechanics is often said one of “classical mechanics” or “completed study”. However, there are still plenty subjects to be investigated in the field of fluid mechanics. Multiphase flow, along with turbulence, is definitely one of them.

Rain from the sky, breaking wave in shore, volcanic eruption by growth of bubble, and so on, are typical examples of multiphase flow seen in nature. From the industrial point of view, modeling of multiphase flow is one of the most important tasks: however, these attempts had not been so successful mainly because multiphase flow is rich in flow regimes such as from bubbly flow to annular flow. In each flow regime, there are many interesting, surprising, and fascinating phenomena (Hewitt, 2002; Lohse, 2003; Magnaudet, 2004; Prosperetti, 2004). And studying the characteristics of each flow regime is very important for the industrial applications.

In the present study, bubbly flow is focused on. Bubbly flow is frequently observed in wide ranges of industrial applications. Some examples can be indicated: the transportation of oil in pipe, in which the flow becomes gas-liquid two phase flow; the boiler in steam power plant and nuclear power plant, in which the flow is bubbly flow and the output is largely dependent on the bubbly flow characteristics; the bubble column, in which bubbles are used for enhancement of mass transfer with the increase of the contact area; the bioreactor, in which the bubbles are used for oxygen supply and the surfactants are added to prevent the death of cells; the ink jet printer, in which the growth of bubble is used to propel the ink; the metal refining, in which the bubbles decides the quality of the metal; the bubble jet bath, in which the bubbles loosen up muscle; the medical imaging, in which the nonlinear oscillation of bubbles are provided as the contrast media . In addition, bubbles are expected to be applied to other fields such as drag reduction of ocean vessels (Kodama, 2000), water quality purification (Fujiwara *et al*., 2003), aquaculture of fish and pearl (Onari, 2001), and cavitation control lithotripsy (Matsumoto *et al*., 2005).

Because of a wide range of applications, the construction of bubbly flow model with a high degree of accuracy is strongly demanded by industries. Those demands are, however, not fully satisfied yet since the modeling of bubbly flow is

far from easy task since the bubbly flow fields essentially consist of multi-scale structures in both time and space (Sugiyama *et al*., 2001). Figure 1.1 shows the schematic of multi-scale structures. The macro-scale structure, for example the Marangoni effect caused by a surfactant distribution on the bubble surface, affects the meso-scale structure such as the coalescence of bubbles. Consequently, macro-scale structure, for example the void fraction profile in pipe, is significantly modified. In other words, to understand the macro-scale structure, it is necessary to understand both the meso-scale structure and the micro-scale structure. This is the root of the basic difficulty in modeling bubbly flow.

Massive works by many researchers have been devoted to the understanding of the micro-scale structure such as the force acting on a bubble. On the other hand, in order to respond the industrial demands, the macro-scale structure of bubbly flow has also been studied by many researchers. However, the significant lack of knowledge of meso-scale structure is noticed.. For example, “When the bubbles encounter, what is the condition of bubble coalescence?”, “What are the differences of motion between a single bubble and interacting bubble?” and so on. This is the motivation of this study.

In the present study, the bubble-bubble interaction and coalescence of bubbles have been investigated. To study bubble-bubble interactions, the simplest configuration of bubbles where the interactions exist, namely a pair of bubbles or bubbles rising in a single chain, are selected. In addition, the criteria of interaction bubbles either collide or not, and either coalesce or bounce are investigated.

Micro-Scale

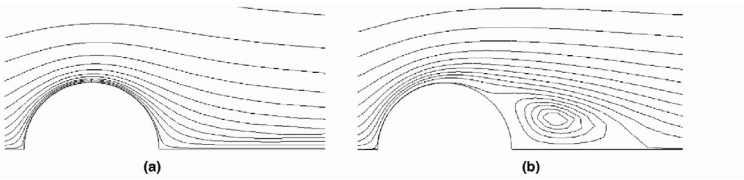

Effects of surfactant (taken from Sugiyama *et al*.; 2001)

Meso-Scale

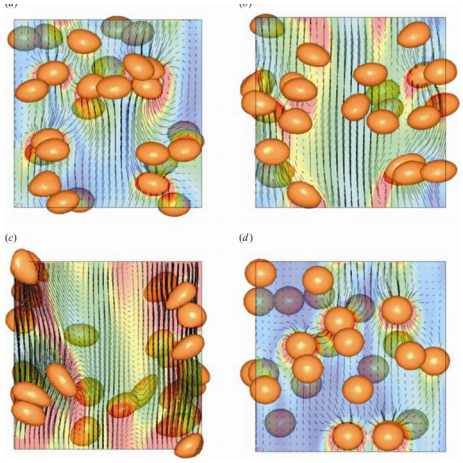

Bubble-bubble interaction
(taken from Bunner & Tryggvason; 2003)

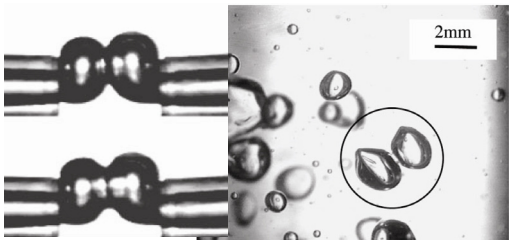

Coalescence
(taken from Tse *et al*.; 1998)

Macro-Scale

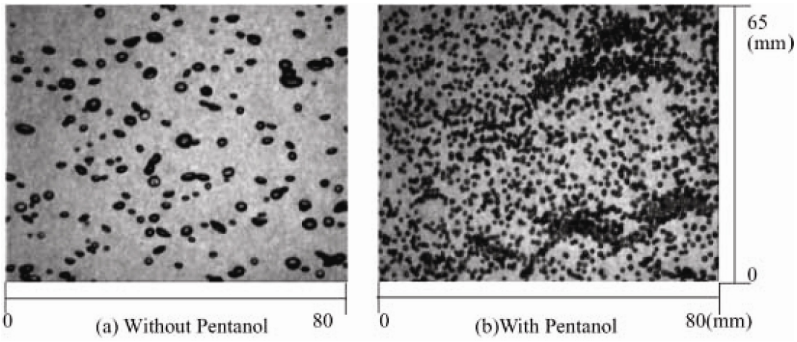

Void fraction profile
(taken from So *et al*.; 2002)

Figure 1.1 Multi-scale structure of bubbly flow

1.2 Outline

This thesis consists of 7 chapters and it is organized as follows.

In chapter 2 the early experimental, theoretical, and numerical studies on the subject of the bubble dynamics are summarized. Especially, the literatures that focused on the physics of fluid are selected.

Chapter 3 is devoted to the description of the experimental setup and the numerical method. In particular, a bubble generator that can control both the bubble diameter and the generation frequency independently is described in detail. The experiments in this thesis are enabled owing to this bubble generator. From chapter 4 to chapter 6 are the main body of this thesis.

In chapter 4, the effects of the bubble-bubble interactions on the motion of a pair of bubbles are studied. Bubbles rise either in line or side by side. Both of the cases are discussed in detail.

In chapter 5, coalescence of a pair of bubbles is studied, motivated by the work by Duineveld (1994). The two types of coalescence are investigated. The first type is that between a rising bubble and a free surface, and the second type is that between of a pair of bubbles rising side by side.

In chapter 6, bubble-bubble interaction effects on bubbles rising in a chain are studied, as the extension of a pair of bubbles rising in line, discussed in chapter 4. The motion of bubbles rising in a bubble chain from a single nozzle, along with the surrounding flow structure of bubble chain, is discussed.

Finally, the conclusions of this thesis are summarized in chapter 7 with future plans and recommendations for the readers.

Chapter II PREVIOUS STUDIES

In this chapter, early studies on bubble dynamics are explored. Although enormous literature has been published, only the basic and deeply related works are selected in this chapter. For comprehensive study, there are good review and books (Bubbles, Drops, and Particles: Clift et al., 1978; Bubble wake dynamics in liquid and liquid-solid suspensions: Fan & Tsuchiya, 1990; The motion of high-Reynolds-number bubbles in inhomogeneous flows: Magnaudet & Eames, 2000).

2.1 Dimensionless number

When a bubble is rising in a quiescent liquid, behavior of bubble depends on physical properties of surrounding liquid. Dimensionless number is useful to investigate bubble behavior because there are many factors. Haberman & Morton (1954) performed the dimensional analysis of a bubble motion focusing on eight physical variables. They used the three dimensionless parameter (by neglecting both density and viscosity of the gas, for the simplicity of the discussion), the Reynolds number *Re*, the Weber number *We*, and the Morton number *Mo*.

$$Re = \frac{u \cdot d}{\nu} \tag{2.1}$$

$$We = \frac{\rho \cdot u^2 \cdot d}{\sigma} \tag{2.2}$$

$$Mo = \frac{g \cdot \nu^4 \cdot \rho^3}{\sigma^3} \tag{2.3}$$

Here, ν and ρ denote the kinematic viscosity and density of liquid, σ the surface tension, u the rise velocity, d the equivalent diameter, and g the gravitational acceleration. The important forces affecting on bubble motion are considered as “inertia force”, “viscous force”, “surface tension force”, and “buoyancy”. Therefore, it should be enough to consider three independent dimensionless

numbers for the study of bubble motion.

The Reynolds number is well-known dimensionless number representing the ratio of "inertia force" to "viscous force". The Weber number is basically the ratio of "inertia force" to "surface tension": hence it measures the bubble deformation. The Morton number is the combination of only physical properties of the fluid. The order of Morton number of water is $O(10^{-11})$. Water belongs to the low Morton number fluid group.

Many other dimensionless numbers were proposed by various investigators (Bhaga & Weber, 1981; Maxworthy *et al.*, 1996; Mougin & Magnaudet, 2002) for each specific purpose. Some of them are listed as follows.

the Eötvös number

$$Eo = \frac{2 \cdot \rho \cdot d^2 \cdot g}{\sigma} \tag{2.4}$$

the drag coefficient

$$C_D = \frac{4 \cdot g \cdot d}{3 \cdot u^2} \tag{2.5}$$

the Froude number

$$Fr = \frac{u^2}{g \cdot d} \tag{2.6}$$

the Galileo number

$$Ga = \frac{g^{1/2} \cdot r^{3/2}}{\nu} \tag{2.7}$$

the aspect ratio

$$\chi = \frac{b}{a} \tag{2.8}$$

Here, a and b denote the minor and major axes of bubble, r the equivalent radius.

The shape regime map by Grace (Clift *et al.*, 1978) is useful for basic understanding of bubble deformation, as shown in Fig. 2.1.

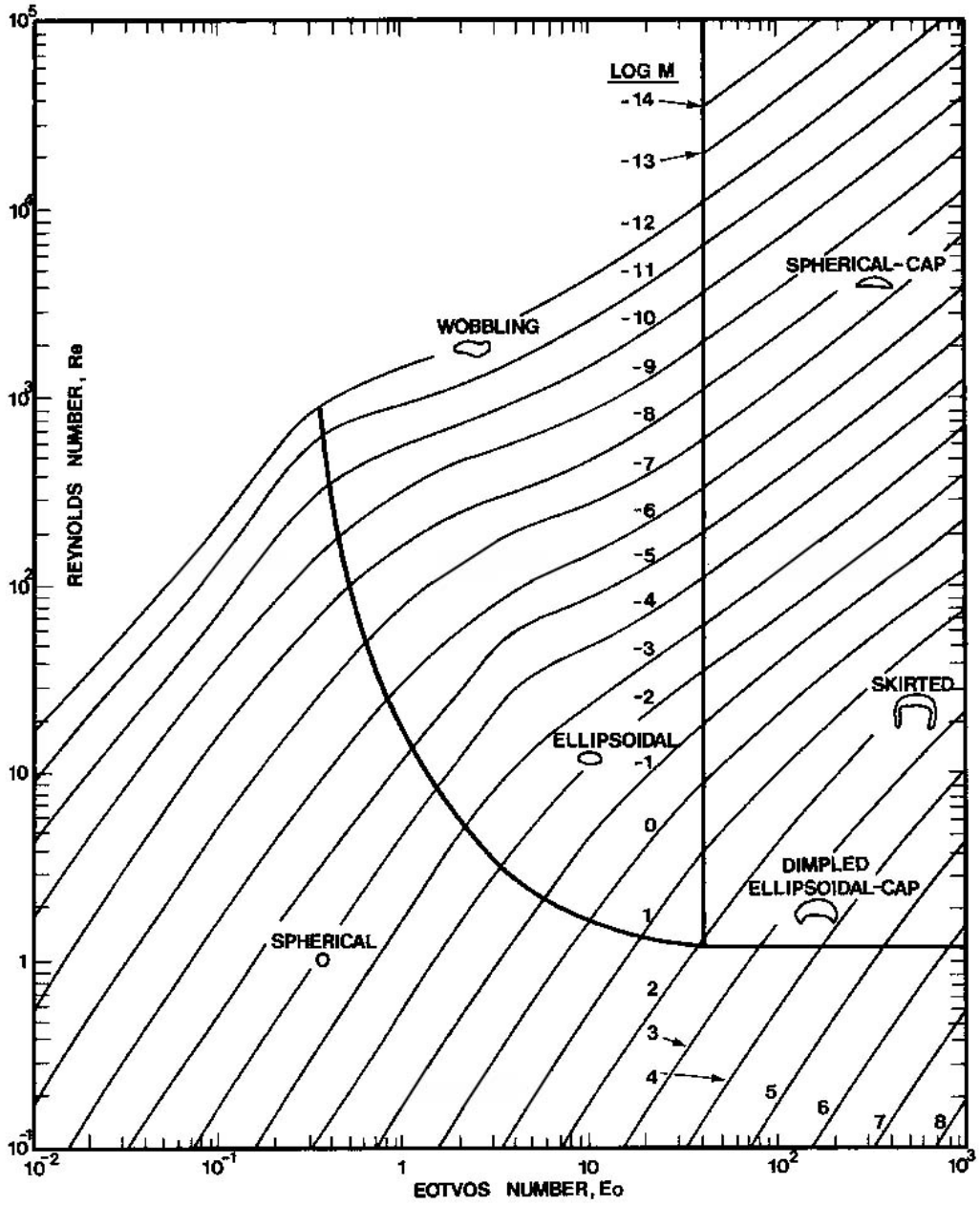

Figure 2.1 Shape regimes for bubbles
(taken from Clift *et al.*, 1978)

2.2 Force acting on bubble

Demands from the industry for the numerical prediction of bubbly flow are large. However, the DNS (Direct Numerical Simulation) of bubbly flow is not realistic because only several bubbles can be handled under the present performance of the computer. Therefore the numeric model constructed by using average equation is, in general, applied to simulate the flow field containing dispersed phase on practice. These equations require the modeling of the various phenomena in the bubbly flow such as force acting on a bubble.

The balance of forces acting on a bubble is written as follows.

$$\rho_G \frac{du}{dt} = F_B + F_{QS} + F_H + F_{AM} + F_L \approx 0 \qquad (2.9)$$

Here, F_B, F_{QS}, F_H, F_{AM} and F_L denote the buoyancy force, the drag force, the historical force, the added mass force and lift force, respectively. The magnitudes of these forces are dramatically changed in contaminated water, and discussed in the next section. The effects of other forces, such as gravity force of bubble, mutual interaction force by other bubble, force from viscous stress and so on, are neglected.

The drag coefficient C_D for a spherical bubble has been examined by a lot of researchers and it is widely acknowledged that the drag coefficient is expressed as the function of Reynolds number *Re*. As for the creeping motion of bubbles where the Stokes approximation valid, the drag coefficient is evaluated by Hadamard-Rybczynski equation (see in Clift *et al*., 1978).

$$C_D = \frac{16}{Re} \qquad (2.10)$$

On the contrary, in flow field on the other end of the spectrum, i.e., potential flow, Levich (1962) derived the drag coefficient by evaluation of the dissipation of the entire flow field. Further more, Moore (1963) derived higher order approximation of the drag coefficient using the perturbation method with matching of inner and outer solution; i.e., matching of region between boundary layer and wake.

$$C_D = \frac{48}{Re} \qquad (2.11)$$

$$C_D = \frac{48}{Re}\left(1 - \frac{2.2}{\sqrt{Re}}\right) \tag{2.12}$$

In addition, Chen (1974) considered the unsteady growth of the boundary layer on a spherical bubble. Moore (1965) also derived the drag coefficient of distorted bubble.

$$C_D = \frac{48}{Re} G(\chi)\left\{1 + \frac{H(\chi)}{\sqrt{Re}}\right\} \tag{2.13}$$

where

$$G(\chi) = \frac{\chi^{\frac{4}{3}}\left(\chi^2 - 1\right)\left\{\sqrt{\chi^2 - 1} - \left(2 - \chi^2\right)\right\}\operatorname{arcsec}\chi}{3\left(\chi^2 \operatorname{arcsec}\chi - \sqrt{\chi^2 - 1}\right)^2} \tag{2.14}$$

$$H(\chi) = 0.0108\chi^4 - 0.157\chi^3 + 1.5725\chi^2 - 2.0195\chi - 1.617 \tag{2.15}$$

It should be emphasized that these equations were derived by analytical method.

For the bridge of the gap between Stokes flow and potential flow, many equations were proposed. Two examples of the drag coefficient of spherical bubble are examined in the followings. The first one was derived by Mei & Klausner (1992) from the result of numerical analysis. The second one was derived by Takemura & Yabe (1997) by correlating experimental result.

$$C_D = \frac{24}{Re}\left\{\frac{2}{3} + \left[\frac{12}{Re} + 0.75\left(1 - \frac{3.315}{\sqrt{Re}}\right)\right]^{-1}\right\} \tag{2.16}$$

$$C_D = \frac{16}{Re}\left(1 + 0.122Re^{0.55}\right) \qquad \left(Re \le 100\right) \tag{2.17}$$

The experimental results on a bubble in pure water (Duineveld, 1995; Takagi *et al*., 2003) show good agreement with the Moore's theory. The numerical results on a spherical bubble (Takagi & Matsumoto, 1996) show good agreement with the Mei's drag coefficient. These C_D are shown in Fig. 2.2.

The lift force acting on a particle in low *Re*, Saffman's lift force (1965) derived analytically is most commonly cited. Auton (1987) also derived the lift force on a bubble in the inviscid flow with a weak shear. However, due to the difficulty of the problem, theoretical study is limited. Legendre & Magnaudet

(1997, 1998) evaluated the lift force in wide range of *Re* using numerical analysis. Their results showed that the direction of the lift force acting on a spherical bubble or particle is the same. However, Kariyasaki (1987) experimentally showed that the strongly deformed bubble in a vertical linear shear flow migrated in the direction opposite to the direction in which spherical bubbles migrated. Takagi & Matsumoto (1995) numerically and Fujiwara *et al*. (2004) experimentally obtained the similar results; however, the lift force mechanism has not yet fully understood. There are several unexplained odd motions of bubble presumably due to the lift force, for example, results reported by Sridhar & Katz (1995), Rensen *et al*. (2001), Lohse & Prosperetti (2003) and so on.

Turning to now the historical force, Basset force is the popular one. Basset force was investigated to act on particles. However, Yang & Leal (1991) showed that no Basset force acted on a bubble. Mei *et al*. (1994) proposed that the historical force acting on a spherical bubble is to be function of *Re*. Takagi & Matsumoto (1996) showed numerically that Mei's historical force is valid in the case of low *Re*; however, it is negligible in the case of *Re*>50.

Finally the studies on the added mass coefficient are briefly reviewed. Takagi & Matsumoto (1996) showed that one half, which is analytically derived in the asymptote of high or low *Re*, is also reasonably valid in the case of intermediate *Re*. The evaluation of the added mass coefficient is crucial especially in expanding bubble (Ohl *et al*., 2003) or oscillating bubble (Vries *et al*., 2002). It is recommended to refer to Magnaudet & Eames (2000) for more detailed reviews.

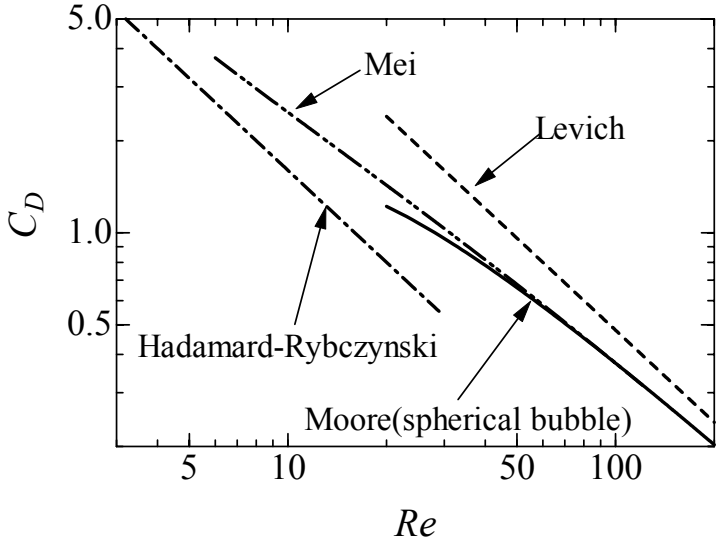

Figure 2.2 Drag coefficient

2.3 Path instability and contamination

Why does bubble rise in helical or zigzag path? Leonardo da Vinch first pointed out this phenomenon (see Ohl *et al*., 2003). Many researchers have devoted themselves into this problem; however, the complete answer has not yet been presented. In the early studies, either bubble shape (*We* effects) or bubble wake (*Re* effects) were mainly investigated. Studies of Miyagi (1925), Haberman & Morton (1954), Saffman (1956), Hartunian & Sears (1957), Tsuge & Hibino (1977) are frequency cited, and they investigated the critical *We* or *Re*.

Nowadays, the main stream of studies shifted to the topics of wake and the effects of the initial shape of the bubble on the motion later on. There are several influential studies on bubble wake. Lunde & Perkins (1997) showed that the wake of spiraling bubble is continuous and consists of a pair of attached vortex. On the other hand, they showed that the wake of a zigzagging bubble is intermittent and consisting of hairpin vortex as is observed in the case of a solid particle. Using Schlieren technique in super purified water, de Vries *et al*. (2002) showed the similar results. They explained that the zigzagging bubble have a double-threaded wake of which the axially vorticity components periodically switch sign. Similar vorticity structure was reported by Johnson & Patel (1999) in the case of the wake of a solid sphere. On the wake of a bubble, Mougin & Magnaudet (2002(a), 2002(b)) solved the generalized Kirchhoff equation and showed the existence of a double threaded wake behind a fixed-shape bubble. In addition they also showed the primary cause both zigzag and spiral paths leading to a double threaded wake. Figure 2.3 shows wakes of a bubble.

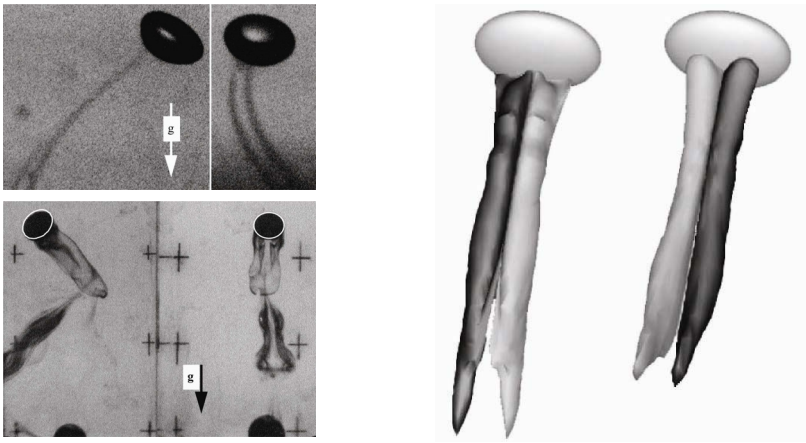

Figure 2.3 Bubble wake
(taken from Lunde & Perkins, 1998; Mougin & Magnaudet,2002)

When the liquid is contaminated, the bubble motion is significantly modified due to the Marangoni effect, as explained first by Frumkin & Levich (see Levich, 1962). The non-uniform surface tension, due to the distribution of surfactants, generates the shear stress jump on the bubble surface; then modifies the boundary condition of bubble surface. For example, the flow structure of bubbly liquid is dramatically altered by addition of small amount of surfactants (So *et al*., 2002). Fdhila & Duineveld (1996) investigated the effect of surfactants on the bubble motion by using both experiment with super-purified water and numerical analysis with stagnant cap model. Cuenot *et al*. (1997) solved the full Navier-Stokes equation and confirmed the validity of the stagnant cap model. In addition, Mclaughlin (1996), Sugiyama *et al*. (2001) extended to the deformable bubble. It was also reported that the steady state velocity of rising bubble in contaminated water depends strongly on the scale of time or space (Zhang & Finch, 2000).

It was also reported that the initial shape deformation of bubble dominates the bubble motion, such as zigzagging or spiraling, even in liquid with no influence of surfactants. Wu & Gharib (2002) and Tomiyama *et al*. (2002) reported that a bubble rose zigzag path when it was released with a small shape deformation, and that a bubble rose spiral under the initial condition of a large shape deformation. Figure 2.4 shows this experimental result. This result is very interesting and controversial, partly because the mechanism is not clear and also because numerical analysis failed to reproduce this phenomenon (Yang *et al*., 2003).

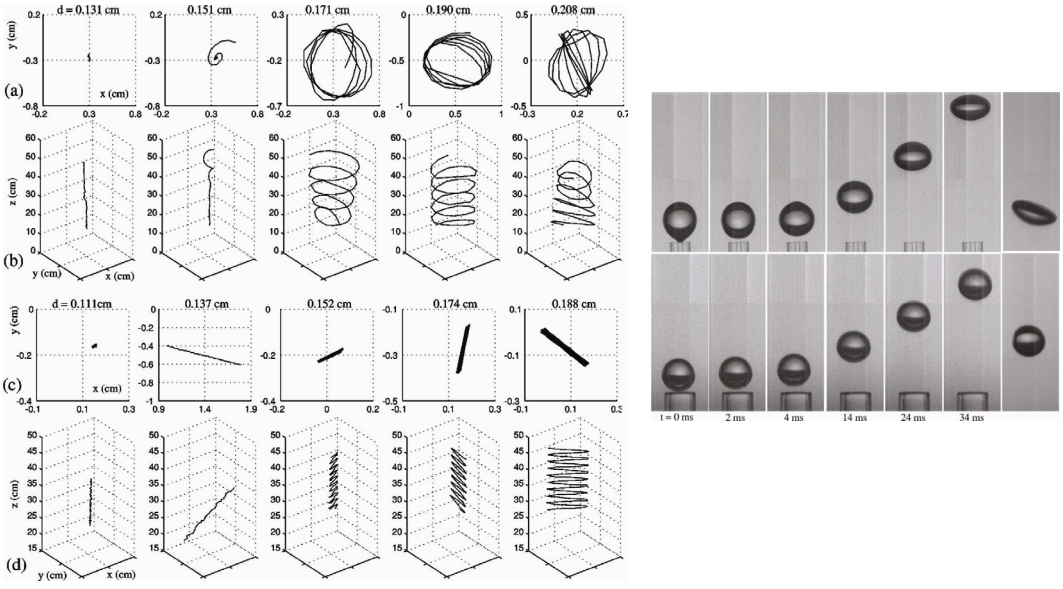

Figure 2.4 Zigzagging or spiral motion of bubble
(taken from Wu & Gharib, 2002)

2.4 Bubble-bubble interaction

Hydrodynamic interactions between bubbles have been studied in order to determine the equivalent viscosity of suspension. In the case of particles, many researchers studied under the condition of creeping motion of particles (Batchelor, 1971; Batchelor & Breen, 1972). In addition, "Stokesian Dynamics" was developed to compute motions of a large number of particles (Brady & Bossis, 1988; Ichiki, 2002). In the case of bubbles, the opposite limit approximation of the creeping flow, i.e., potential flow, is widely used. Group of Prof. Wijngaarden published a lot of papers (Wijngaarden, 1976; Biesheuvel & Wijngaarden, 1982; Wijngaarden, 1982; Kok, 1993(a); Kok, 1993(b); Wijngaarden, 1993). They showed that irrotational flow approximation can predict experimentally and theoretically the motion of a pair of bubbles rising in a quiescent liquid due to the buoyancy. Irrotational flow is also used to predict a suspension of bubbles. Sangani & Didwania (1993), Smereka (1993) computed the motion of a lot of bubbles in a box with periodic boundary condition. However, the result showed the tendency of horizontal clusters, which is not observed in experiment. Although they took the influence of the viscous force into account by evaluating the viscous energy dissipation of the entire flow field, both thin boundary layer and wake of the bubble are the regions where the most energy dissipated in reality. Therefore the finite Reynolds number effects should be considered.

Group of Prof. Tryggvason simulated bubbly flow directory in the cases from low *Re* to intermediate *Re* (Esmaeeli & Tryggvason, 1996; Esmaeeli & Tryggvason, 1999; Esmaeeli & Tryggvason, 1999; Bunner & Tryggvason, 1999; Bunner & Tryggvason, 2002(a); Bunner & Tryggvason, 2002(b); Bunner & Tryggvason, 2003) with the number of O (10^2) of bubbles. They investigated the effects such as the bubble-bubble interaction, bubble deformation, bubble arrangement, and so on, on the bubbly flow. Their method is powerful for understanding microstructure of bubbly flow; however, it is difficult to capture thin boundary layer and wake on the fixed grid. Therefore, their calculations are restricted in the range of *Re* of O (10) currently.

It is widely recognized that the experimental studies of interaction of several bubbles are eagerly required to verify the predictions obtained by either mathematical or numerical analysis. The studies composing this thesis satisfy these demands. The interaction effects on a pair of bubbles and multiple bubbles are investigated in detail in chapter 4 and chapter 6, respectively.

2.5 Bubble production

What size of bubble is produced from a submerged nozzle? This is one of the most essential problems in bubble column, because the size of bubble decides the contact area of gas-liquid interface; hence, it has been investigated especially in the fields of chemical engineering. If a bubble is always released from a submerged nozzle when the buoyancy increases more than the surface tension, the problem is simple. However it seldom occurs. The physical reason is explained in Section 3.2.3.

The production of bubble has been studied extensively (Ramakrishnan et al., 1969; Satyanarayan et al., 1969; Khurana & Kumar, 1969; Bowonder & Kumar, 1970). In addition, many models of production have been proposed (Wraith, 1971; Pinczewski, 1981; Terasaka & Tsuge, 1993). However, the physical process of bubble production was not clearly understood until Oguz & Properetti (1993) investigated the dynamics of bubble growth and detachment from a needle using both of a simple model and a boundary-integral potential flow calculation. They proposed the novel method to produce a small bubble. The detail is explained in §3.2.3.

Not only the observations of bubble production, but also the controls of bubble production were reported. Sirota & Kameda (2001) developed a bubble generator using fast-acting electromagnetic valve. They succeeded in producing a bubble with radius of 0.1mm from a pinhole of 35μm in silicon oil, having the kinematic viscosity of 100 mm^2/s. Ohl (2001) developed a single bubble generator by injecting a short burst of gas into a liquid channel flow. The radiuses of the bubble were controlled continuously from 300 μm to 3mm. These apparatus are powerful, especially for single bubble generation.

Kariyasaki *et al*. (1999) developed a bubble generator in which the gas pressure was actively controlled by using an audio speaker. This generator with combined with multiple orifices produced multiple bubbles simultaneously (Kariyasaki & Osaka, 2001). The detail of this bubble production controller is explained in Section 3.2.3. It also should be noted that Sirota *et. al*. (2004) developed a generator of 0.1mm bubbles using supersonic wave without audio speaker.

2.6 Bubble coalescence

When a pair of bubbles encounter in the liquid, what is the condition for bubbles to coalesce? Although coalescence is widely known and observed physical process, it has not been clearly explained, at least from the view point of fluid mechanics.

When a pair of bubbles approaches each other, van der Waals force becomes dominant and bubbles coalesces at the thickness of liquid film between each bubble surfaces of *O* (100Å) (Chesters, 1974),. When the liquid film between bubbles decreases constantly, coalescence is explained simply by the prediction of the thinning process (Allan *et al.*, 1961). However, in the case of bubbles with large approaching velocities, bubbles bounce. It was first pointed out by Kirkpatrick & Lockett (1974). The mechanism of bouncing is discussed in papers (Chesters & Hofman, 1982; Kok, 1989; Duineveld, 1994; Tsao & Koch, 1994), and they concluded that the pressure of liquid film between bubbles becomes extremely high, and bubbles bounce. Because of the high pressure, they predicted the formation of "dimple". Figure 2.5 shows the sketch of dimple (left) and bouncing bubbles (right). However, their conclusion raised the question whether it is possible for the pressure to increase extremely high. It should be noticed that a bubble has essential no mass; hence a bubble itself carries no inertia. This problem is discussed in this thesis.

In addition, coalescence becomes complicated by other factors. By the mixing a tiny amount of either a surfactant or an electrolyte into the liquid phase, bubble coalescence is prevented (Marrucci & Nicodemo, 1967; Lessard & Zieminski, 1971; Drogaris & Weiland, 1983; Prince & Blanch, 1990; Duineveld, 1994). Moreover, it was reported that mechanism of coalescence is significantly modified in turbulent flow (kamp et al., 2001) or in sound field (Duineveld, 1996).

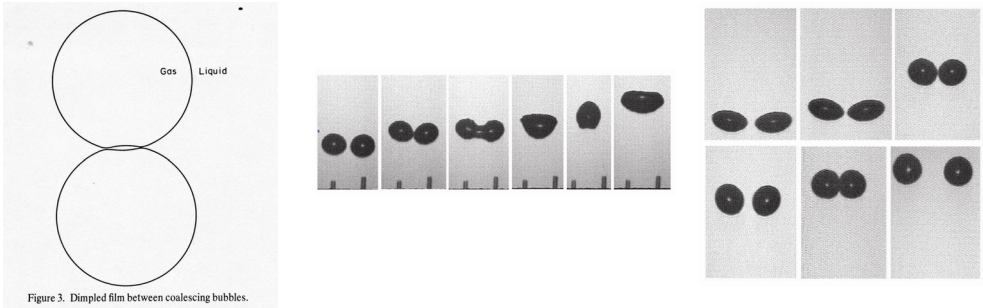

Figure 2.5 Bounsing of bubbles
(taken from Chesters, 1975; Duineveld, 1994)

Chapter III EXPERIMENTAL AND NUMERICAL METHODS

In this study, both experiments and numerical analyses were performed for the understanding of the bubble-bubble interaction and coalescence. This chapter describes the outline of the experimental apparatus and methods especially for bubble production controller which was originally developed by Kariyasaki, et al. (1999). Combined with flow visualization technique, motion of multiple bubbles, whose diameters and generation frequencies were independently and accurately controlled owing to this controller, were analyzed for the understanding of meso-scale structure. This chapter also describes the outline of the numerical analysis, which is powerful tool to investigate the detailed structure of the flow field, such as pressure distribution near a bubble. In this study, Level Set Methods and Finite Element Method were used for the understanding of micro-scale structure.

3.1 Experimental setup

Experiments were performed with distilled water or silicone oil in the acrylic tank. Four types of experimental tanks, which are different in size, were used. All experiments were conducted in quiescent liquid pool with the assumption of no influence of the solid wall throughout this thesis. The nitrogen bubble was generated by using the bubble production controller. Owing to this controller, both bubble size and bubble frequency (distance of the bubbles) were accurately and independently controlled. The detail of the control system is described in Section 3.2. Figure 3.1 shows the schematic of the experimental apparatus. The production controller was equipped between the pressure tank and the nozzle. Nitrogen gas was supplied from a pressure tank, which was installed downstream of a gas cylinder. The pressure tank was made of stainless steel, and its volume was 0.018 m^3. The pressure inside the pressure tank was regulated by a needle valve (Fujikin; No.UN-14mA-S) and measured by a manometer. Both bubble behavior and the liquid flow field were observed through a flat optical opaque acrylic wall and recorded by either a high speed video camera (nac; Hi-Dcam PCI 8000s) or an analog single-lens-reflex camera (Nikon; F3).

Measurements such as bubble diameter, the bubble center, and the rising

velocity, etc. were calculated as the results of a series of image processing of the image data taken by the high speed video camera. The detail of the image processes is described in Section 3.4.

Silicone oil (Shinetsu; KF96) or commercially available distilled water was used as the test liquid. Physical properties of the liquid were measured as followings; liquid viscosity was measured by a viscosity meter (A&D; SV-10) and density was measured by a standard densimeter. The values of surface tension between liquid and gas were those listed in the table provided from the suppliers (Shinetsu; KF96). The liquid temperature was measured by a thermometer. Table 3-1 shows the physical properties of liquid that were used in this study.

The recording system consisted of a high speed video camera (nac; Hi-Dcam PCI 8000s), a zoom lens (CANON; SPACECOM TV ZOOM LENS H6X8-2 8-48mm 1:1.0), a flat light (Sakai Glass Sci.; HF-SL-A214-LC) and a traverse camera apparatus (THK; KT30A-B06-060B). Table 3.2 shows the specification of the image recording system.

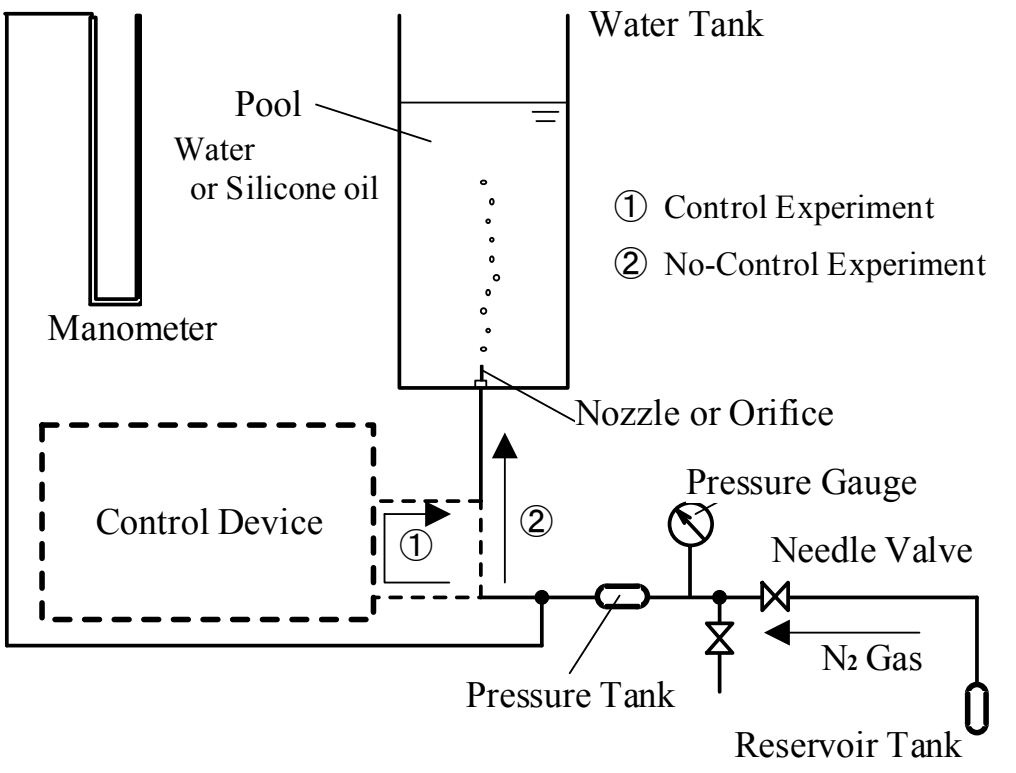

Figure 3.1 Schematic of experimental setup

Table 3.1 Physical properties of liquid

	water	**K0.65**	**K1**	**K1.5**	**K2**	**K5**	**K20**
ν [mm^2/s]	1.00~0.89	0.68~0.72	1.02~1.16	1.54~1.72	2.04~2.49	5.12~5.91	20.28~22.7
σ [mN/m]	72.8	15.9	16.9	17.7	18.3	19.7	20.8
ρ [kg/m^3]	998~997	762~764	819~882	853~858	874~882	916~922	950~955
Mo	$(1.6\sim2.5)\times10^{-11}$	$(2.3\sim2.8)\times10^{-10}$	$(1.2\sim4.2)\times10^{-9}$	$(6.2\sim9.7)\times10^{-9}$	$(1.9\sim4.2)\times10^{-8}$	$6.8\times10^{-7}\sim 1.1\times10^{-6}$	$(1.6\sim2.5)\times10^{-4}$

Table 3.2 Specification of the recording system

Recode rate [Hz]	60	120	250	500	1000	2000
The number of pixels	480×420	480×420	480×420	320×280	240×210	160×140

Camera; Shutter speed 1/60~1/40000, 8bit (nac; Hi-Dcam PCI 8000s)
Traverse apparatus; velocity 0~450mm/s, Stroke 600mm (THK; KT30A-B06-060B)
Light; size 600×425mm, frequency 34kHz (Sakai Glass Eng.; HF-SL-A214-LC)

3.2 Bubble production control

3.2.1 Description of apparatus

Production of the controlled bubbles (diameter, distance of bubbles) is necessary and essential for the experimental study of the interaction between bubbles. However, production of the controlled bubbles is far from easy task. For example, Oguz & Prosperetti (1993) commented that the production control of bubbles is "maddeningly difficult task" in their study of the dynamics of bubble growth and detachment from a needle. The reason of this difficulty is discussed in detail in Section 3.2.3.

There are various kinds of bubble production devices. For example, Sirota & Kameda (2001) developed a bubble generator using fast-acting electromagnetic valve. They succeeded in production of a 0.1mm of radius of bubble from a pinhole of 35μm in silicon oil having the kinematic viscosity of 100 mm^2/s. Ohl (2001) developed a single bubble generator by injecting a short burst of gas into a liquid channel flow. His generator produced bubbles whose radii were controlled in the range from 300 μm to 3mm, continuoulsly. These devices are powerful and useful for single bubble generation.

The most important feature of the bubble production controller used in this study is to produce not only one but two or more controlled bubbles, since the bubble-bubble interaction should be mainly discussed in this study. Therefore the bubble production controller developed by Kariyasaki *et al.* (1999) were implemented. Figure 3.2 shows the schematic of bubble production controller. This controller consists of three elements, i.e., a frequency synthesizer (NF; WF1946), a power amplifier (KENWOOD; KAF-3030RF), and an audio speaker (Fostex; FF125K). The frequency synthesizer generated rectangle wave signals of required frequency. These signals were amplified by the power amplifier. Figure 3.3 shows an example of generated rectangle wave and amplified signal. Figure 3.4 shows the characteristic of amplifier. The audio speaker was driven by this signal and produced a change of the gas volume inside the connecting pipe between the nitrogen pressure tank and the nozzle. Consequently, the bubbles were produced by the accurate release of the controlled volume of nitrogen gas from the nozzle, with accurately controlled generation frequency. In using this production controller, the parameters such as frequency of synthesizer f, volume of amplifier A_m, pressure inside the pressure tank p_t, duty ratio (on/off ratio of the time of the signal from a frequency synthesizer) d_u, and nozzle or orifice diameter

d_n (radius r_n) were optimized. The effects of these parameters on the characteristics of the bubble production are discussed in Section 3.2.3.

Either an orifice or a nozzle was used for bubble production. As the nozzle, three types of capillary glasses, which are widely used for a micro-pipetter, were used. The length of nozzle was 32 mm. The diameters were 204 μm, 285 μm and 350 μm respectively. As the orifice, two adjustment holes were drilled on the nylon tube (outside diameter 6 mm and internal diameter 4 mm), by hand drills, whose diameters were either 300 μm or 500 μm,. The end of this nylon tube was sealed off. The orifice diameter was measured by using a microscope (Moritex; SCOPEMAN MS-6500Pro). The examples of observation results of both nozzle and orifice are shown in Figure 3.5.

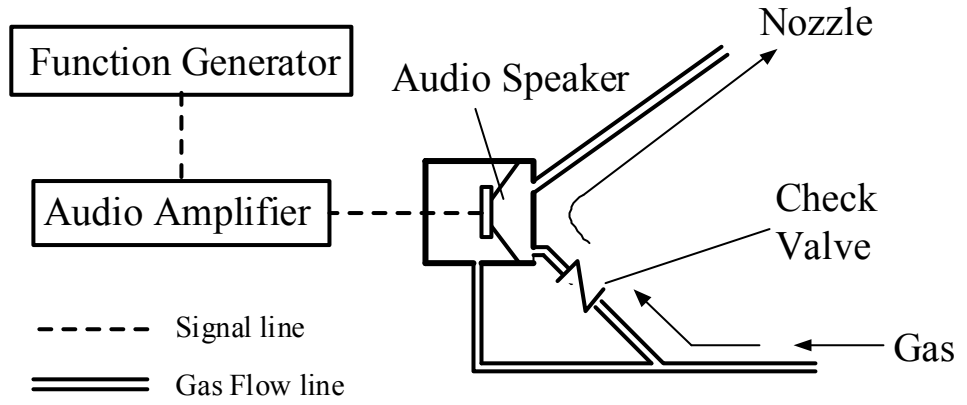

Figure 3.2 Schematic diagram of bubble generation control

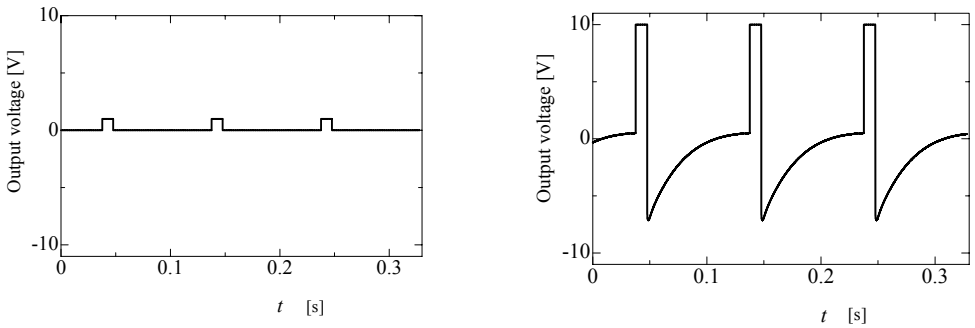

(a) function synthesizer (b) amplifier

Figure 3.3 Example of electric signals (f=10Hz)

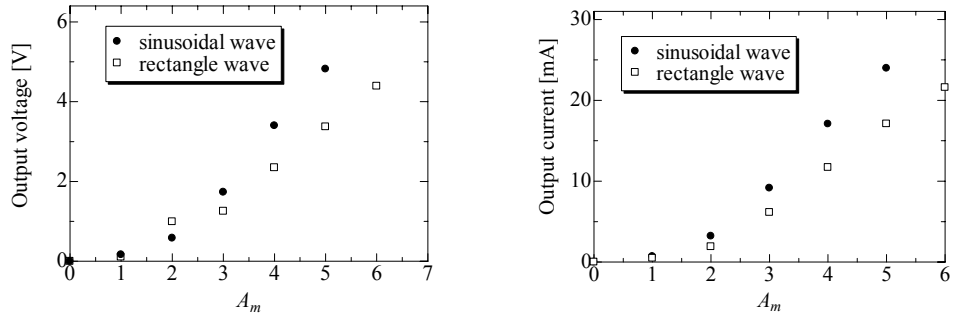

(a) voltage (b) current

Figure 3.4 Effect of amplitude of the amplifier (f=20Hz)

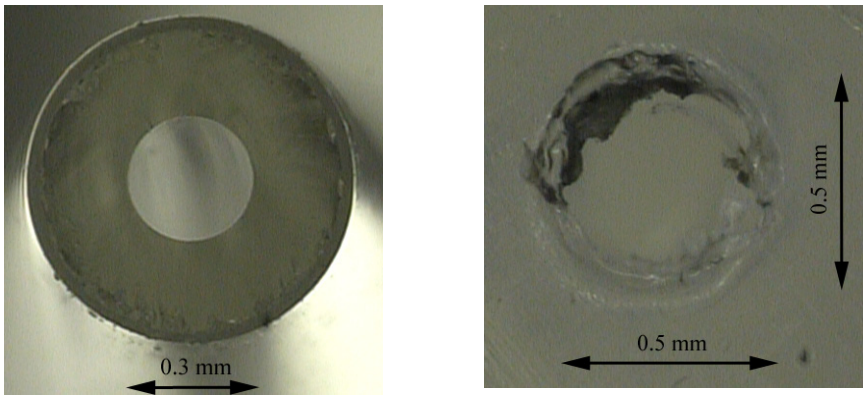

(a) nozzle (b) orifice

Figure 3.5 Examples of observation results of nozzle and orifice

3.2.2 Bubble production

Typical examples of bubble production in distilled quiescent water using the present bubble production controller are shown in Fig. 3.6. Figures 3.6 (a) and 3.6 (b) show the examples of the control of bubble diameter and the one of bubble production frequency f (distances of bubbles), respectively. In Fig. 3.6 (a), only the pressure inside the pressure tank p_t was changed with f fixed. The bubble diameter became smaller with the decrease of p_t . On the other hand, in Fig. 3.6 (b) only the frequencies of the signals fs were changed with p_t fixed. It was clarified that only the distance of bubbles were changed with the diameters of bubbles unchanged.

It was confirmed that the possible controllable values of d obtained by using the present bubble production controller ranged from 0.5 mm to 2.5 mm. Further, it was also confirmed that the controllable f ranged from 1 Hz to 80 Hz in the cases with d greater than 1.0 mm, and from 1 Hz to 20 Hz in the cases with d of approximately 0.5 mm. Corresponding vertical distance between bubbles, l, were approximately 300 mm, 30 mm and 15 mm for f = 1 Hz, 10 Hz and 20 Hz, respectively in the case of d = 1.0 mm.

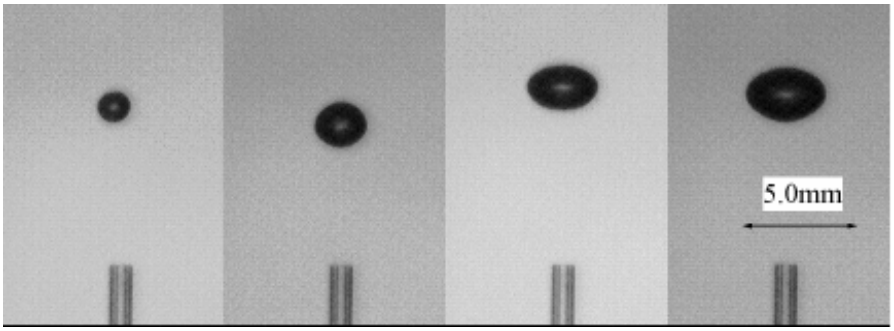

d = 1.2 mm d = 1.6 mm d = 2.0 mm d = 2.5 mm

(a) bubble diameter control (f = 1 Hz)

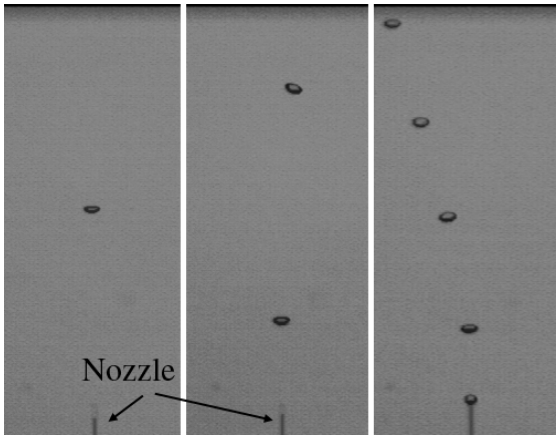

f = 1 Hz f = 10 Hz f = 20 Hz

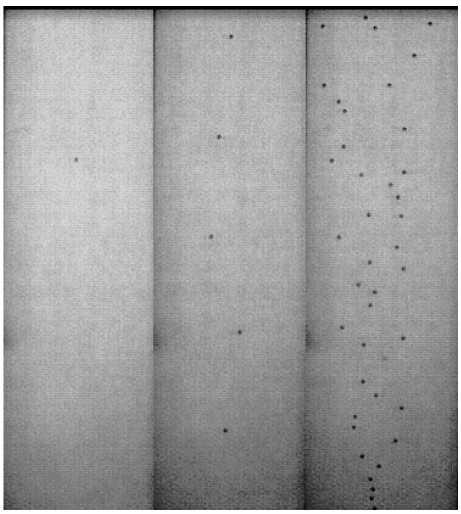

f = 1Hz f = 10 Hz f = 80 Hz

(1) d = 2 mm (2) d = 1 mm

(b) bubble frequency control

Figure 3.6 Example of production control of bubbles

3.2.3 Mechanism of production control

Oguz & Prosperetti (1993) investigated the bubble growth and the detachment from a needle. They reported that the producing of a small bubble is a difficult task. The reason for the difficulty is explained as follows.

Consider that the first incipient conditions in which the gas-liquid interface is just outside the needle's mouth and that gas flow is so slow that $p_B \approx p_C$ where p_B is the pressure in the bubble and p_C is the pressure in the chamber connected to the needle. As the bubble grows, the interface remains on the needle tip and its radius of curvature decreases, reaching a minimum value equal to the needle radius r_n. For this to occur, evidently, the chamber pressure must be at least equal to or greater than, a minimum value given by

$$p_{C,\min} = p_\infty + 2\frac{\sigma}{r_n} \tag{3.1}$$

where p_∞ is the pressure at the needle's tip under quiescent conditions and σ is the surface tension. As the bubble radius increases past r_n, the pressure inside bubble becomes progressively higher than the value needed to ensure quasi-equilibrium of the gas-liquid interface and the bubble growth proceeds dynamically. If the needle radius is very small, this overpressure is significantly large and consequently bubble grows very rapidly. This is the essence of the basic difficulty in producing small bubbles.

In addition, they categorized the bubble growth into two different regimes, depending on the gas flow rate Q into the bubble, comparing with a critical value. In the case that the gas flow rate Q is smaller than the critical value, the bubble detaches only when $r \approx r_F$. Here, r_F is the radius generated due to the balances between buoyancy and surface tension of the spherical bubble, defined by Fritz (see Kumar & Kuloor 1970).

$$r_F = \left(\frac{3}{2}\frac{\sigma r_n}{\rho g}\right)^{\frac{1}{3}} \tag{3.2}$$

It is only when the bubble has an equivalent radius greater than Fritz radius r_F that buoyancy is sufficiently stronger than surface tension to detach a bubble from the needle. In the other case, the bubble radius at detachment is proportional to $Q^{2/5}$. In this case, bubble radius is determined by many factors (surface tension, nozzle radius, nozzle flow resistance, chamber pressure, and so on). Therefore, the various models of bubble production have been proposed (see Section 2.5).

Let's return to the bubble production control. First, the results of Kariyasaki & Osaka are shown in Fig. 3.7. Figure 3.7 (1) shows the bubble shape. In Figs. 3.7 (1) (c) and (d), bubble shape was considerably different from those produced by the conventional method. As mentioned above, first stage of bubble growth requires the highest pressure. Kariyasaki reported that much higher pressure rather than the $p_{C,\min}$ was supplied to the bubble, consequently the strong air jet developed and, the bubble top was deformed like a hat. Therefore the bubble growth proceeded dynamically. In Fig. 3.7 (2), however, the pressure inside orifice decreased because of the opposite direction movement of the cone of the speaker. Then bubble volume was decreased or unchanged. Due to the surface tension, bubble tends to return to the spherical shape. Finally the bubble detached itself from the orifice.

Sirota *et al*. (2004) also reported the similar results, using the similar controller. They investigated the time history of the radius r and the distance from the orifice to bubble center s_o. In the early stage of bubble growing period s_o became greater than r and then the bubble detached. In short, the effects of displacements of bubble center and surface tension were the main factors. Moreover, by applying the acoustic pressure field, they enlarged the effect of this displacement of bubble center and they succeed in the production of small bubbles.

Figure 3.8 shows the typical examples of the present results using an orifice. Figure 3.9 shows the time history of bubble diameter in the case of Fig. 3.8. Dashed line in Fig. 3.9 is the Fritz diameter from Eq. 3.2. After production, coalescence was observed in Fig. 3.8 (a), so the diameter of bubble was larger than Fritz diameter. Figures 3.8 (b) and (c) show the time history of bubble shape when the bubble production controller was activated. Bubble shapes are elongated similar to the result of Kariyasaki *et al*. In this case, it is considered that bubbles were produced by the same mechanism as reported by Sirota *et al*. (2004). Moreover, these figures show the effects of amplitude of amplifier A_m and duty ratio d_u. Because the initial air jet was important to produce a small bubble, the bubble became smaller with either the increase of A_m or the decrease of d_u.

On the contrary, when the glass was nozzle, bubble production was controlled by the mechanism different from described above. Figures 3.10, 3.11 and 3.12 show the time histories of bubble shapes and bubble diameters using glass nozzle with d_n=285 μm. In the case of free release of bubble (i.e. without using controller of bubble production), the bubble diameter reached the Fritz diameter. This result implied that the bubble diameter was determined only the nozzle diameter and was independent of the flow rate Q (Oguz & Prosperetti, 1993). However as

shown in Fig. 3.10 (b) it is possible to produce the smaller bubble size than the Fritz diameter with the same diameter nozzle under the condition of no liquid flow.

Next the mechanism of this production control is discussed. Figure 3.11 shows the close up images of Fig. 3.10 (b), especially the periods of bubble detachments. First, bubble grew almost spherical (Fig. 3.11,(a)). For the d_u = 5 % and f = 5 Hz, signal duration was 0.01 s and the pressure in the nozzle decreased (Fig. 3.11(b)). With the decrease in the pressure of the nozzle, bubble shape was elongated (Fig. 3.11(f)). Due to the rapid decrease in the pressure, bubble was necked (Fig. 3.11 (g)) and the liquid around the neck flew into the nozzle (Fig. 3.11 (h)). Finally, bubble detached itself from the nozzle and bubble shape returned to almost spherical due to the surface tension. The mechanism of bubble production from the nozzle is considerably different from the one from the orifice. In the case of orifice, at the early stage of bubble growth, bubble was elongated due to the air jet. However, in the case of nozzle, the bubble detached from the nozzle first and then bubble shape returned to spherical one. In short, the decrease in pressure inside the nozzle "cut" the bubble.

Furthermore, another type of bubble production was observed. Figures 3.13 and 3.14 show the time histories of bubble shapes and bubble diameters using the glass nozzle with d_n = 204 μm. In this case, the diameters reached the Fritz diameter in each case with and the without production controller. It should be emphasized that there is a difference in the period of producing bubbles. In Fig. 3.13 (a), it took 24ms to produce the second bubble after the first bubble was produced in the case of free release. However as in Fig. 3.13 (b), it took 36ms to produce the bubble with the bubble production controller activated.

Oguz & Prosperetti (1993) showed the possibility of production of the small bubbles using an imposed liquid flow field parallel to the nozzle, and also demonstrated that the bubble which grew slowly detached itself from the nozzle with smaller diameter without the surrounding flow field. They proposed that the similar effects were achieved by the change of the flow resistance in the nozzle (to change the nozzle length). If the similar production to those in Fig. 3.13(b) are achieved in the range of over the critical Q of Fritz volume, it is possible to produce small bubble under the same mechanism proposed by Oguz & Prosperetti (1993) with the flow resistance in the nozzle unchanged.

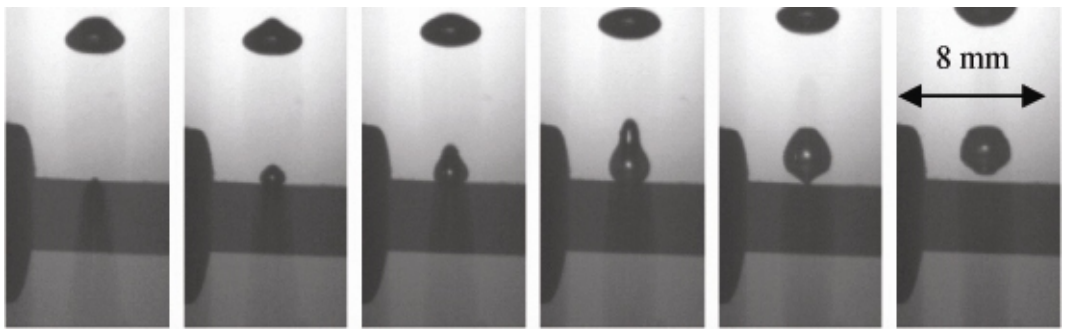

(a) (b) (c) (d) (e) (f)

(1) bubble shape

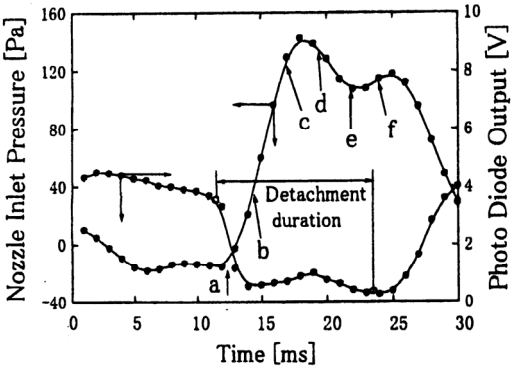

(2) nozzle pressure and bubble signal

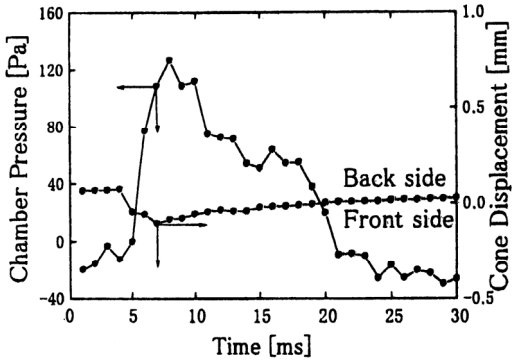

(3) chamber pressure and cone displacement

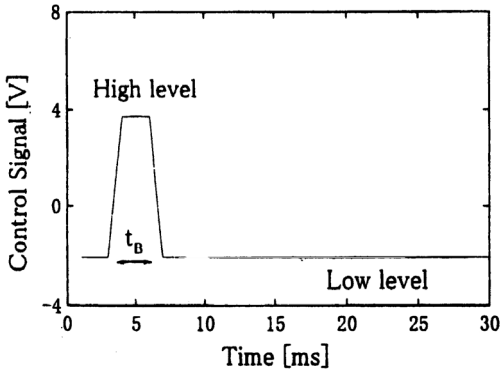

(4) signal of function generator

Figure 3.7 Bubble shape, chamber pressure, and electrical signal (d_u = 8 %, f = 30 Hz, taken from Kariyasaki & Osaka, 2002)

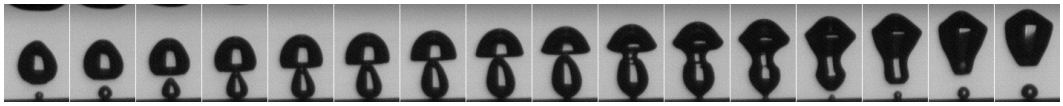

(a) without control (Δt = 1 ms)

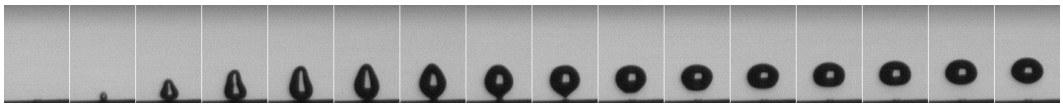

(b) d_u = 2 %, A_m = 2.0 (Δt = 1 ms)

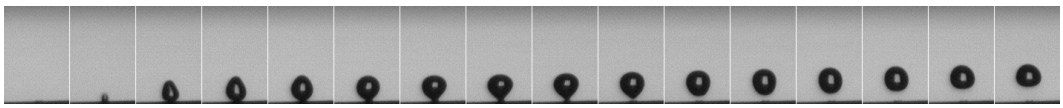

(c) d_u = 1 %, A_m = 4.0 (Δt = 1ms)

Figure 3.8 Bubble production with orifice (d_n = 212 μm, f = 5 Hz)

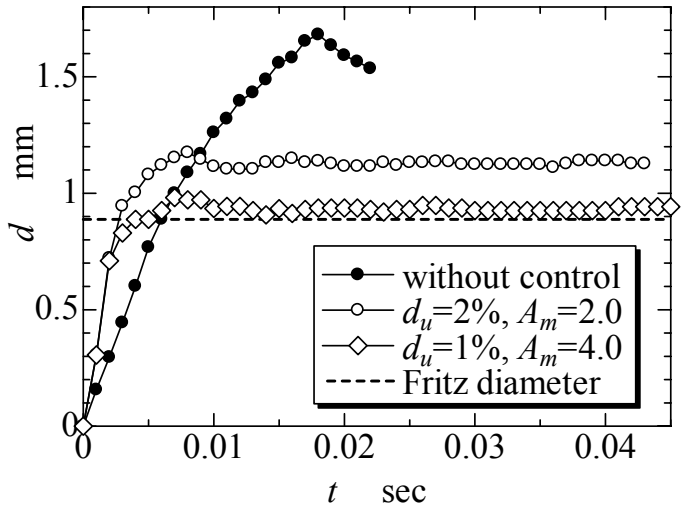

Figure 3.9 Bubble diameter versus time (orifice, d_n = 212 μm, f = 5 Hz)

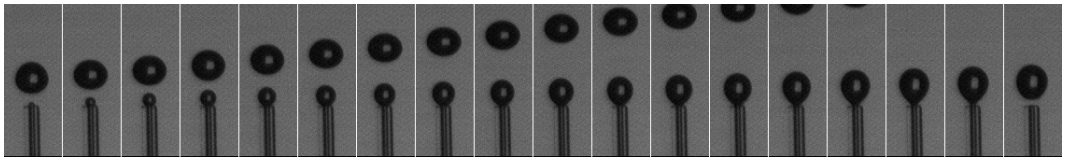

(a) without control (Δt = 2 ms)

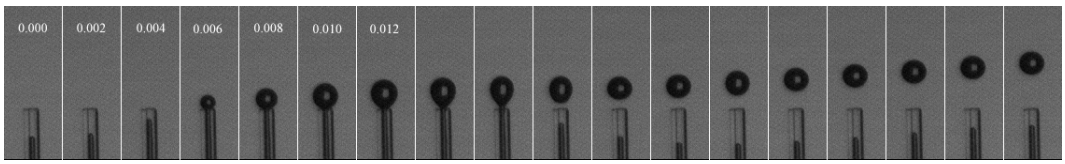

(b) d_u = 5 %, A_m = 3.0 (Δt = 2 ms)

Figure 3.10 Bubble generation with glass nozzle (d_n = 285 μm, f = 5 Hz)

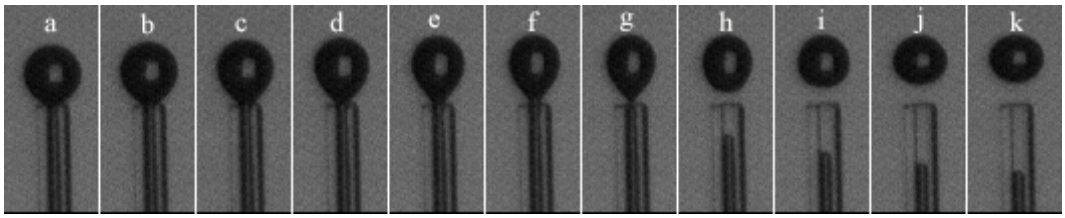

Figure 3.11 Close up of Fig. 3.10 (Δt = 1 ms)

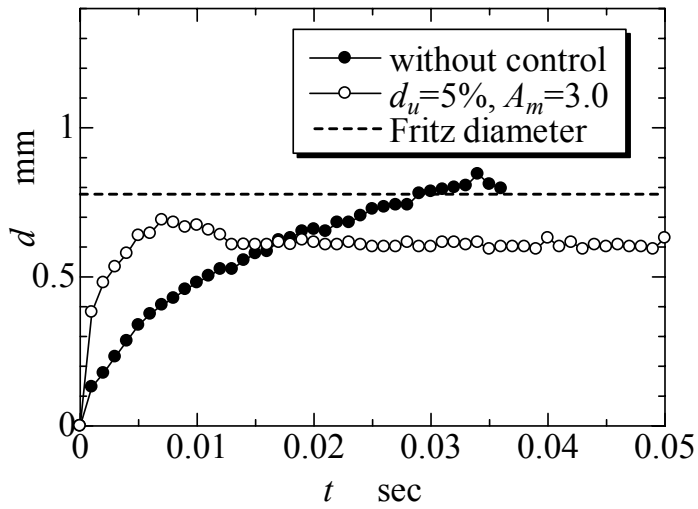

Figure 3.12 Bubble diameters versus time

(glass nozzle, f = 5 Hz, d_n = 285 μm)

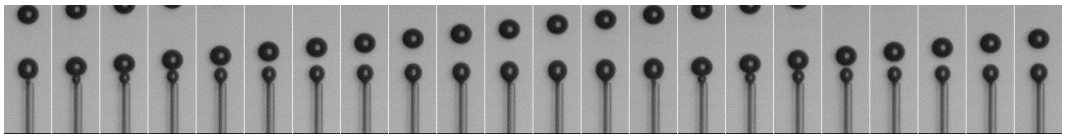

(a) without control (Δt = 2 ms)

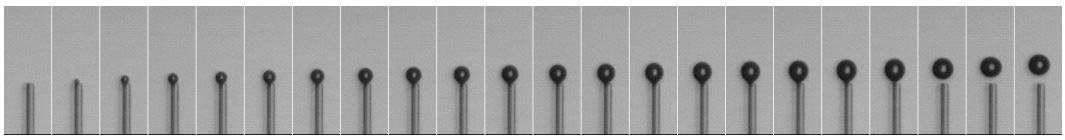

(b) d_u = 10 %, A_m = 0.5 (Δt = 2 ms)

Figure 3.13 Bubble generation with glass nozzle (d_n=204 μm, f=5Hz)

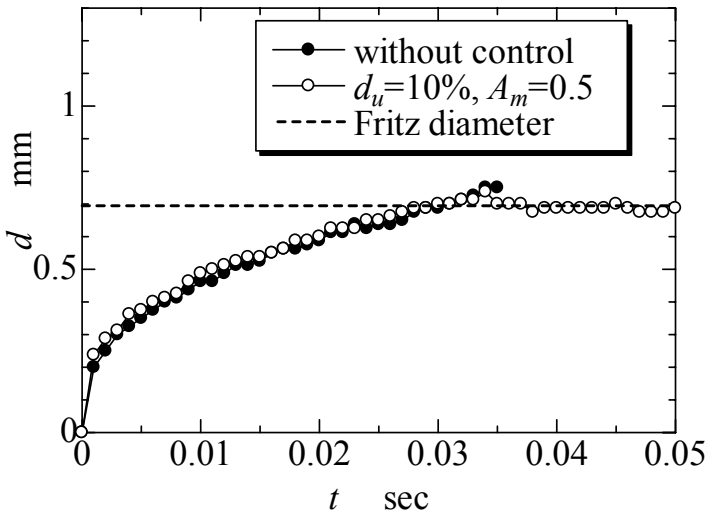

Figure 3.14 Bubble diameter versus time

(glass nozzle, f = 5 Hz, d_n = 204 μm)

3.3 Image analysis

Large number of images was obtained by the high speed video camera. The values, such as bubble diameter, bubble deformation, bubble center, rising velocity, and so on, were calculated as the results of series of image processing. Two different protocols of image processing were applied depending on the magnification of the image.

When a image contains many bubbles i.e. in the case of low magnification, the locations of bubbles were calculated by following process, i.e., the edges intensification of bubble surfaces using Prewitt filter (Prewitt, 1970), the binarization with a threshold and the labeling processes. An example of application of this protocol is shown in Fig. 3.15.

On the contrary, when the bubble is relatively large compared with the image size, bubble center should be calculated with a higher degree of accuracy when the motion of bubble is captured by mobile camera synchronized with the bubble vertical motion. In this protocol, we used a pair of images, original bubble image and background image. First, the bubble image was extracted, by comparison with the background image, and then the noise was removed with a median filter with 9 pixel-stencil. The discriminant analysis method (Otsu, 1980) was used for the bit quantization and the threshold value was evaluated automatically. In addition, the bubble shape was reconstructed by using Fourier Descriptors (Lunde & Perkins, 1995) and the bubble center was recalculated, for the accuracy enhancement. This Fourier Descriptor protocol was used in the experiment of a pair of bubbles rising in side by side. In this Fourier Descriptor, the bubble contour r (θ) was represented by a periodic function of θ with period 2π and written as Equation (3.3).

$$r(\theta) = A_o + \sum_{n=1}^{N} A_n \cos(n\theta) + \sum_{n=1}^{N} B_n \sin(n\theta) \tag{3.3}$$

The center of bubble was calculated by the iteration to eliminate n=1 term. The typical example of the series of image processes and the effect of the cut-off number N of Fourier Descriptors are shown in Fig. 3.16.

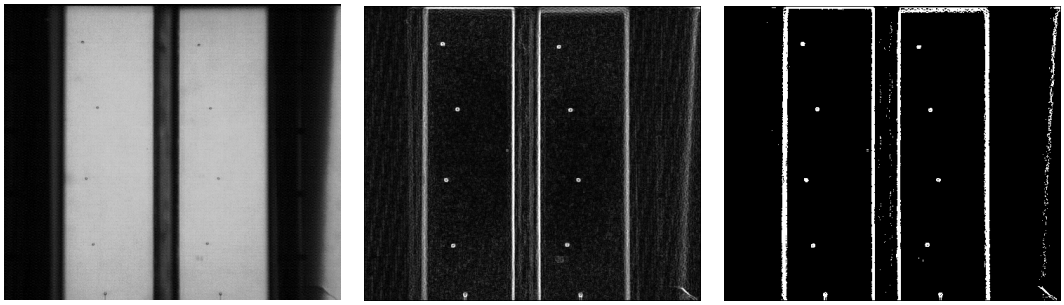

(a) original (b) prewitt filter (c) binarization

Figure 3.15 Example of image analysis

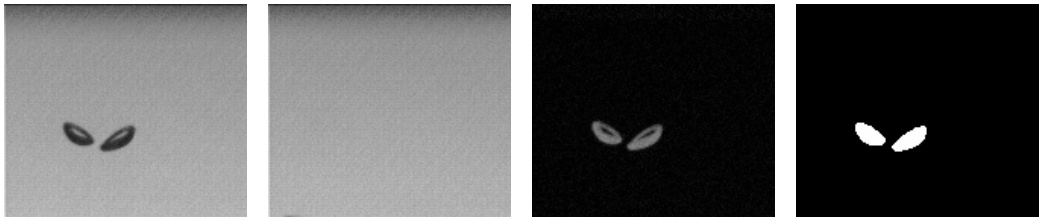

(a) original (b) background (c) background subtraction (d) binarization

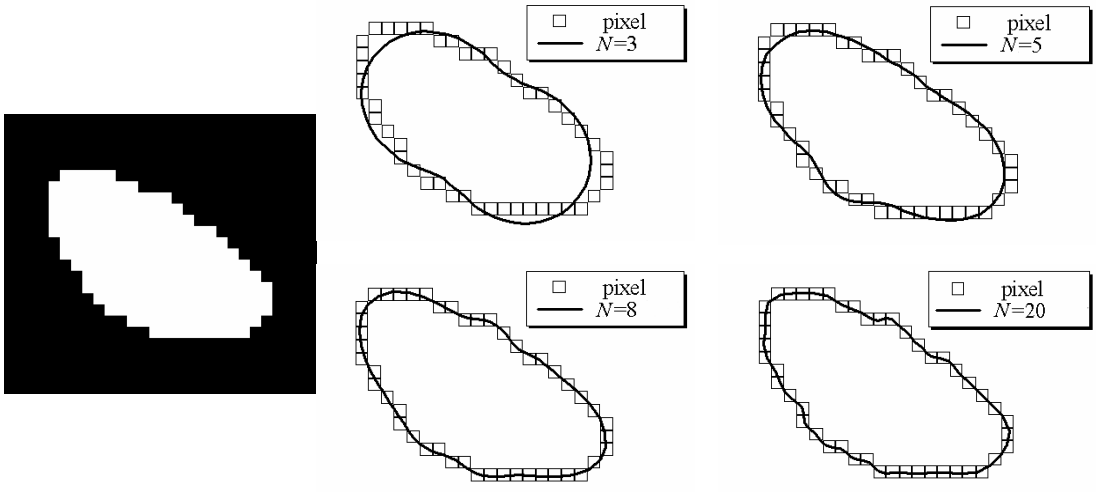

(e) fourier descriptor (original 1bit image, N=3,5,8, and 20)

Figure 3.16 Example of image analysis

3.4 Numerical method

3.4.1 Level set method

The level set methods for capturing moving front was introduced by Osher & Sethian (1987). The level set method is applied widely in various problems ranging from capturing multiphase fluid dynamics, to image analysis. The detailed explanations of the level set method from theory to application are available in general text books (Sethian, 1999; Osher & Fedkiw, 2003; Osher & Paragios2003) and journal reviews (Osher & Fedkiw, 2001; Sethian & Smereka, 2003).

In this study, level set method was used for capturing the interface between gas and liquid. The fundamental concept of level set method is to represent mathematically singular functions, such as the delta function, the heaviside function etc., by the functions of using a smooth distance function ϕ. Sussman *et al.* (1994) extended this level set concept to incompressible two-phase flow. In multiphase flow, the distance function ϕ is defined by the distance from the interface. The discontinuous quantities over interface such as density and viscosity are described by pseudo discontinuous functions of the distance function ϕ with a finite thickness 2α. Figure 3.17 shows the concept of the level set methods.

Fluid flow was calculated by solving the Navier-Stokes equation with this distance function ϕ advected by instantaneous each velocity expressed in Eq. 3.4.

$$\frac{\partial \phi}{\partial t} + \boldsymbol{u} \cdot \nabla \phi = 0 \tag{3.4}$$

In order to maintain the nature of ϕ as a distance function, a re-initialization process was developed. Sussman *et al.* (1994) proposed an iterative procedure to maintain ϕ as a distance function. Their re-initialization procedure is based on solving partial differential Eq. 3.5 until a steady state solution was obtained at each time step.

$$\frac{\partial \phi}{\partial t} = \operatorname{sign}(\phi)\left(1 - \left|\nabla \phi\right|\right) \tag{3.5}$$

Example of the effect of re-initialization is shown in Fig. 3.18.

Sussman *et al.* (1994) solved Eq. 3.5 without special treatment to enforce mass conservation. However, several authors have pointed out that the total mass was not conserved as calculation time passed even with the above re-initialization procedure applied. Chang *et al.* (1996) proposed to introduce another

re-initialization procedure aimed at preserving total mass in time. Their re-initialization procedure involved solving the following Eq. 3.6 to a steady state,

$$\frac{\partial \phi}{\partial t} + \left(m_0 - m(t)\right)\left(-P + \kappa\right) = 0 \tag{3.6}$$

where m_0 denotes the total mass at the initial condition. P is a positive constant and κ is curvature and can be express by ϕ. Sussman et al. (1998) reported a different procedure to enforce mass conservation, and Takahira *et al*. (2004) improved it. In this thesis, the procedure of the mass conservation enforcement in the re-initialization by Chang *et al.* (1996) was employed. Figure 3.19 shows the change of mass. The convergence criterion was set to 10^{-5} as well as Chang *et al.* (1996). The mass was successfully conserved by employing this method since the change in mass was 10^{-5} or less and the significant improvement was confirmed as compared with the results without any treatment, shown as the dashed line.

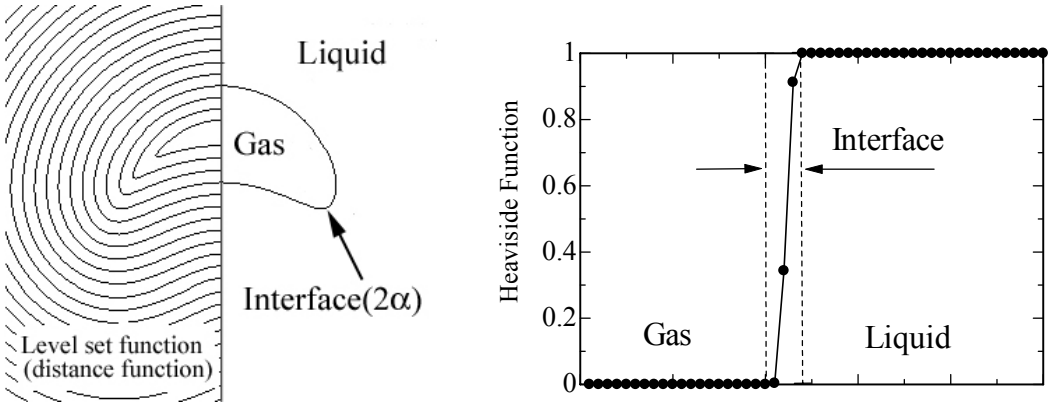

(a) distance function (b) heaviside function

Figure 3.17 Concept of the level set methods

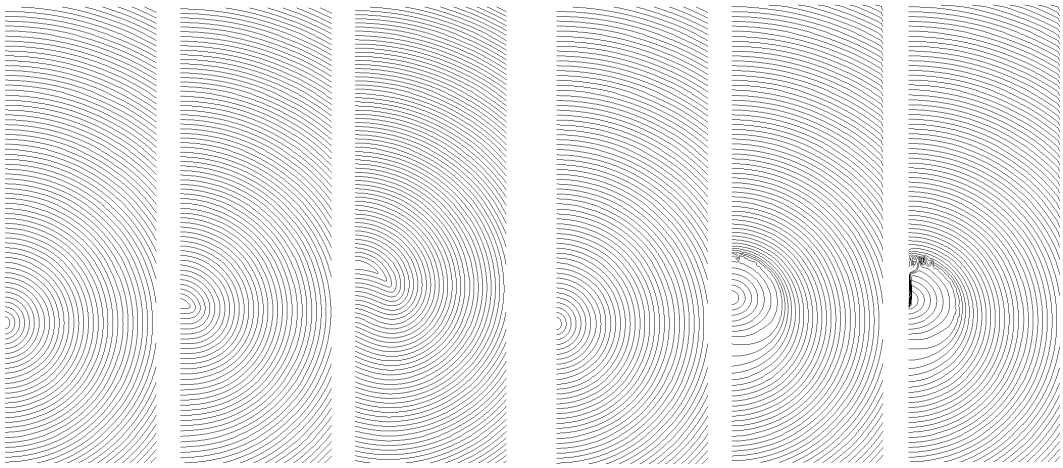

(a) with re-initialization (b) without re-initialization

Figure 3.18 Effect of re-initialization

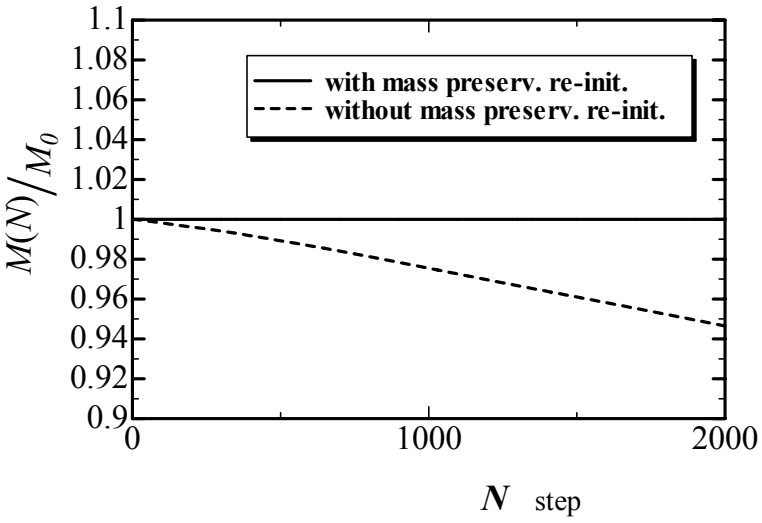

Figure 3.19 Effect of mass conservation re-initialization

3.4.2 DSD/ST finite element method

The deforming-spatial-domain/space-time (DSD/ST) finite element method was applied to study the rising motions of a pair of bubbles in line. The DSD/ST method has been developed by Tezduyar and his group (Tezduyar *et al.*, 1992a; Tezduyar *et al.*, 1992b) to compute the flow field involving moving boundaries and interfaces, especially free surface flows, two-liquid flows, and flows with solid objectives. The characteristic and advantage of this scheme are discussed in this section.

The first characteristic of DSD/ST method is the choice of both interpolation and weight function spaces. These spaces are formed not only in space but also in time. Therefore the function spaces are defined on the space-time slab. The use of these spaces made it possible to take both the calculation point movement and the mesh deformation easily into consideration. The space-time slab finite elements in the present study were the frustum of pyramid as shown in Fig. 3.20, and constructed as follows. The 2-dimensional space (r, z, $t = t$) was divided by using Delauney triangulation. The bottom triangles of the space-time slab frustum were in (r, z, t) plain and the top triangles were in the (r, z, $t = t + \Delta t$) plane which was the plane with time passed by Δt. There were six unknowns for each space-time slab. This choice of the number of unknowns to be calculated, which lead to generate larger matrix than the other ordinary method, caused the major disadvantage of DSD/ST.

The flexibility of the mesh configuration, especially at the interfaces, when the time dependent non-structured deforming mesh was employed, made DSD/ST powerful tool for analysis of moving interface problem, since the boundary conditions at the interfaces were to be easily and rigorously satisfied. The mesh movement was controlled by the following two rules. (i) The rising velocities of each calculation points far from bubble were the same as the bubble rising velocity, and (ii) those on the interfaces moved with the normal velocities to the interfaces with the same normal fluid velocities at the corresponding points. The redistribution of the points were obtained by solving the elastic equation to satisfy the displacement boundary condition at the bubble interfaces, on the center axis, and upper, lower and side boundaries. The typical initial configuration of the meshes around a bubble in the (r, z) coordinates and the one after certain time passed are shown in Figs. 3.21 (a) and 3.21 (b), respectively. The concentration of the calculation points in the neighborhood of the interface had the significant advantage in order to capture the sharp change of the physical properties at the

interface. Although DSD/ST was flexible for adding or deleting the calculation points, the mesh topology of this study was set to be constant.

DSD/ST can easily treat the stress jump at the interface. This characteristic is the another reason for this method to be applied for the analysis of bubble motion. The stress jump at the interface was taken into consideration by adding the term of the basic equation in the variational form.

The DSD/ST was so stabilized that the choice of the same order of the functions for velocities and pressure, typically linear functions in both space and time, was allowed. This property was useful for constructing the simpler matrix by reducing the number of the element connections. The interpolation functions and the weight functions for the velocities were continuous everywhere in space and piece-wise continuous in time, those for the pressure were piece-wise continuous in time also, however, were allowed to have discontinuity at the interface.

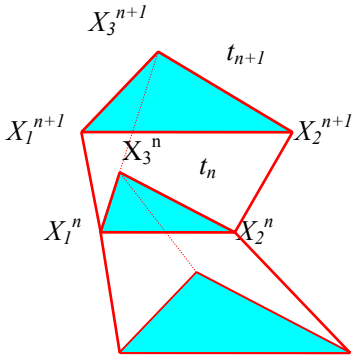

Figure 3.20 The space-time slab for DSD/ST formulation

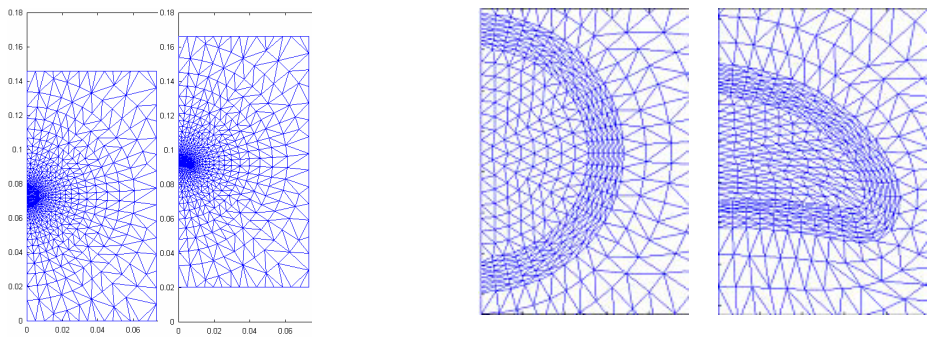

(a) global displacement (b) local displacement

Figure 3.21 Mesh moving strategy

3.5 Computational performance and graphical post-process

In this section, computational performance and graphical post-processing of calculation are commented. Table 3.3 shows the computational performance of the workstation used in this study. All programs were written by FORTRAN language, and were compiled and executed on the Linux machine. The typical calculation run was for about from 1day to 7days.

The calculation results should be post-processed, i.e., visualized for the further investigation. In this study, two visualization soft wares were used. The first one was a free-soft ware named “AVASE” (URL: http://hp.vector.co.jp/authors/VA011972). This software was written by Delphi (Microsoft Windows software development environment), and visualized various flow field characteristics, such as the distribution, of scalar quantities, vector map, iso-contour lines, and so on. The other one was in-house software developed on Linux OS with GTK and Open-GL. The results obtained by FEM, which used the non-structural grid, were visualized by this in-house software. This software also visualized calculation grid structures, pressure distributions, velocity vector maps and iso-contour lines of vorticity. The examples of the visualization results processed by these soft wares are shown in Fig. 3.22.

Table 3.3 Performance of computers

Machine	HPC-ALPHA UP264	HPC-ALPHA UP264	HPC-IA642	Dell
CPU	Alpha 21264 833kHz	Alpha 21264 667kHz	Itanium 2 1.5GHz	Xeon 2.0GHz
CPU (number)	2	2	2	2
RAM	2GB	512MB	8GB	2GB
Cache(KB)	128KB(L1) 4MB(L2)	128KB(L1) 4MB(L2)	16KB(L1) 256KB(L2) 1.5MB(L3)	8(L1) 256(L2)
OS	SuSE Linux 7.1	SuSE Linux 6.4	Red Hat RHAS2.1	Red Hat 7.2
Compiler	Compaq Fortran 1.1	Compaq Fortran 1.1	Intel® Fortran 7.0	Intel® Fortran 7.0

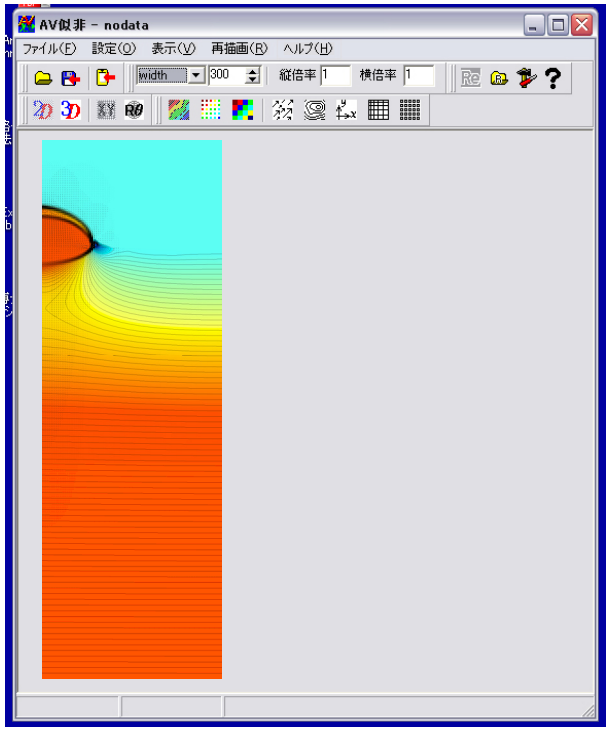

(a) AVASE

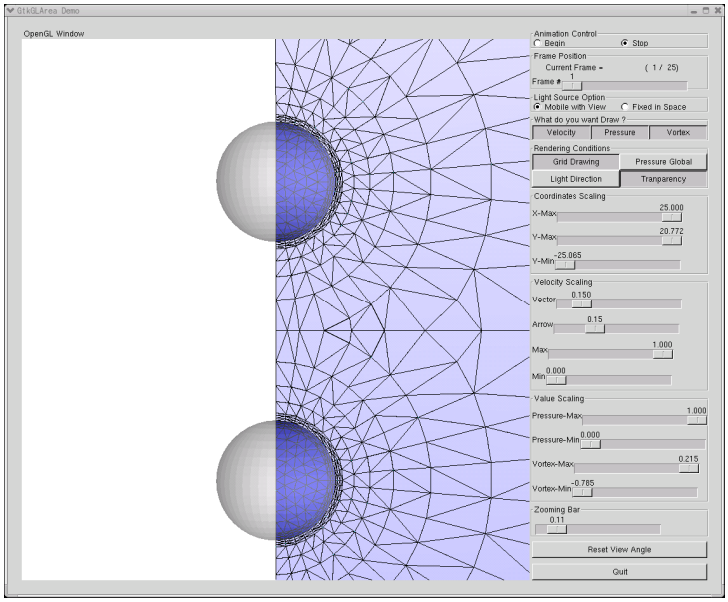

(b) GTK + Open GL

Figure 3.22 Example of post processing

Chapter IV HYDRODYNAMIC INTERACTION OF A PAIR OF BUBBLES

Interaction effects on the bubble motion were experimentally and numerically studied. The motion of bubbles which rose in line and side by side were intensively investigated. Bubble diameter and liquid kinematic viscosity were taken as the experimental and numerical parameters. In the experiment, the motion of bubbles in a quiescent silicone oil pool was recorded by a high-speed video camera. In the numerical study, the DSD/ST finite element method, which took the bubble deformation effect into consideration, was used. The effects of Reynolds number on the motion of a pair of bubbles were focused on. There are many literatures on this subject: however most of them were theoretical and numerical studies. The most significant contribution of this study is that the experiments with a higher degree of accuracy were conducted on the physical processes which both theoretical and numerical approach had been taken, and that experimental results were provided to support the predictions ever proposed.

4.1 Introduction

The hydrodynamic interactions between bubbles play a dominant factor in the meso-scale structure of bubbly flow. In this chapter the hydrodynamic interactions between a pair of bubbles are mainly investigated, since a pair of bubbles is one of the simplest fundamental elements where the hydrodynamic interactions between bubbles exist. The studies devoted to the motion of a pair of bubbles are divided into two categories. The one is the studies of the bubbles rising in line and another is the bubbles rising side by side.

The study of Yuan & Prosperetti (1994) belongs to the former category, i.e., studies of bubbles rising in line. They evaluated the “true drag coefficients” of a pair of bubbles in the intermediate Reynolds number ($50 \leq Re \leq 200$), by directly solving the Navier-Stokes equation with the assumption of axisymmetric flow filed and the spherical shape of bubbles. They showed that the drag coefficient of the leading bubble was almost the same as the one of the single bubble: however the one of the trailing bubble greatly decreased due to the flow field generated by the leading bubble, and that a pair of bubble approached and reached the equilibrium distance. Harper (1997) also obtained the similar results with Yuan & Prosperetti (1994), by constructing the theoretical model which was the extension

of the one of Moore (1963). On the contrary, it was shown by experimental (Tsuji *et. al*., 1982) and numerical (Sirignano, 1993) studies that no equilibrium distances between a pair of either droplets or particles exist. Katz & Menevau (1995) also showed that the bubbles rising in a single vertical line repeatedly collided, by showing the experiment results in low Reynolds number ($0.2 \leq Re \leq 35$). The possible origins of this paradox were proposed by Yuan & Prosperetti (1994), namely the effects of (1) the bubble deformation, (2) surfactant.

There are also fruitful and interesting results reported in the second category, i.e., studies of bubble rising side by side. Kok (1989) theoretically predicted the motion of a pair of rising bubbles horizontally interacting with each other. He also compared his theoretical results with the experimental results conducted in the purified water. He showed that a pair of bubbles rising side by side in high Reynolds number attracted each other. Duineveld (1994) investigated the criterion of either coalescence or bouncing of the contacting bubbles. He showed that the criterion expressed by the Weber number *We,* based on the approach velocity was 0.18. Legendre *et al*. (2003) clarified by using numerical analysis (DNS) that the sign of the lift coefficient reversed within the range of $30 < Re < 100$.

In addition, de Vries (2002) investigated that the bubble bounced from the wall and he showed that the criterion of the bubble whether bouncing or sliding is similar value of Duineveld (1994).

In this study, the motion of a pair of bubbles was investigated, focusing on the flow field with intermediate Reynolds number of about $O(10^1 \sim 10^2)$, which is widely observed in the practical application. An answer to the question: “Is there an equilibrium distance?” was proposed, by showing the experimental evidence, which were not obtained until the bubble production controller, which controlled both bubble diameters and bubble distances accurately and independently, were developed. The nitrogen bubbles were generated from a nozzle in quiescent silicone oil. The effects of the surfactant adsorption on the gas-liquid interface in silicone oil were assumed to be negligible. The experimental results were compared with the numerical results, by using DSD/ST finite element method taking the bubble deformation effects into consideration.

In addition, the motion of a pair of bubbles generated from two orifices horizontally placed were investigated, and the horizontal hydrodynamic interactions between bubbles and the *Re* number effects on the bubble motion were also discussed. Moreover, the details of bouncing bubbles were investigated, by comparing to the experimental results of bubble bouncing with the solid wall.

4.2 Experimental and numerical method

In this study, the motion of bubbles, in the diameter range from 1.0 mm to 2.5 mm released from a single nozzle or two orifices in quiescent silicone oil pool ($150 \times 150 \times 800$ mm^3), were intensively investigated. A pair of bubbles in liquid pool was generated by using the bubble production controller. The pool was filled with commercially available silicone oil, the level of which was kept at 500 mm above a nozzle tip. Typical bubble growth sequences using this controller are shown in Fig. 4.1. These images were taken by a high-speed video camera at a frequency of 1000 Hz. Bubbles were generated from a nozzle for the study of bubbles rising in line. When bubbles were generated from nozzle, it should be noted that this bubble production method caused no significant oscillation on bubbles, which is easily confirmed by Fig. 4.1 (a), hence bubbles immediately reached the steady shapes. On the other hand, bubbles were generated from a pair of orifices horizontally placed for the study of bubbles rising side by side. It was confirmed that a pair of bubbles was simultaneously generated as shown in Fig. 4.1 (b).

In the numerical study, the calculation was conducted with the assumption that bubbles were initially at rest with spherical shapes. The initial distance between bubbles was five times of bubble radius because of the restricted computer performance and the calculation time. The calculation area was twenty fives times and fifty times of bubble radius in r and z direction, respectively. The typical initial mesh configuration around a bubble in the (r, z) coordinates are shown in Fig. 4.2. The node and element numbers were 694 and 1206, respectively. Only the liquid viscosity was taken as the calculation parameter, and the bubble diameter, liquid density, gas density, and surface tension coefficient were fixed, such as $d_i = 0.8$ mm, $\rho_L = 1000$ kg/m^3, $\rho_G = 1.172$ kg/m and $\sigma = 0.0728$ N/m. The corresponding Eo and Re are 0.34 and from 27 to 134, respectively.

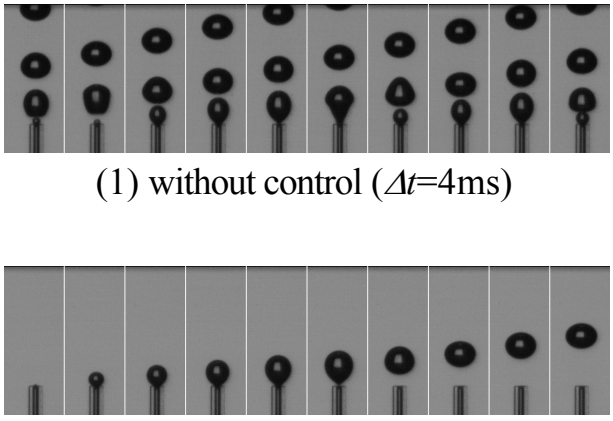

(1) without control (Δt=4ms)

(2) with control (Δt=4ms)

(a) Bubble production from a nozzle

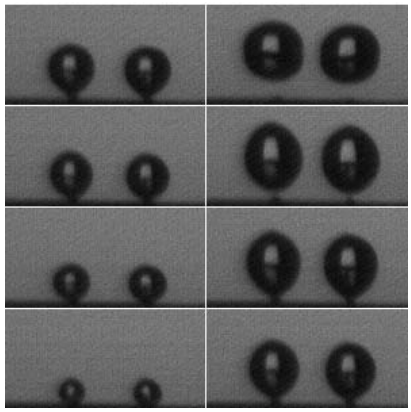

(b) Bubbles production from a pair of orifices

Figure 4.1 Typical example of bubble production

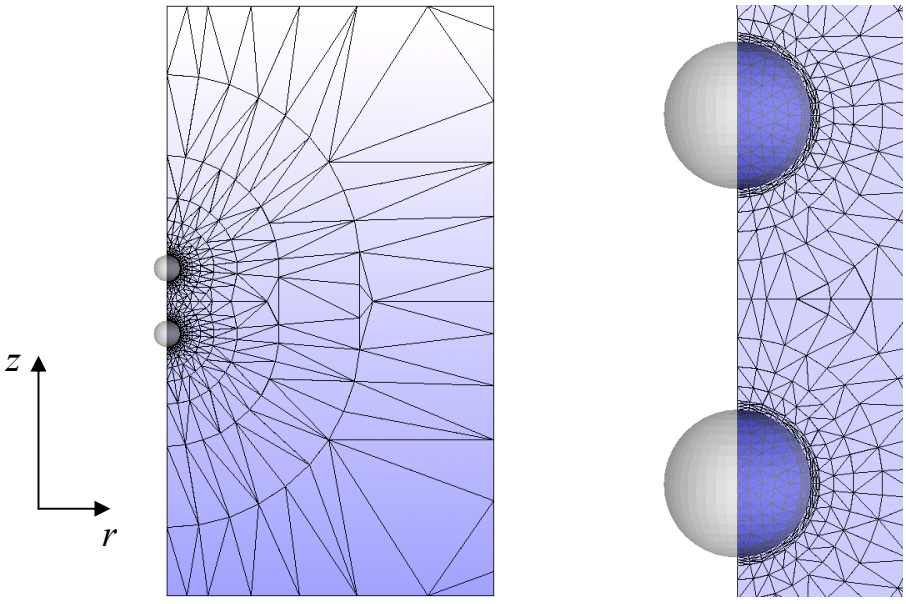

(a) calculation grid

(b) close up

Figure 4.2 Typical example of computational grid

4.3 Non-dimensional parameters of the onset condition of path instability

First, the onset condition of the path instability of the bubble was investigated, in order to distinguish the bubble motion caused by own instability from the one caused by the hydrodynamic interaction between bubbles. Table 4.1 shows the criteria of the bubble either rising in a nearly straight vertical trajectory or rising in a inclined line. Figure 4.3 shows the four series of the superimposed images of the single rising bubble, corresponding to the cases listed in table 4.1. It was clearly observed that the bubble rose in nearly a straight trajectory in the case 1 and case 2. On the other hand, the bubble either in the case 3 or case 4 rose slightly inclined. It is considered that this difference originated from the onset of path instability.

Numerous literatures have dealt with the onset of path instability of a single bubble. Duineveld (1995) showed that the onset conditions of path instability were $Re > 662$, $We > 3.3$, in super-purified water, while silicone oil was used in present study. In silicone oil the surfactant adsorption on the gas-liquid interface was assumed negligible. It should be noted that the surface tension itself of silicone oil-air is almost one third of the one of water-air. It was shown that the criteria of the onset of path instability were $Re > 295$ and $We > 2.9$ obtained in this study, as listed in table 4.1. These values differed from those obtained by Duineveld (1995). However, the criteria described in terms of χ and Ga, $\chi > 2.0$ and > 55, agreed well with the result of Mougin & Magnaudet (2002). Therefore, it was considered that the interacting bubbles in this chapter, which rose in a non-straight trajectory under the condition of Reynolds number $Re < 290$, were significantly affected by the bubble-bubble interaction in the present study.

Table 4.1 Onset of path instability (K1)

	Re	*We*	χ	*Ga*	straight?
case1	268	2.72	1.92	48	yes
case2	270	2.73	1.95	48	yes
case3	295	2.98	2.03	55	no
case4	296	2.99	2.04	56	no

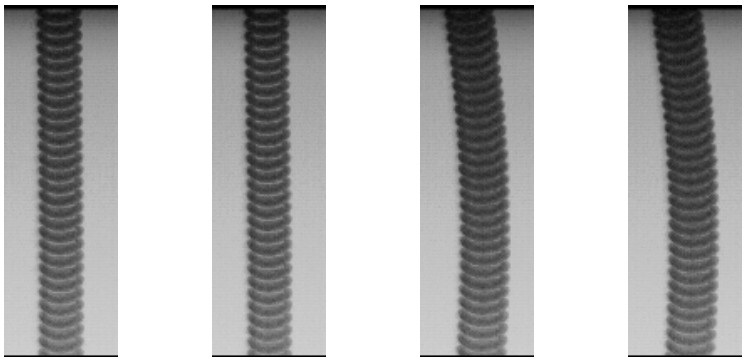

(a) case1 (b) case2 (c) case3 (d) case4

Figure 4.3 Superimposition of bubbles (Δt = 2 ms)

4.4 A pair of bubbles rising in line

4.4.1 Effects of Reynolds number (experiment)

First the motion of a pair of bubbles rising in line with low Reynolds number was examined. Katz & Menevau (referred to as KM: 1996) experimentally showed that a bubble chain, in $0.2 < Re < 35$, rose in the manner of paring, which led to the collision repeatedly and to the coalescence. Figure 4.4 shows the typical results of the motion of a pair of bubbles in the present experiments with silicone oil of K20. The trailing bubble collided with the leading bubble, as shown in Fig. 4.4. It is considered that this collision was caused by the bubble wake effects, as studied in KM. All experimental results with K20 showed that the trailing bubble approached the leading bubble and collided with it. The collided pair of bubbles, however, never coalesced contrary to the results of KM. Figure 4.5 shows the transient velocities of a pair of bubbles as the function of non-dimensional distance L ($L = l / r$). The trailing bubble always rose faster than the leading bubble. The velocities of both trailing and leading bubbles were accelerated as they approached with each other. These results qualitatively agreed well with those of KM.

Next the motion of a pair of bubbles with intermediate Reynolds number is discussed. Yuan & Prosperetti (referred to as YP: 1994) showed by using the numerical analysis that there existed the equilibrium distance between a pair of bubbles. Auther's experimental results, as in Fig. 4.6, clearly showed that the trailing bubble ceased to approach the leading bubble when the distance between bubbles (mutual distance) reached a certain value, and that a pair of bubbles rose keeping the constant mutual distance. It is considered that this constant mutual distance developed as the result of the balance between the "potential repelling force" and the attractive force due to the viscous effects, as YP predicted. It was also observed that some pairs of rising bubbles escaped from a vertical line as shown in Fig. 4.7. These bubbles are referred to as the escaped bubbles in the followings.

These results were quantitatively compared with those of YP with respect to the equilibrium non-dimensional distance Le. The equilibrium distance Le was defined as the constant distance, as shown in Fig. 4.8, which was asymptotically achieved after a pair of bubbles approached, divided by the initial bubble radius. When a pair of bubbles was escaped bubbles, Le was defined as the mutual distance on the vertical line just before the bubbles escaped from the vertical line.

It was reported by YP that the equilibrium distance *Le* was uniquely defined for given *Re*, and that, for example, *Le* was 3.1 in the case of *Re*=50. It was also pointed out that the equilibrium distance was stable. On the contrary, auther's experimental results showed that *Le* was in the range of approximately 10 to 25, which was considerably larger than the prediction of YP, and varied depending on the initial bubble mutual distance, *Li*, with the same *Re*.

The effects of the initial distance, *Li* on the equilibrium distance, *Le*, were investigated by keeping *Re* constant as shown in Fig. 4.9. The equilibrium distance increased as the initial mutual distance increased. This difference was considered to originate from both the bubble deformation effects and three-dimensional bubble motion effects, since YP studied the motion of a pair of bubbles with the assumption of both spherical shape of bubbles and the axisymmetric motion of bubbles. Furthermore YP obtained their results with the initial condition where both bubbles were stationary. On the other hand in our experiment, the trailing bubble was generated after the wake of the leading bubble developed to some extent. From the above discussion, it is concluded that the difference in Reynolds number plays the most important role in the paradox of YP and KM.

Next, the motion of a pair of bubbles with higher *Re* number with less viscous liquid: K2 is discussed. As shown in Fig. 4.10, the trailing bubble approached the leading bubble for a while after the trailing bubble was generated, and then the trailing bubble escaped from the vertical alignment, with large deformation. It is considered that the equilibrium distance is considerably unstable, contrary to the results of YP, with the bubble deformation prominent.

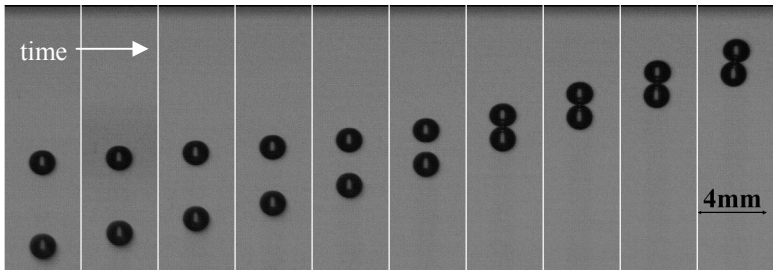

Figure 4.4 Motion of low Reynolds number bubbles

(Re = 5, K20, d = 1.4 mm, Δt = 48 ms)

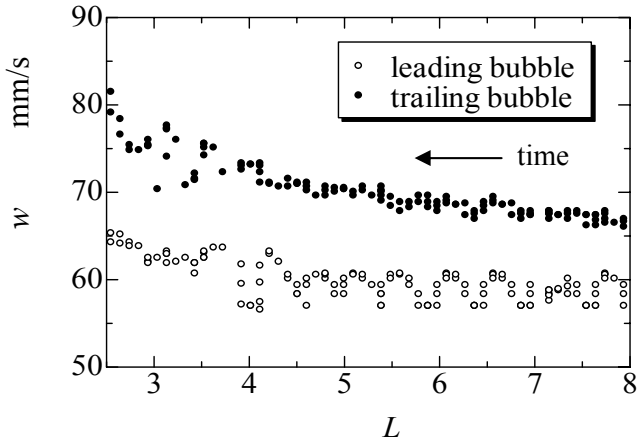

Figure 4.5 Rise velocity of low Reynolds number bubbles
(Re = 5, K20, d = 1.4 mm)

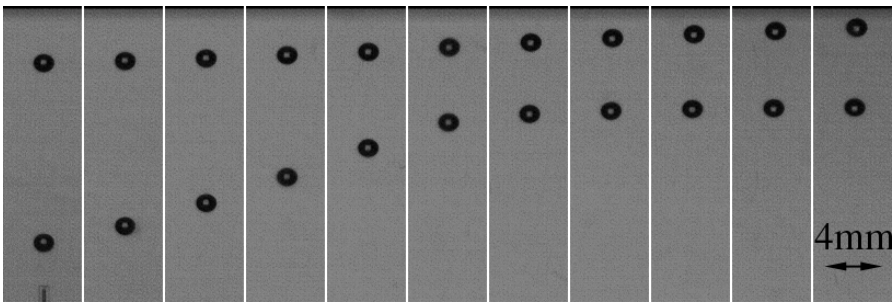

Figure 4.6 Behavior of intermediate Reynolds number bubbles
(Re = 25, K5, d = 1.1 mm, Δt = 112 ms)

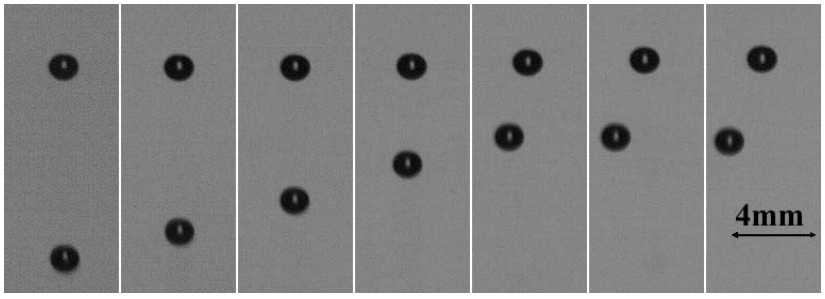

Figure 4.7 Bubble distance of intermediate Re
(Re = 25, K5, d = 1.1 mm)

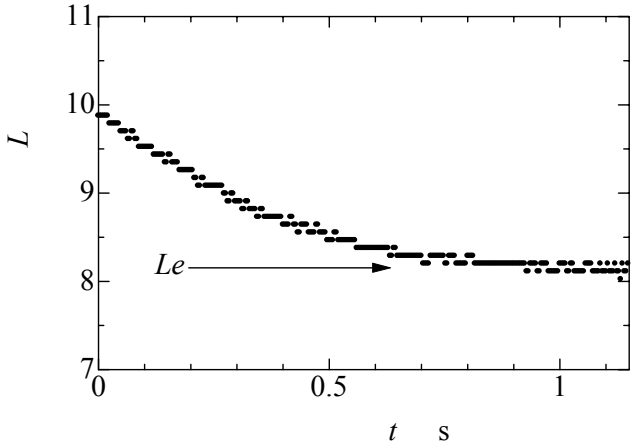

Figure 4.8 Behavior of intermediate Reynolds number bubbles

(Re = 40, K5, d = 1.4 mm, Δt = 96 ms)

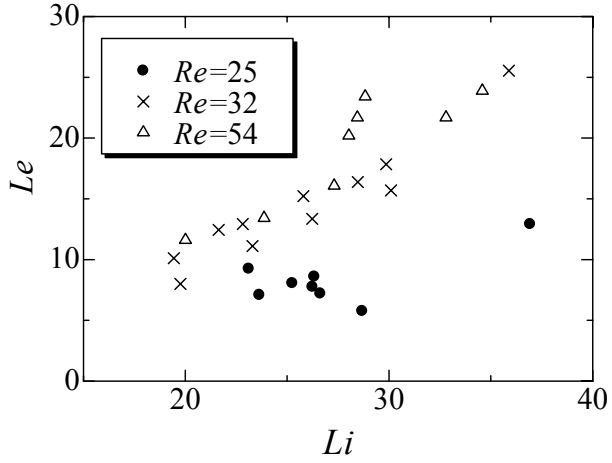

Figure 4.9 Effect of initial distance on equilibrium distance

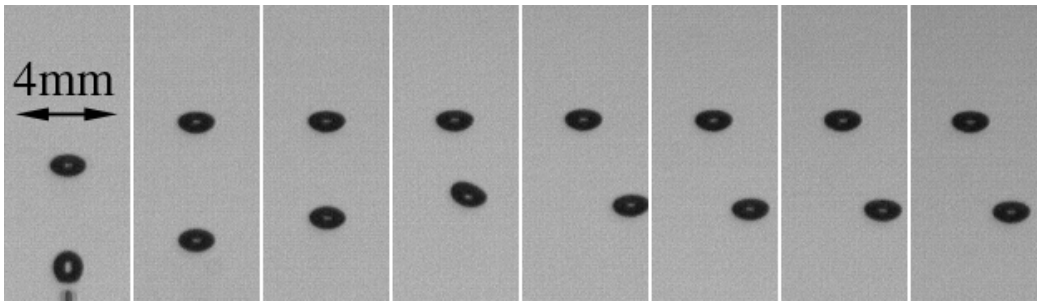

Figure 4.10 Behavior of intermediate Reynolds number bubbles

(Re=145, K2, d=1.4mm, Δt=32ms)

4.4.2 Axisymmetric motion of a pair of deformable bubbles

In this section, the motion of a pair of deformable bubbles rising in line is numerically analyzed. First the numerical results of the single rising bubble are compared with other numerical (Himeno & Watanabe, 1999) and experimental (Takagi, 1994) results. The calculation conditions (ν=5 mm^2/s, d=2.562mm) were chosen as the same as Himeno & Watanabe (1999). The present calculation result estimated the bubble rising velocity at approximately 6 % faster than the one obtained by experiment, as shown in Table 4.2. The vorticity distribution and velocity vector map at the steady state are shown in Fig. 4.11. It is clearly observed that the present numerical scheme can capture the remarkably thin boundary layer developed around the bubble.

Next, the motion of a pair of bubbles is discussed by focusing on the equilibrium distance. The calculations were carried out with various liquid kinematic viscosities, in the range of 1.2×10^{-6} m^2/s $\le \nu_L \le 5.0\times10^{-6}$ m^2/s. A pair of bubbles collides in the cases of $\nu_L \ge 2.7\times10^{-6}$ m^2/s and the equilibrium distance was observed in other cases. A pair of bubble was defined to have collided when the minimum element area became 1×10^{-20} m^2 or less. The equilibrium velocity and the equilibrium distance were defined as the distance and the rising velocity of a pair of bubbles, respectively when the calculation reached the steady state. The equilibrium *Re* number, Re_e, was defined with this equilibrium velocity.

The distances between bubbles were plotted against the time with liquid viscosity as the parameters in Fig. 4.12. In the case of 1.8×10^{-6} m^2/s $\le \nu_L \le$ 2.6×10^{-6} m^2/s, the distance between bubbles decreased initially, and then it became a certain constant value, that was defined as the equilibrium distance. With the increase of Re_e, when the viscosity is small such as 1.5×10^{-6} m^2/s or less, the oscillations of the distance between bubbles were observed. These oscillations were considered mainly due to the shape oscillation of trailing bubble. The equilibrium Reynolds number Re_e is also shown in Table 4.3.

The equilibrium distance was plotted as a function of *Re*, in Fig. 4.13. The black circles are present calculation result, and white circles are the calculation results of Yuan & Prosperetti. Yuan & Prosperetti simply showed the equilibrium distance *Le* as a functions of *Re* as shown in Eq. 4.1, mainly because they assumed a spherical bubble and conducted a dimensionless calculation.

$$Le = 4.40 \log_{10} Re - 4.38 \qquad (4.1)$$

In the present study, on the other hand, *Le* was shown in Eq. 4.2.

$$Le = 3.85 \log_{10} Re - 3.79 \qquad (4.2)$$

Of course, *Le* depended on not only *Re* but also *We* and *Eo*. In this study, however, *Le* was written as the function of only *Re* just for the simplicity.

Equation 4.2 predicted the smaller equilibrium distance than the one of Yuan & Prosperetti. It is considered that this discrepancy is mainly due to the deformation of the bubble, which was taken into consideration in the present calculation. For instance, the aspect ratio of the leading bubble was about 0.95 in the case of *Re*=72. It is well known that the drag force acting on the deformed bubble increases due to the increase of the viscous dissipation. Therefore, viscous force of the deformed bubble increased more than the spherical bubble when the bubbles rose with the same velocity. On the contrary, the dipole term, which is the main contribution of potential repelling force, in the potential field expansion of flow field, largely depends on the velocity of bubble and the effects of the slight deformation to the dipole term are generally considered to contribute to the higher order terms. In short, the deformation effect on the potential repelling force was considered to be small. Equation 4.2 predicted the shorter equilibrium distance than Eq. 4.1 because the increase of the attractive force (viscous force) dominated the one of the repulsive force (potential force).

Finally, the flow fields, bubble distance, and bubble velocity are presented in Figs. 4.14 ~ 4.17. Bubbles either collided or kept an equilibrium distance between them. When a pair of bubbles collided, velocity of the trailing bubble was always faster than the leading bubble as shown in Fig. 4.17. The velocities of both the trailing and the leading bubbles were accelerated as they approached with each other. These results qualitatively agreed well with those of experiment and KM. When a pair of bubbles kept an equilibrium distance between bubbles, the vorticity of a leading bubble was advected to lower and touched the trailing bubble (t=0.04s). And then the velocity of trailing bubble increased, and the velocities of the leading and the trailing bubbles reached the same value. Finally bubbles kept an equilibrium distance.

Table 4.2 Comparison with other studies

	Present cal.	Himeno & Watanabe cal.	Takagi exp.
d mm	2.562	2.562	2.562
w m/s	0.193	0.172	0.182
Re	98.9	88.4	93.7
We	4.432	3.545	3.981

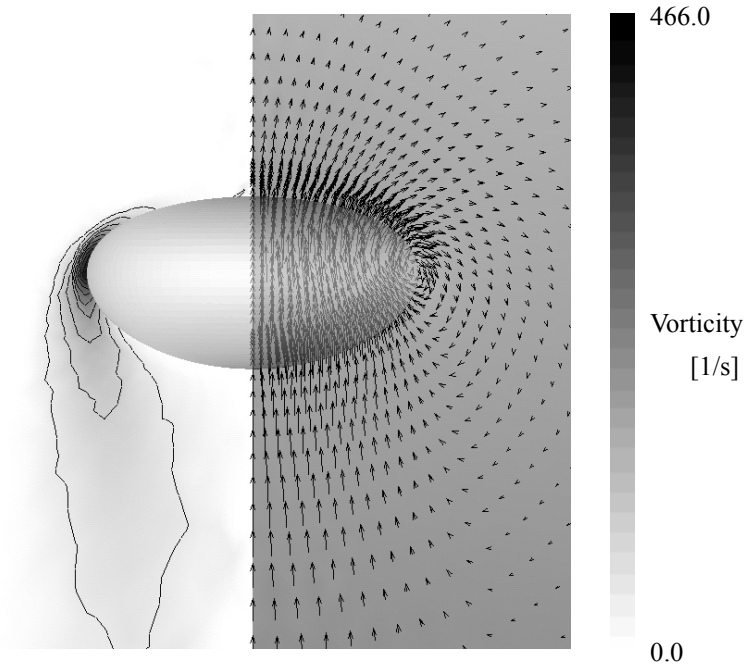

Figure 4.11 Velocity and vorticity distribution of single bubble

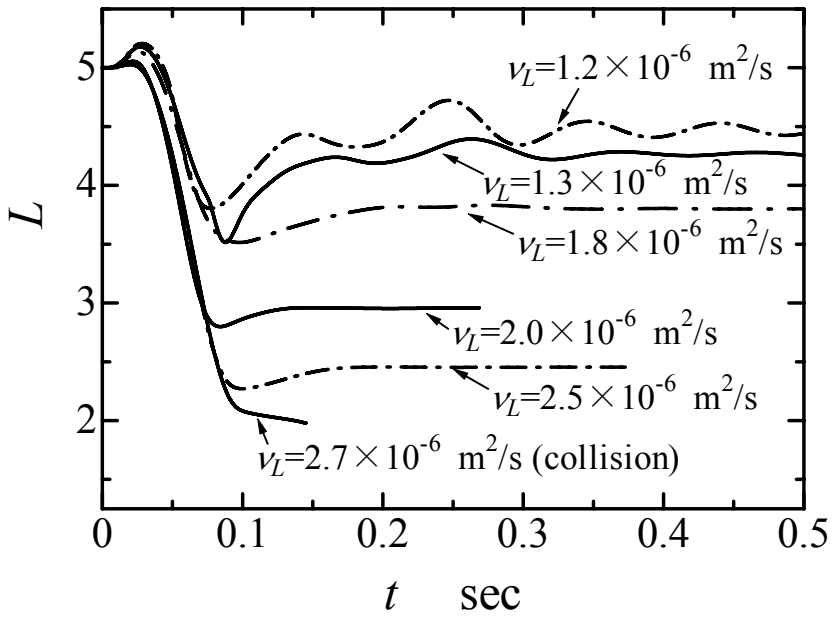

Figure 4.13 Effect of liquid viscosity on bubble distance

Table 4.3 Equilibrium Reynolds number

ν_L (×10^{-6}) m^2/s	2.6	2.5	2.0	1.8	1.5	1.3	1.2
Re_{eq}	37	40	59	71	93	116	134

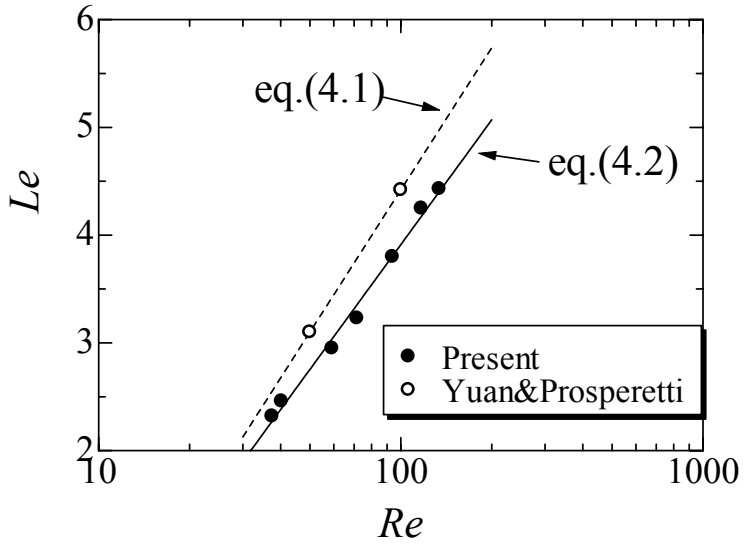

Figure 4.13 Equilibrium distance between two bubbles as a function of the Reynolds number

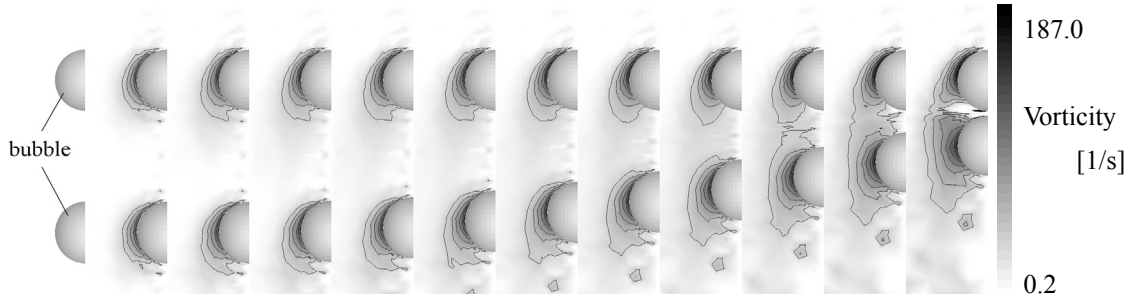

Figure 4.14 Vorticity distribution in the case of low Reynolds number
(Re=27, Δt=0.01s)

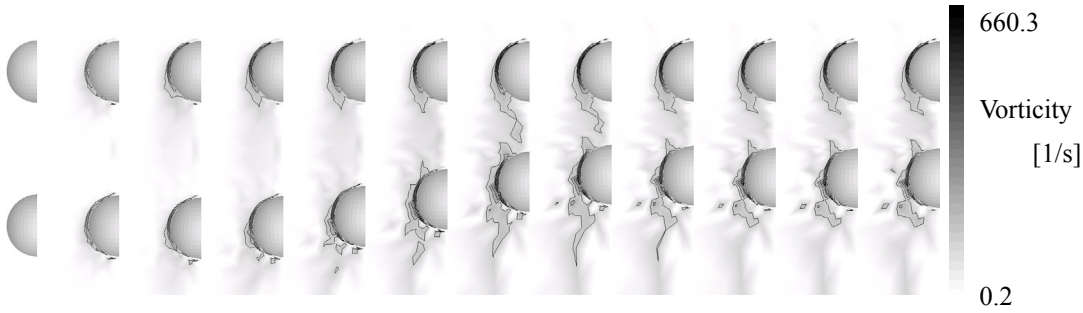

Figure 4.15 Vorticity distribution in the case of intermediate Reynolds number
(Re=72, Δt=0.01s)

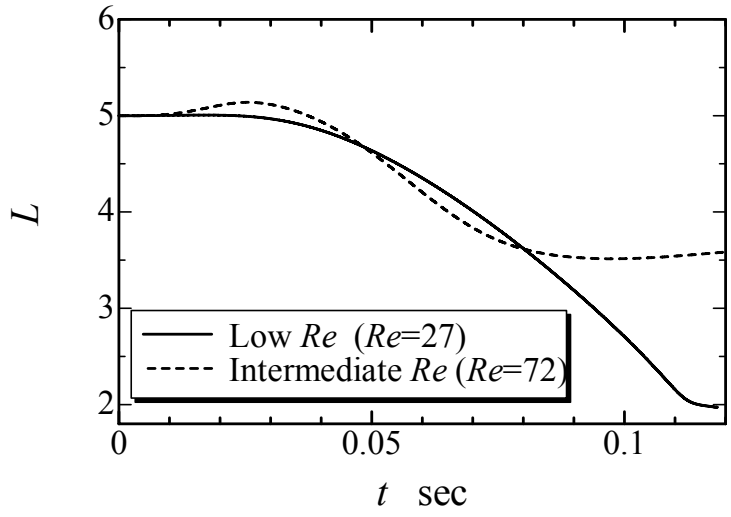

Figure 4.16 Bubble distance

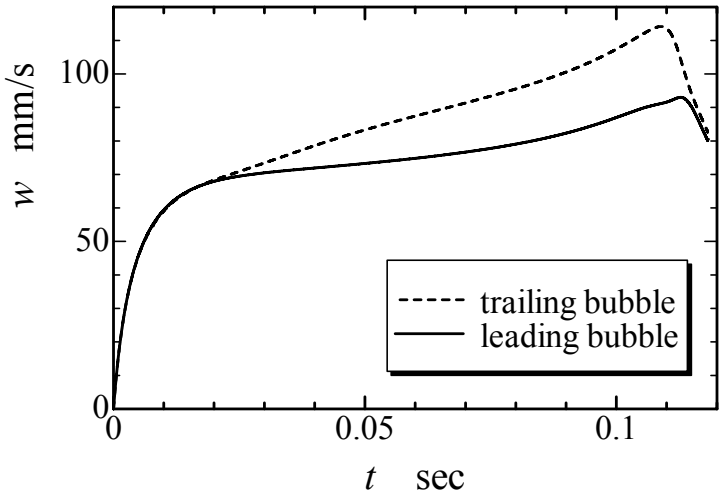

(a) *Re*=27

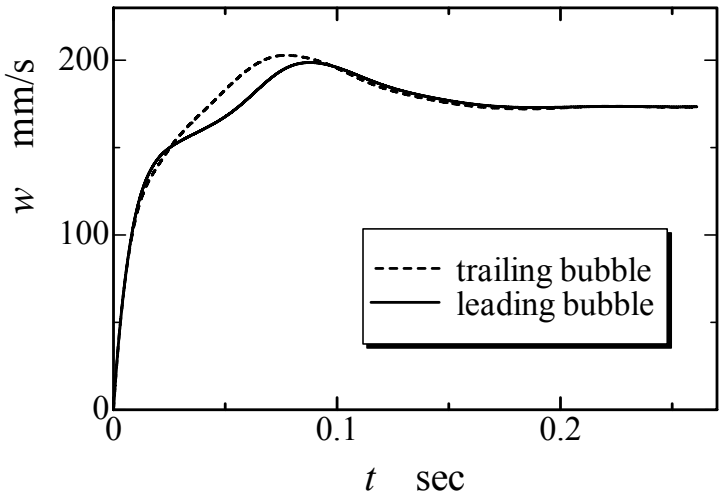

(b) *Re*=72

Figure 4.17 Rise velocity of a pair of bubbles

4.5 A pair of bubbles rising side by side

4.5.1 Effects of Reynolds number

The motion of a pair of equi-diameter bubbles rising side by side is considered in this section. A pair of bubbles was generated simultaneously from a pair of pin-holes on a pipe horizontally placed. Legendre *et al*. (2003) studied the lift force acting on the spherical bubbles rising side by side by numerical analysis. They showed that the direction of the lift force acting on the bubble was altered due to the vorticity generated bubble surface with a transitional region with $30 \leq Re \leq 100$, and that with *Re* greater than these values the attractive force dominated, and that the repulsive force dominated otherwise.

Figure 4.18 shows the motion of a pair of bubbles with various Reynolds number *Re*. The low *Re* cases (by using high kinematic viscosity liquid with K5 and K20) are shown in Figs. 4.18 (a) and (b). On the other hand, the high *Re* cases (by using low kinematic viscosity liquid with K1), are shown in Figs. 4.18 (c) ~ (f). First of all, the results of the low *Re* are discussed. A pair of bubbles separated from each other as they rose after the generation, as shown in Fig. 4.18(a). It is considered that this separation caused by the vorticity generation on the bubble surface, as predicted by Legendre *et al*. (2003). With the increase of *Re*, bubbles rose almost straight line as shown in Fig. 4.18 (b) due to the decrease of the lift force acting on the bubbles.

On the contrary, a pair of bubbles was attracted each other in the case of high *Re* as shown in Figs. 4.18 (c) ~ (f). A pair of bubbles (in the case of $Re = 109$) coalesced at $z = 15$ mm above the orifices immediately after the generation, as shown in Fig.10 (c). On the other hand, those with slightly larger $Re = 160$ bounced at $z = 15$ mm, then rose straight with the separation of the larger distance between bubbles than the initial horizontal distance, as shown in Fig. 4.18 (d). The criteria of either coalescence or bouncing are discussed in the next section.

With the further increase of *Re*, bubbles repeatedly bounced with each other as shown in Figs. 4.18 (e) and (f). In this case, two types of bouncing were observed, namely bubbles rose in either symmetry or asymmetry. The detail of this bouncing is discussed in next section.

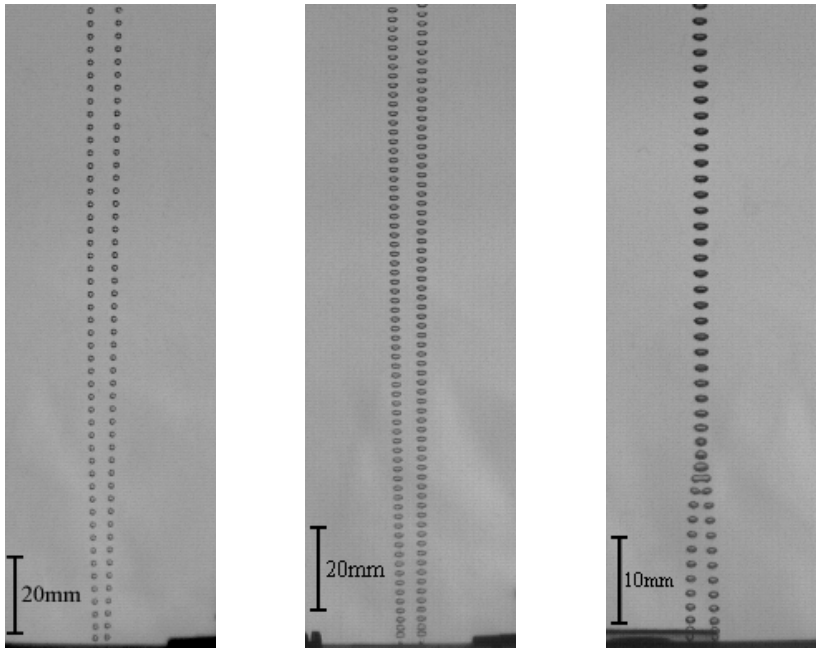

(a) Re=6, l_i=2.2mm (b) Re=49, l_i =4.5mm (c) Re=109, l_i=3.0mm

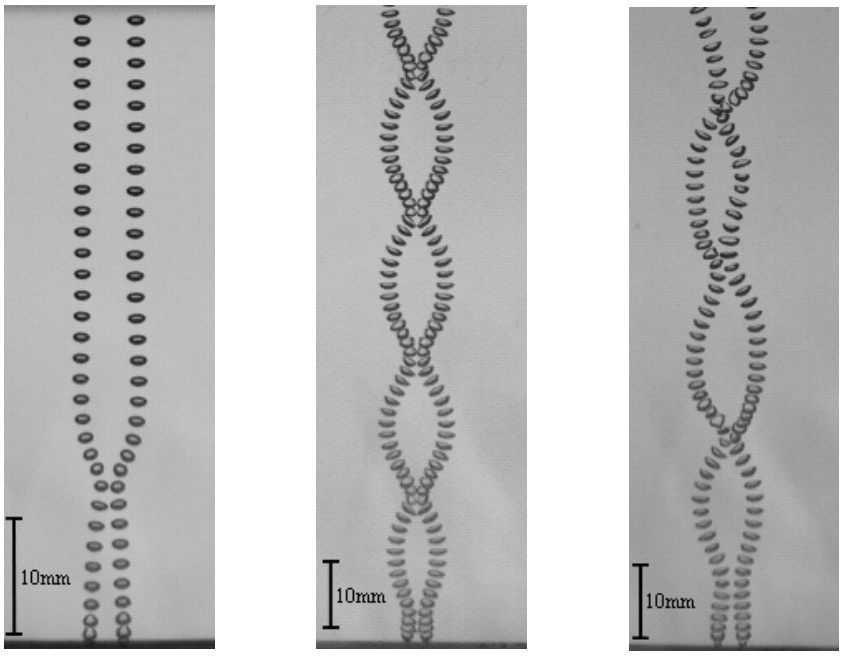

(d) Re=160, l_i=2.2mm (e) Re=341, l_i=2.5mm (f) Re=304 l_i=3.0mm

Figure 4.18 Motion of a pair of bubbles rising side by side

4.5.2 Bouncing of Bubbles

As shown in the previous section that a pair of bubbles bounced repeatedly in the case of high *Re* (Figs. 4.18 (e) and (f)), a pair of bubbles rose in symmetry in some cases, and in asymmetry in other cases. These differences are investigated. Figures 4.19 and 4.20 show the close up images of bubble bouncing. Figure 4.21 shows the bubble velocity corresponding to the case of Figs. 4.19 and 4.20. First, the motion of bubbles rising in symmetry is investigated by comparing the motion of a bubble that rose bouncing with a wall. It is well known that the velocity of bubble bouncing a wall is decelerated and was almost zero due to the formation of a vortical region (de Vries, 2002). However, from Fig. 4.21 (a), rising velocity w was not so decelerated. It is considered that the vortical region was not formed in the range of the present experimental condition.

On the other hand, the velocities of the bubbles rose in asymmetry were slightly decelerated. This deceleration of rising velocities was always observed when the edge of bubbles shifted and then collided. Because of the shift of the collision point, the interaction of the wake of each bubble is different. From Figs. 4.20 and 4.21 (b), it is assumed (or speculated) that the bubble-2 was accelerated due to the wake of bubble-1 when the bubble-1 was decelerated and rotated.

Next, the motion of a pair of bubbles that repeatedly bounced in symmetric is investigated by comparing to the bubble bouncing with the wall (Takemura & Magnaudet, 2003). Figure 4.22 shows that the bubble trajectories corresponding to the one in Fig. 4.18 (e) and the results of Takemura & Magnaudet (2003). It was clearly observed that the amplitude of the bouncing of bubbles was significantly larger than the case of bouncing with a wall. It is considered that this is due to the difference in *Re*. On the other hand, the frequency was slightly higher. It is considered that this difference was caused by the deceleration of bubble velocity at the bouncing in the case of bouncing with a wall.

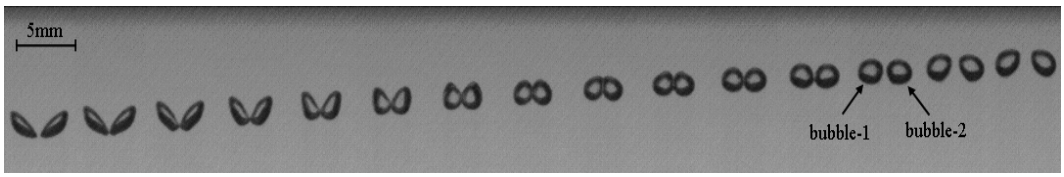

Figure 4.19 Bouncing of bubbles with symmetric shape oscillation (Δt = 2 ms)

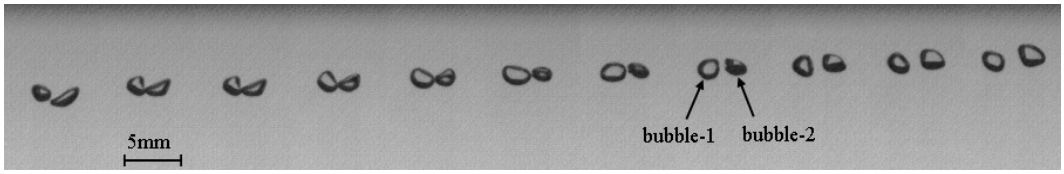

Figure 4.20 Bouncing of bubbles without symmetric shape oscillation (Δt = 2 ms)

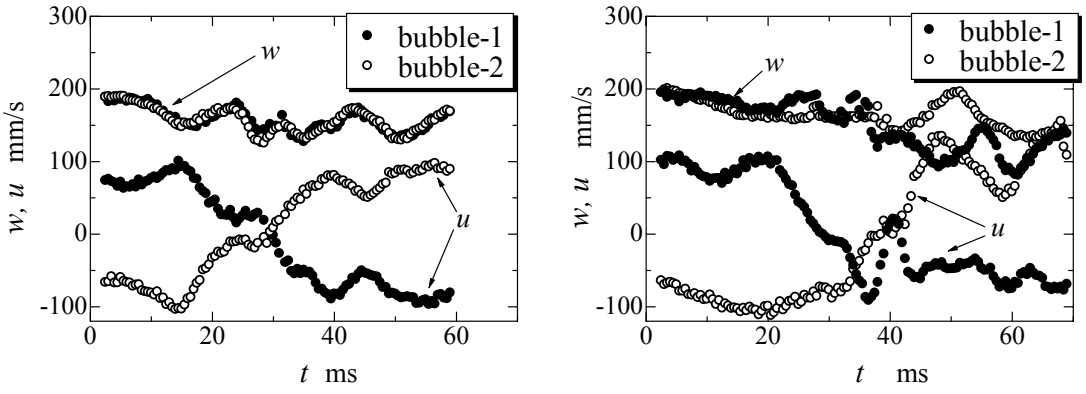

(a) with symmetric shape oscillation (b) without symmetric shape oscillation

Figure 4.21 Velocity of bubbles

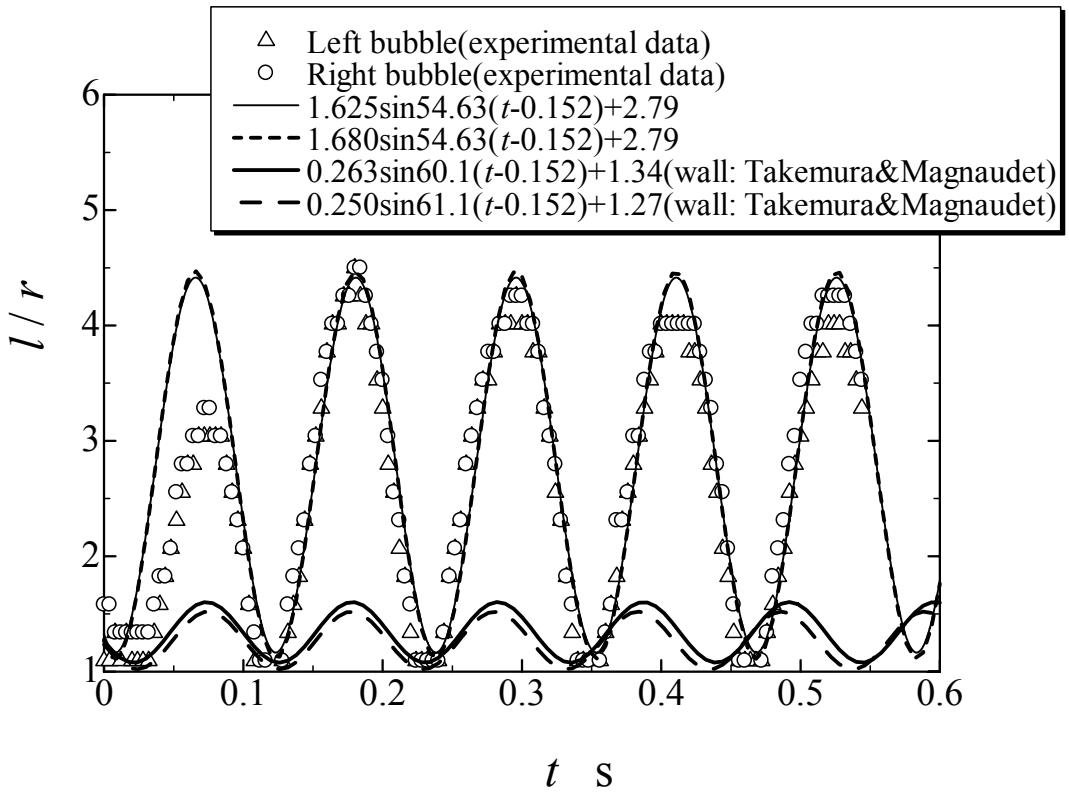

Figure 4.22 Bouncing of bubbles

4.6 Conclusion

The motions of a pair of bubbles with the same diameter were experimentally studied. A pair of bubbles rising either in a vertical line or side by side, interacting with each other was investigated. These accurately controlled spatial configurations of a pair of bubbles were realized for the first time owing to a high accuracy bubble production controller. It was observed that the Reynolds number significantly affected the motion of a pair of bubbles rising both in vertical line and side by side.

When a pair of bubbles rose in vertical line, the trailing bubble was attracted by the wake of the leading bubble, and then it reached an equilibrium distance between bubbles due to the balance between the leading bubble wake attractive force and potential repulsive force, in the case of intermediate *Re*. As *Re* further increased, the trailing bubble deformed and then escaped from the vertical line.

When a pair of bubbles rose side by side, they attracted each other and then coalesced when *Re* was smaller than a critical value, in the case of large *Re*. At the moment of the bouncing of a pair of bubbles, it was observed that the bubble rising velocity was not so decelerated with asymmetric shape deformation. In addition, it was also observed that the frequency of bouncing bubble is slightly higher and the amplitude of bouncing bubble is significantly larger than the bouncing bubble with a wall.

Chapter V VISCOSITY EFFECTS ON COALESCENCE OF A PAIR OF BUBBLES

In this chapter, effects of liquid viscosity on coalescence of a pair of bubbles were studied both experimentally and numerically. Following the footsteps of Duineveld (1994), two types of coalescence/bouncing of bubbles were focused on. The first type was those between a rising bubble and a free surface, and the second type was those between of a pair of bubbles rising side by side. The former is considered as the extreme case, which is equivalent to coalescence/bouncing between bubbles with finite and infinite diameters. The later is more practical. That is, bubbles were generated simultaneously from a pair of pin-holes on a pipe horizontally placed. We investigate the effects of liquid kinematic viscosity which was not considered by Duineveld (1994) on the criteria of two types of coalescence/bouncing of bubbles.

5.1 Introduction

Coalescence, in particular, is one of the most important elementary physical processes occurring in bubbly flow. For example, So *et al*. (2002) demonstrated that bubble coalescence can be prevented by adding a small amount of surfactant and that the structure of bubbly flow is significantly modified, by observing turbulent bubbly channel flow. However, the current understanding of the coalescence process is insufficient for accurate modeling. Consequently, the most typical computer simulations carried out in the literature, such as the direct numerical simulation (DNS) of bubbly flow, failed to take the coalescence process of bubbles into account.

In general, studies concerned with the coalescence of bubbles can be grouped into two categories—those investigating the effects of impurities dispersed in liquid phase and those focusing on the mechanism of coalescence, which is considered in this paper. With regard to the former category, for instance, the effects of mixing a tiny amount of either a surfactant or an electrolyte into the liquid phase to prevent bubble coalescence were examined (Marrucci & Nicodemo, 1967; Lessard & Zieminski, 1971; Drogaris & Weiland, 1983; Prince & Blanch, 1990; Duineveld, 1994). Chesters (1991) has provided a comprehensive review of these studies.

With regard to the second category, the coalescence mechanism has been discussed from the viewpoint of the liquid film that exists between a pair of bubbles by applying the lubrication theory. The study of the flow structure in this

thin liquid film reported a good agreement between the theory and the experimental results (Allan *et al*., 1961; Marrucci, 1969). On the other hand, Kirkpatrick *et al*. (1974) showed that the bubble "bounced" in the case of a large approach velocity to a free surface and that it coalesced without bouncing in the case of a small approach velocity. Chesters & Hofman (1982) developed the model of the thinning process of liquid film that led to a rupture. Neglecting liquid viscosity, they showed that the characteristic shape of the thin liquid film, referred to as a "dimple," was formed and that this dimple played an important role when a pair of bubbles bounced. The results of the thickness of liquid film between a bubble and a free surface obtained by Doubliez (1991) were in good agreement with those of Chesters & Hofman (1982), when the alcoholic solutions were not in distilled water. Through the use of super-purified water, Duineveld (1994) investigated the coalescences between a rising bubble and a free surface and between a pair of bubbles rising side by side. He showed that the conditions of bubbles coalescing or bouncing were strongly dependent on Weber number (*We*), and that the threshold *We* was predicted using models by Chesters & Hofman (1982). However, Duineveld (1994) only considered the effect of *We* number and never discussed the effects of viscosity, Capillary number (*Ca*), and Reynolds number (*Re*).

Furukawa & Fukano (2001) investigated the influence of liquid viscosity on fluid flow patterns in vertical upward gas-liquid two phase flow. They showed that, under a high liquid viscosity condition, the transition from a bubbly flow to a slug flow occurred in the case of low superficial gas and liquid velocities. Bubble coalescence is an important parameter in this transition process (Das & Pattanayak, 1994). It is therefore necessary to investigate the influence of liquid viscosity on bubble coalescence, which was not considered by Duineveld (1994).

The aim of the present study is to investigate the effects of liquid viscosity on the coalescence of a pair of bubbles. A qualitative evaluation of both the coalescence time and the thresholds of the bouncing/coalescence of a bubble with a free surface were experimentally performed. In addition, both the shape of the liquid film between the bubble and the free surface and the structure of the liquid flow and pressure field were numerically analyzed by the level set method. This method is clearly distinct from the lubrication theory in computing not only the flow field in the thin liquid film between a bubble and a free surface but also the entire flow field around the bubble. Furthermore, following the footstep of Duineveld (1994), both the coalescence and the bouncing of a pair of bubbles rinsing side by side were investigated with focusing on the viscosity effect, in the same way as the experiment of a free surface.

5.2 Experimental apparatus and procedure

In the experiment, a single bubble or a pair of bubbles was generated, the diameters of bubbles were accurately controlled by releasing nitrogen gas from a single orifice or a pair of orifices horizontally placed into a pool (150 mm × 150 mm × 400 mm) filled with quiescent silicone oil. The bubble diameter d and the kinematic viscosity of the liquid ν, were selected as two characteristic experimental parameters. The diameter d ranged from 0.30 mm to 1.66 mm. Six types of silicone oils with different viscosities were used; we refer to them as K065, K1, K1.5, K2, K5, and K20. Morton number (Mo) ranged from O(10^{-10}) to O(10^{-4}), where Mo is a dimensionless number depends only on fluid properties. The effects of both We and Re on the experimental results were carefully examined. The rising velocity w was observed to be constant until the upper surface of the rising bubble disappeared in the meniscus; hence, this velocity was considered to be equivalent as the bubble approaching velocity to the free surface. The characteristic diameter d was considered to be that of an equivalent sphere having the same volume as the bubble, the shape of which was assumed to be spheroid. As observed by Kirkpatrick *et al*. (1974), no deceleration of the bubble was apparent prior to contact between the bubble and the free surface. The experimental ranges of We and Re numbers were from O(10^{-3}) to 1.70 and from 1 to 200, respectively.

5.3 A bubble upon impact with a free surface (experiment)

5.3.1 Bubble behavior and coalescence time

First, the coalescence time was measured, in order to investigate how differences in viscosity modify the bubble coalescence with a plane-free surface. The coalescence time was defined by Kirkpatrick *et al*. (1974), as the elapsed time from contact between the bubble and interface to the rupture of the contact film. The coalescence time was evaluated using both the real and the mirror images of a bubble near a free surface as shown in Fig. 5.1. Figure 5.1 is a typical example of images of bubble motion near a free surface. It is considered that the contact between the real and mirror images of the rising bubble, as shown in Fig. 5.1 (c), to be the contact between the bubble and the free surface. In other words, it was assumed that the bubble made contact with the free surface when it reached the initial undisturbed free surface. Thereafter, the bubble continued to rise and partially disappeared with the rise of the free surface. The bubble then bounced and moved further upward (Fig. 5.1 (f)). it was also considered that the bubble coalesced with the free surface when the bottom part of the bubble disappeared, as shown in Fig. 5.1 (g). Consequently the coalescence time was 48 ms in the case of Fig.5.1.

We distinguished between the coalescence and bouncing in the following manner. Three typical results of the bubble either coalescing with or bouncing off the free surface are shown in Fig. 5.2. it was considered that a bubble coalesced without bouncing when it disappeared immediately after making contact with the free surface as shown in Figure 5.2 (a); otherwise, it was considered the bubble to have bounced. Both Figs. 5.2 (b) and 5.2 (c) are typical examples of bubble bouncing. After the bubble made contact with the free interface, it either bounced repeatedly, as shown in Fig. 5.2 (b), or remained at the free surface until it coalesced, as shown in Fig. 5.2 (c). Figure 5.3 shows typical detailed images of the bubble bouncing both before and after contact with the free surface. In this case (We = 1.7, K1), the bubble bounced three times before it coalesced with the free surface. The first bounce is shown in Figure 5.3.

The bouncing number n and the coalescence time in the case of low kinematic viscosity liquids (K1 and K2) are shown in Figure 5.4. It should be emphasized that, in this liquid viscosity range, the coalescence time was proportional to We, and consequently to the square of the approach velocity. Kirkpatrick *et al*. (1974) was the first to show that the approach velocity played an important role in

coalescence time; however, he only provided a qualitative discussion.

It should be also noted that the coalescence time increased with an increase in n and also with an increase in We in the case of equal n. For instance, in the case of $n = 2$, coalescence times of 0.03 s and 0.05 s were obtained with We of 0.75 and 1.75, respectively, as shown in Fig. 5.4. Figure 5.5 shows the transient positions of the bubble bottom for two different We (A and B) using the same kinematic viscosity of liquid, K1. Both the bubbles bounced twice ($n = 2$). After the bubble made contact with the free surface, the bubble bottom immediately moved downward in the case of low We (A). On the other hand, the bubble bottom continued to rise as a result of both bubble shape deformation and free surface rise in the case of high We (B). After reaching the highest possible point, the bubble started to decline further than the point observed in the case of low We, and then began to rise again to make contact with the free surface. Consequently, the distance traveled by the bubble increased considerably. On the basis of a straightforward application of Newton's law on mass moving in a potential field, neglecting drag, the time between the first and second contact is evaluated to be approximately proportional to the square root of the distance traveled by the bubble. Therefore, the coalescence time increased with an increase in We, even with the same bouncing number, as shown in Fig. 5.5.

With the increase in the liquid viscosity, the bubble motion in the vicinity of the free surface was considerably modified as compared with the cases in which K1 or K2 was used, as shown in Fig. 5.6 (K5). The bubble pushed the free surface upward direction after making contact with it and then bounced back slightly. However, clear bouncing—the separation of the real image from the mirror image as shown in Fig. 5.3—was not observed, and the bubble remained at the free surface until it coalesced with the free surface. The coalescence time varied widely for higher kinematic viscosities, even with the same We, as observed in the case of lower viscosities.

Figure 5.7 shows the effects of kinematic viscosity on bubble coalescence time. Bubble coalescence time was a function of only We in the case of both K1 and K2, regardless of the viscosity, as already observed in Fig. 5.4. However, the bubble coalescence time increased significantly in the case of K5 or K20 and showed a low correlation with We; this is a considerable deviation from the results of K1 and K2. The magnitude of the order of the coalescence times of K5 and K20 is different from those of low viscosity liquids (K1 and K2) although the coalescence time tended to shorten with smaller We, even in the case of K5 or K20.

Chesters *et al*. (1982) and Duineveld (1994) constructed the bubble bouncing

model and showed that two equally sized bubbles coalesced if *We* was below a critical value, namely, *We* = O(0.1), irrespective of the effect of the viscosity, and that they bounced otherwise. It was found that critical *We* was 0.1 in the case of K1. It is expected, considering the preceding experimental results, that this influence of kinematic viscosity also affects the critical *We* of the coalescence of bubbles. In the next section, the effects of viscosity on the threshold of coalescence are discussed.

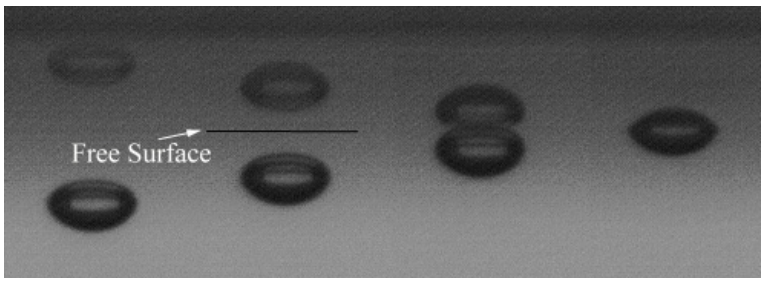

(a) $t = -4$ (b) $t = -2$ (c) $t = 0$ (d) $t = 2$ (ms)

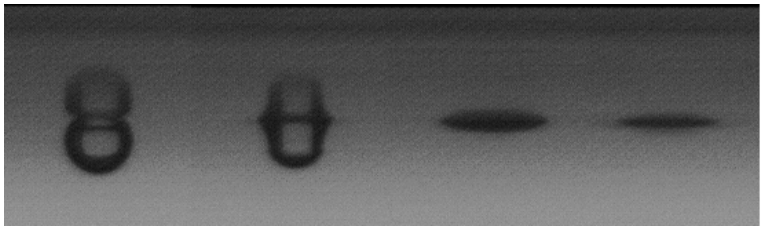

(e) $t = 44$ (f) $t = 46$ (g) $t = 48$ (h) $t = 50$ (ms)

Figure 5.1 Evaluation of free surface location and coalescence moment

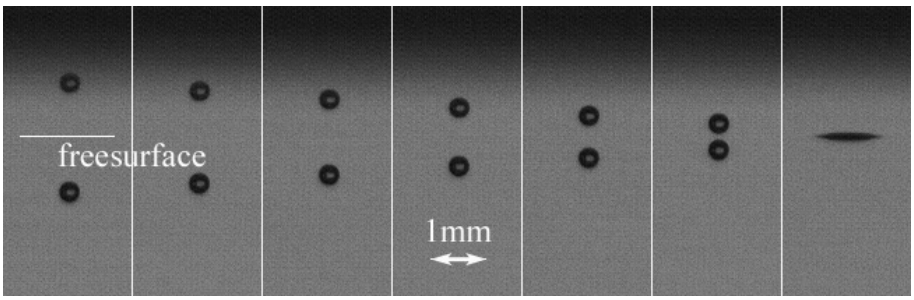

(a) Coalescence (Δt = 4 ms)

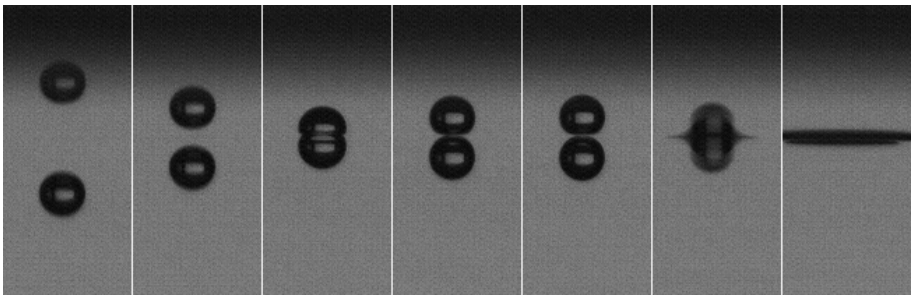

(b) Bouncing (Δt = 4 ms)

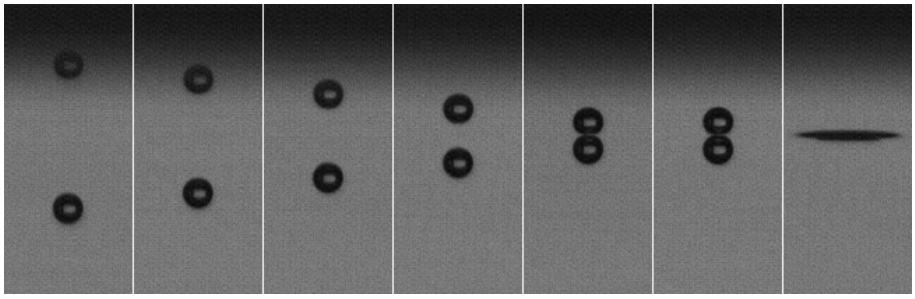

(c) Bouncing (Δt = 4 ms)

Figure 5.2 Distinction between coalescence and bouncing

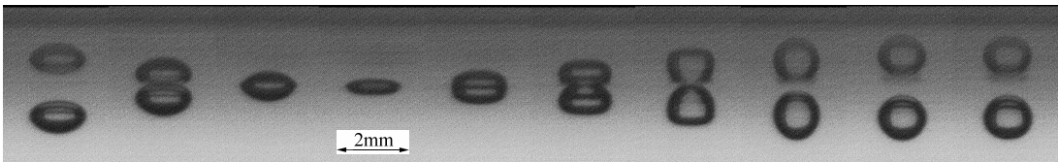

Figure 5.3 Bubble motion near the free surface in a low viscosity liquid (We = 1.7, K1, Δt = 2 ms)

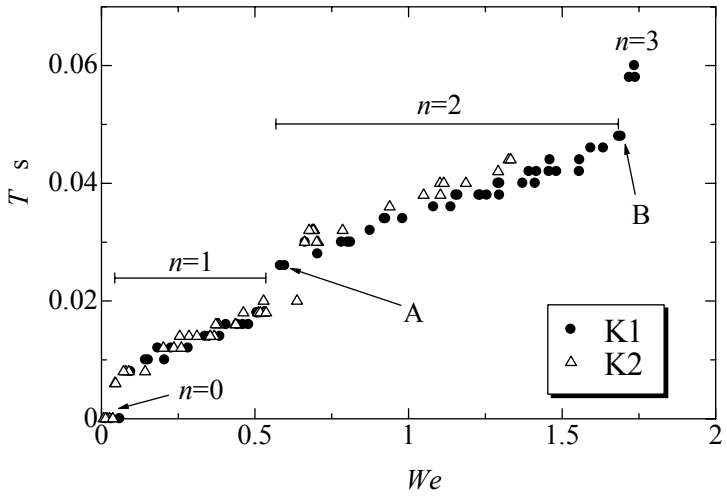

Figure 5.4 Coalescence time and bouncing number (K1 and K2)

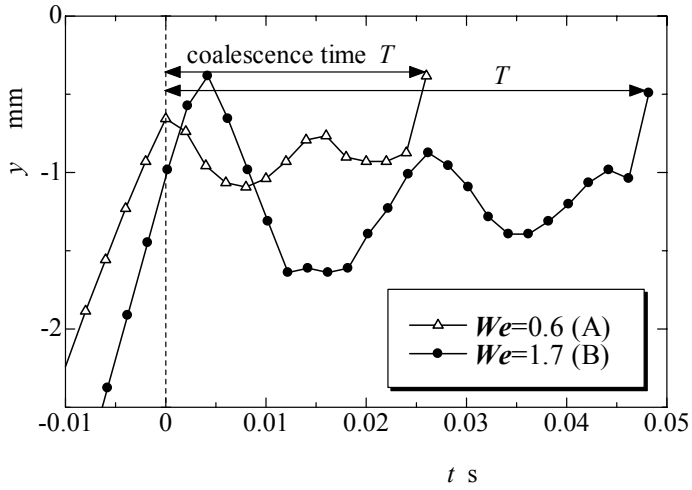

Figure 5.5 Transient vertical position of bubble bottom

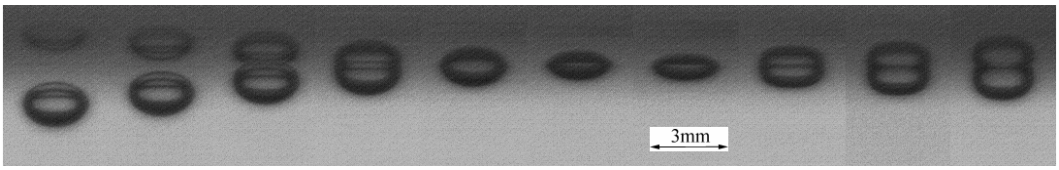

Figure 5.6 Bubble motion near the free surface in a high viscosity liquid (We = 1.1, K5, Δt = 2 ms)

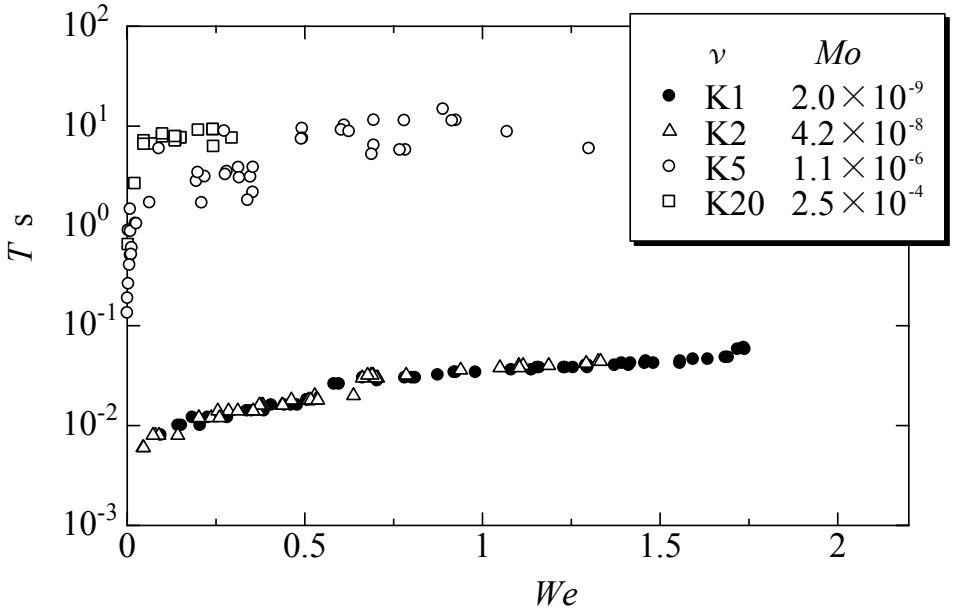

Figure 5.7 Coalescence time (liquids of all viscosity ranges)

5.3.2 Criteria of bouncing and coalescence

In this section, in order to discuss the effects of viscosity, it is investigated whether a rising bubble coalesced with or bounced off a free surface using five types of silicone oil with different kinematic viscosities, i.e., K0.65, K1, K1.5, K2, and K5. Duineveld (1994) conducted a similar experiment using super-purified water and showed that We = 0.104 was the critical We below which the bubble coalesced. However, he did not discuss the viscosity effects.

Figure 5.8 shows that a rising bubble either coalesced with or bounced off a free surface. Weber numbers, We, were calculated and plotted as the open circles when bubble bounced, and as the crosses when bubble coalesced with a free surface. The critical We for bubble coalescence was focused on, in the case of both K0.65 and K1, which are relatively low kinematic viscosity liquids. It was observed that the critical We for K0.65 and K1 are 0.088 and 0.087, respectively. These results agreed well quantitatively with the experimental result of Duineveld (1994). The discrepancy between these results and the results of Duinveld's was considered to be the integration of multiple effects such as the difference in liquid molecular structure, experimental errors, and so forth. It should be emphasized that, regardless of the difference in the liquid kinematic viscosity, whether a bubble coalesced with or bounced off the free surface was determined only by We, as reported by Chesters *et al*. (1982). Further, the influence of the difference in the kinematic viscosity was scarcely detected.

On the other hand, the results of K1.5 and K2, which have relatively higher kinematic viscosities, were significantly different from those obtained with less viscous liquid. The critical We for K1.5 and K2 were significantly modified and reduced to 0.061 and 0.051, respectively. These results revealed the strong effects of the difference in the liquid kinematic viscosity, which sharply contradicted those of the low liquid viscosity. It is noteworthy that the bubble even did not coalesce in the case of K5 in the range of the present experimental We (consequently $We = O(10^{-3})$). It was understood that the strong effects of the liquid kinematic viscosity on the critical We for coalescence were observed in the case of liquids with high viscosity, such as K1.5, K2, and K5.

Next, the effects of the Reynolds number are considered. Chesters *et al*. (1982) numerically investigated the Reynolds number effects on the thinning rate of the liquid film between two approaching bubbles. They found that a dimple was formed on the flat surface of the bubble in the inviscid liquid and that the surface area of bubble increased before the film ruptured, causing the bubbles to

bounce. They also discussed the influence of *Re* on the thinning rate of the liquid film. The thinning rate of a low viscosity liquid with *Re* = 100 was indistinguishable from that with the inviscid assumption. With an increase in the liquid viscosity, a decrease in *Re* was observed, and the thinning rate with *Re* = 10 was also similar to that of the inviscid result with a slight difference in the early stage of liquid film development. The dimple formation was suppressed only in the case of *Re* = 1.

Re were calculated and plotted when a bubble bounced (open circles) and when it coalesced (crosses) as shown in Fig. 5.9. As is clearly seen, the critical *Re* for coalescence decreased with an increase in liquid viscosity. It was found that the critical *Re* in the case of K1 was approximately *Re* = 40 and that in the case of K1.5 was *Re* = 25. It was also observed that the viscosity affected on critical *Re* only in the latter case. In contrast to the results of Chesters *et al*. (1982), which reported that a significant difference in liquid film development occurred only when approximately *Re* = 1, it was shown that the liquid viscosity effects on bubble coalescence became remarkable for high *Re; Re* = 25 in the case of K1.5. It is considered that whether bubbles coalesce or bounce depends not only on *We* but also on *Re*; hence, this determination should not be solely based on *We*.

Using liquids of different kinematic viscosities, it have been shown that the theory proposed by Chesters *et al*. (1982), which states that whether a bubble coalesces with or bounces off a free surface depends only on *We*, should be applied in more restricted conditions. Further, it also have been shown that, due to the influence of a liquid kinematic viscosity, critical *We* should not be determined as a single value in high kinematic viscosity liquids (Mo = O(10^{-8})~O(10^{-7})). In next section, we investigate the viscous effects in greater detail by numerical analysis.

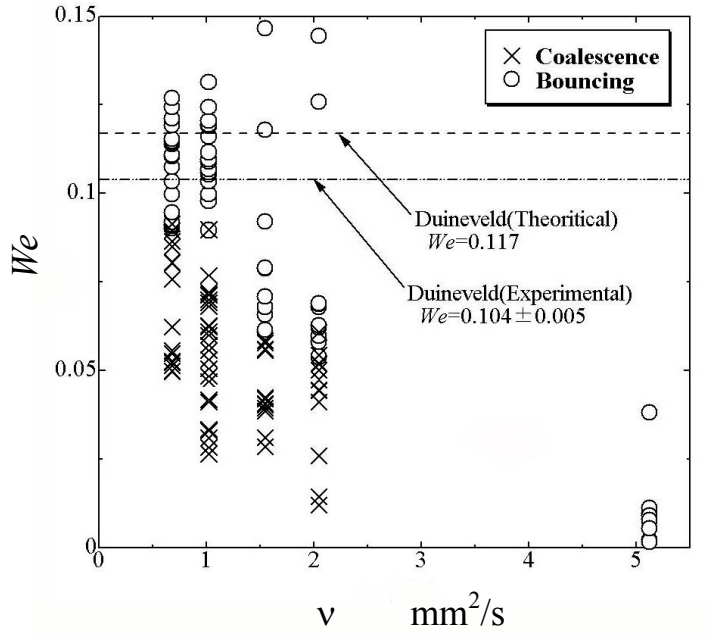

Figure 5.8 Critical Weber number for bouncing

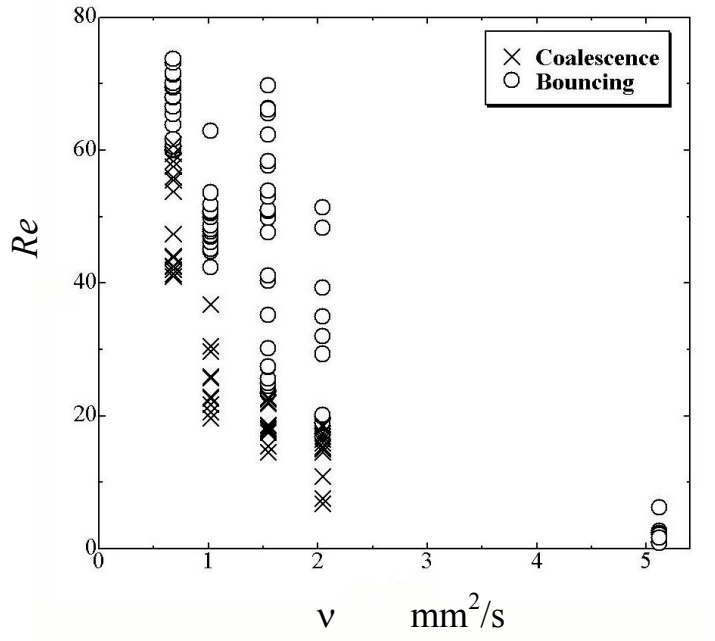

Figure 5.9 Critical Reynolds number for bouncing

5.3.3 Effects of viscosity on foam formation

Consecutive images of the free surface and of the bubbles generated at a fixed frequency (5 Hz) are shown in Figs. 5.10 (a) and (b). Figure 5.10 (a) shows the low kinematic viscosity case (K1) while Fig. 5.10 (b) shows the high kinematic viscosity case (K5). It was observed that surface waves occurred only in the case of K1 due to immediate coalescence after the bubbles collided with the free surface, and that foam was formed in the case of K5, as shown in Fig. 5.10 (b), as the consequence of the large coalescence time for K5.

It is remarkable that the existence of foam in non-polar liquids depends on the liquid kinematic viscosity. It is generally considered that foam exists in due course of the existence of the surfactants, which prevent thin liquid films between a free surface and bubbles from disappearing. However, silicone oil is non-polar liquid; hence, surfactant effects are assumed to be negligible. It is considered that the flow condition plays an important role in foam formation in a high viscosity liquid. The results of the numerical analysis, from the point of view of the liquid flow fields and pressure fields surrounding a bouncing bubble, are discussed in the next section.

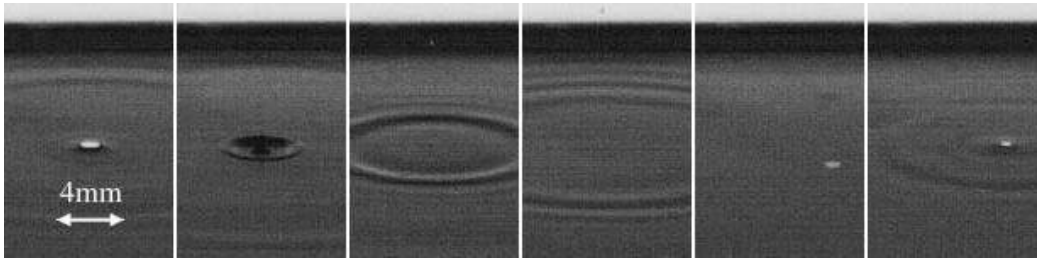

$t = 0$ $t = 0.017$ $t = 0.033$ $t = 0.050$ $t = 1.0$ $t = 2.0$ (s)

(a) K1, d = 1.3 mm, 5 Hz

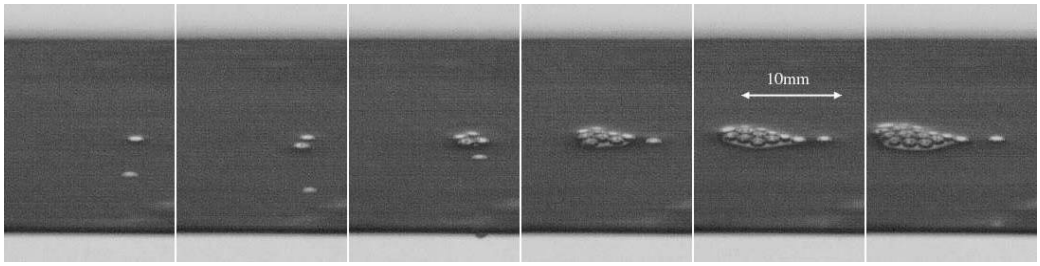

$t = 0$ $t = 0.2$ $t = 1.0$ $t = 2.0$ $t = 3.0$ $t = 4.0$ (s)

(b) K5, d = 1.4 mm, 5 Hz

Figure 5.10 Foam formation on the free surface of silicone oil

5.4 A bubble upon impact with a free surface (numerical analysis)

5.4.1 Numerical method and verification

In the calculation, the axisymmetric shape of the bubble and the incompressibility of both the gas and the liquid were assumed. The governing equations of the flow used are the equation of continuity, the Navier-Stokes equation, and the transport equation of the level set function.

$$\nabla \cdot \boldsymbol{u} = 0 \tag{5.1}$$

$$\frac{\partial \boldsymbol{u}}{\partial t} + \boldsymbol{u} \cdot \nabla \boldsymbol{u} = \frac{1}{\rho}\left\{-\nabla p + \nabla \cdot \left(\mu \nabla \boldsymbol{u}\right)\right\} + \boldsymbol{f} \tag{5.2}$$

$$\frac{\partial \phi}{\partial t} + \boldsymbol{u} \cdot \nabla \phi = 0 \tag{5.3}$$

In this study, the level set function ϕ, the delta function $\delta(\phi)$, the Heaviside function $H(\phi)$, the viscosity $\mu(\phi)$, and the density $\rho(\phi)$ were defined in the same way as in Sussman *et al*. (1994, 1998). In the Sussman's technique, the physical properties at the interface is approximated as the function of smoothed Heaviside function as shown Fig. 3.17 (b). In addition, the surface tension was evaluated as a body force by employing the CSF method (Brackbill *et al*., 1992).

In this calculation, the fundamental equations were discretized by the finite difference scheme with the staggered grid system. The SMAC method was used as a solver, with the third-order accuracy ENO scheme for the advective term and the second-order accuracy central difference scheme for the other terms. The Adams-Bashforth method of second-order accuracy was used for time integration and the Bi-CGSTAB method (van der Vorst, 1992) with the imperfect LU decomposition preconditioner was used to solve the Poisson equation of pressure correction.

The level set function was reinitialized using the scheme proposed by Sussman *et al*. (1998), and reinitialization was achieved by repetitive calculation of the following equation.

$$\frac{\partial \phi}{\partial \tau} = \boldsymbol{S}(\phi_0)\left(1 - \left|\nabla \phi\right|\right) \tag{5.4}$$

In the above equation, S is the sign function andϕ_0 is the level set function prior to

reinitialization. The solution of ϕ has the same sign as ϕ_0; hence, the interface position is not modified with the accuracy of the grid size, and it satisfies $|\phi| = 1$. Therefore, ϕ is a distance function from the interface. The second-order accuracy ENO scheme and the second-order Runge-Kutta method were used for the discretization of $|\nabla\phi|$ and the time integration, respectively. The special treatment for the mass conservation of the bubble of each time step was provided by applying the method proposed by Chang *et al*. (1996).

In this study, two different gas-liquid interfaces namely bubble surface and free surface, co-existed in the calculation domain. These two interfaces were identified by defining two different distance functions through which each interface was described and independently transporting these distance functions to the calculation domain. Therefore, coalescence between the bubble and the free surface was prevented. The method developed by Chang *et al*. (1996) was used for the mass reinitialization. The convergence criterion was set to 10^{-5}, as in Chang *et al*. (1996). The mass was successfully conserved by employing this method since the change in mass was 10^{-5} or less.

The boundary conditions such as no slip on the bottom wall, zero shear stress on the right wall, and free outflow on the upper side of the pool were imposed. The CFL condition with the Courant number ranging between 0.2 and 0.4, the mesh size from 120×300 to 120×600, and the bubble diameter of d = 1.6~2.0 mm were employed as the calculation conditions. The physical properties of both the gas and the liquid used were those of nitrogen, and silicone oil with ν = 1~5 mm^2/s, respectively. Figure 5.11 shows this calculation domain and the boundary conditions.

Figure 5.12 shows the computational results of both the bubble shape and the bubble bottom position with $\nu = 2$ mm^2/s. These results were compared with the experimental ones and plotted as a function of time; *We* for both cases were approximately equal. *We* was calculated using the maximum velocity for u. It was observed from the experiment that the bubble bounced off the free surface under this condition. Both the bubble shape and the bubble bottom position are in good agreement with the experimental results. The difference was observed after t = 0.04 because of the no-coalescence assumption in the calculation. It is considered that the calculation reproduces both the bubble shape and the bouncing phenomenon with the free surface.

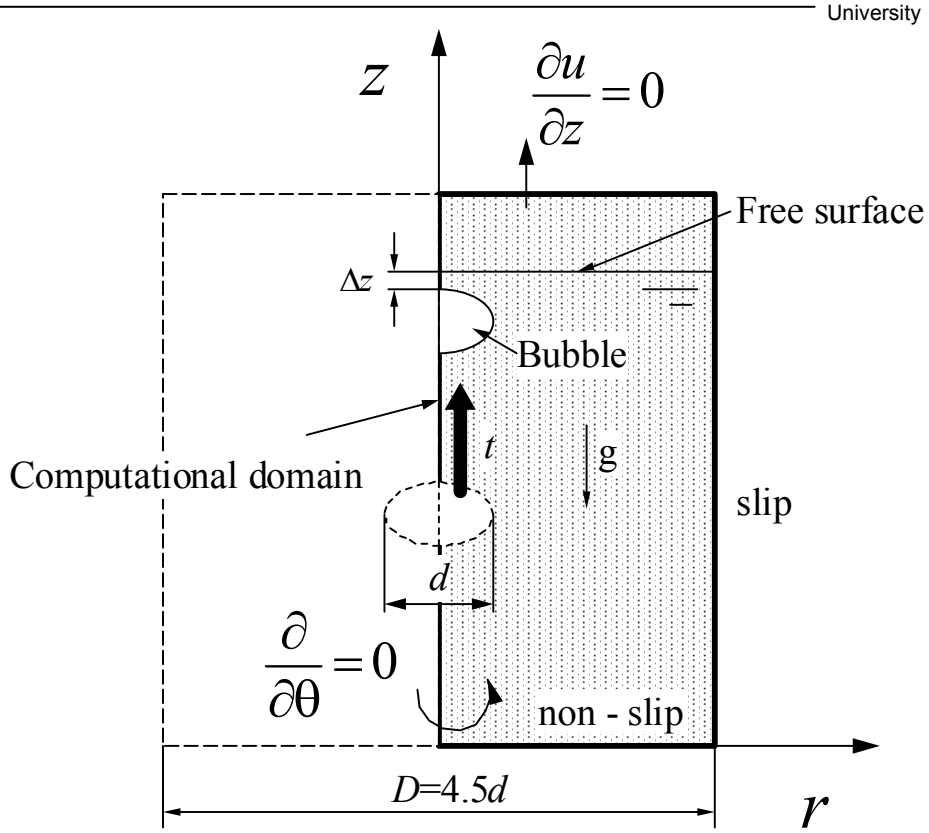

Figure 5.11 Computational domain and boundary condition

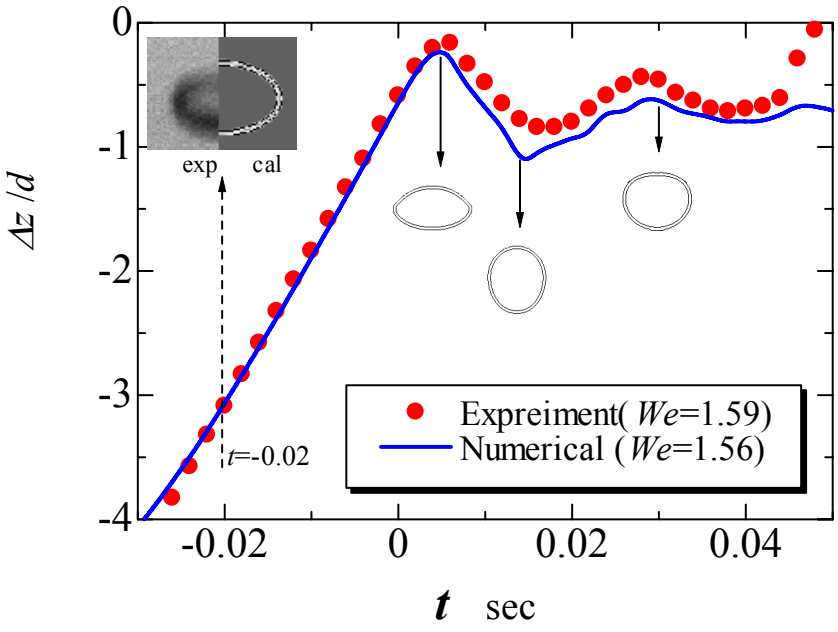

Figure 5.12 Comparison of experimental results and calculations

($\nu = 2$ mm^2/s, $We \cong 1.6$)

5.4.2 Bubble bouncing with a free surface

First, the bubble bouncing with the free surface was investigated. Figure 5.13 shows the velocity vector, the pressure contour line, and the pressure distribution on the axis in the case of d = 1.6 mm and ν = 2 mm^2/s. Figure 5.13 (a) shows the image of the result when a bubble was well underneath the free surface. The internal pressure of the bubble was greater than the surrounding fluid pressure due to the magnitude of surface tension resulting from the pressure jump across the gas-liquid interface. When the bubble approached the free surface as shown in Fig. 5.13 (b), the horizontal component of the liquid above the bubble did not increase sufficiently for the bulk of the liquid to escape from the liquid film between the bubble and the free surface; hence, the bulk of the liquid was trapped in the film, which was consequently pushed up toward the free surface. At the same time, a downward force acted on the liquid due to the gravity and surface tension of the free surface; hence, the upper side of the bubble surface decelerated. On the other hand, the bulk of the liquid underneath the bubble continued to rise due to the inertial force of the liquid. Therefore, the bubble was distorted and became oblate. Moreover, the pressure between the bubble and the free surface increased; however, did not exceed the internal pressure of the bubble. Simultaneously, a reverse-pressure gradient was generated in the vertical direction in the liquid under the bubble and a downward liquid flow was induced as observed in Fig. 5.13 (c). Further, the bubble surface was driven by this flow and moved downward. Consequently, due to the surface tension, the bubble departed from the free surface and recovered its shape from oblate to round. That is, the bubble bounced off the free surface.

Based on the numerical results, the novel interpretation of the bubble bouncing off the free surface is proposed. This interpretation is essentially different from the model proposed by Duineveld (1994) and Tsao *et al*. (1994). Their interpretation is that “The bubble bounces because pressure in the liquid film between bubbles is extremely high, and the internal pressure of the liquid film at this time becomes about from several tens to hundreds times of the *We* number as large as the initial pressure jump due to the surface tension.” On the contrary, the present numerical analysis proposed that the bubble bounces without extremely high pressure in the liquid film between the bubble and the free surface. Since the numerical and experimental results were in excellent agreement within the scope of the present study, it is considered that the physical process in the liquid film is not a predominant factor of bubble bouncing.

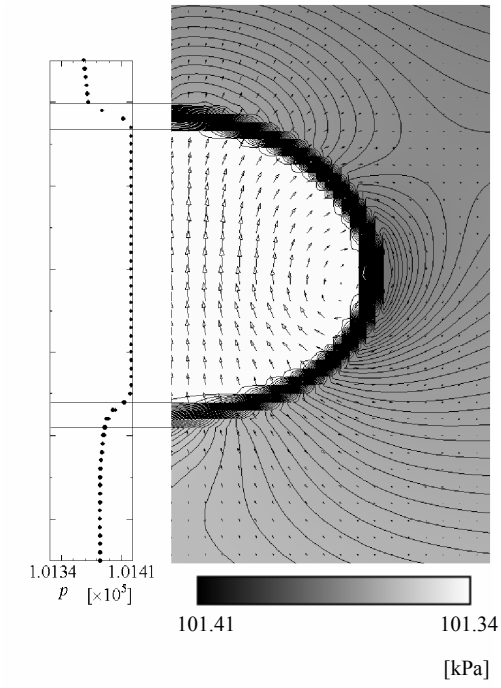

(a) t = –0.024 s

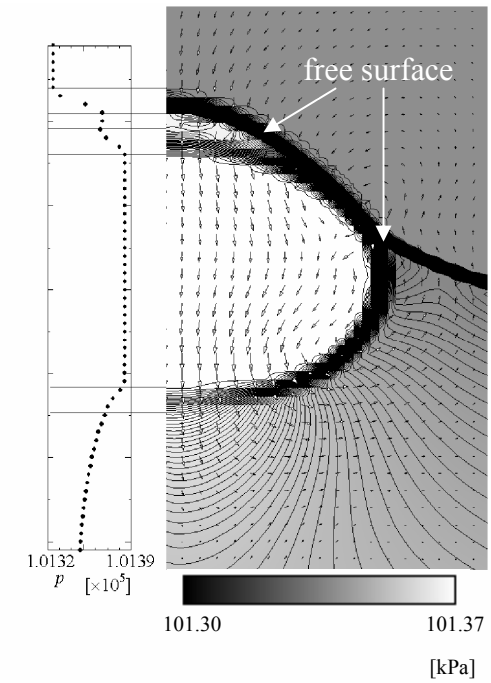

(b) t = 0.002 s

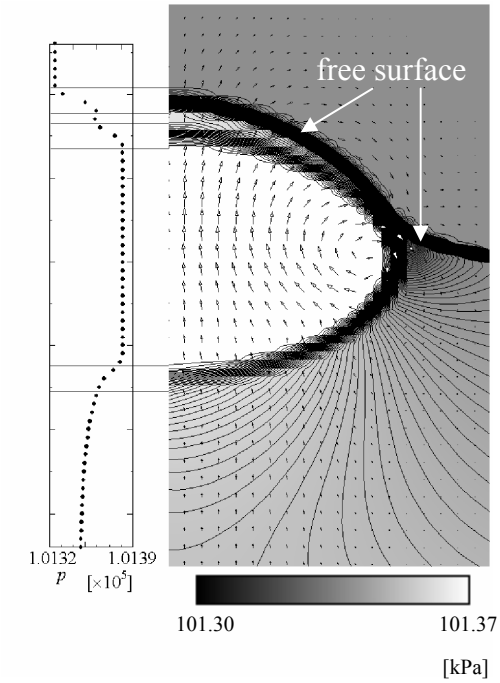

(c) t = 0.005 s

Figure 5.13 Velocity and pressure distribution of a low viscosity liquid (d = 1.6 mm, ν = 2 mm^2/s, We = 1.56)

5.4.3 Effects of inertia and viscosity

It was clarified in section 5.3.1 that an increase in *We* led to the bubble bouncing off the free surface and simultaneously extended the duration of the coalescence time. In this section, the influence of liquid inertia force on the liquid film between the bubble and the free surface is investigated. The calculation was executed by setting only gravity *g* as a variable parameter in order to change the rising velocity of the bubble and setting other parameter, such as the bubble diameter, liquid kinematic viscosity, and the surface tension coefficient as constants.

Figure 5.14 (a) shows the three images of the bubble shape in the vicinity of the free surface, obtained with different gravity values with d = 1.6 mm and ν = 2 mm^2/s. The variations in the shape of the liquid film between the bubble and the free surface were observed to be dependent on *We*. In the case of small *We*, the liquid film was the thinnest at the bubble top and gradually became thicker toward the peripherals. In contrast, when *We* increased, the liquid film was thicker in the bubble top than in the peripherals and the characteristic liquid film shape, i.e., a dimple (Chi *et al*., 1989), was clearly observed, as shown in Fig. 5.14 (a). It was recognized (Chesters *et al*., 1982; Duineveld, 1994; Tsao *et al*., 1994) that the dimple possessed a shape that prevented the bulk of the liquid from flowing out from the liquid film, and that the dimple played an important role in bubble coalescence and bouncing. Moreover, as *We* increased, the bubble became more oblate and the upsurge of the free surface grew prominent.

Next, the pressure distribution in the liquid, particularly in the liquid film between the bubble and the free surface, is investigated in detail. Figure 5.14 (b) shows the pressure distribution in the liquid in the cases with and without the dimple. In the case of small *We*, the dimple was not formed and the pressure decreased from the top of the bubble toward the peripherals, as shown in Fig. 5.14 (a)–(1). When the dimple was formed, the pressure distribution was comparatively constant in the liquid film. Although Duineveld (1994) and Tsao *et al*. (1994) predicted that the internal pressure of the liquid film should be extremely high, the numerical analysis results confirmed that the internal pressure of the liquid film was not high enough to form a dent on either the bubble surface or the free surface, and that it was about the same order as the internal pressure of the liquid just underneath the bubble, as shown in Fig. 5.14 (b).

As discussed in the previous section, Chesters *et al*. (1982) and Duineveld (1994) reported that the bubble bounced off the free surface due to dimple

formation as *We* increased; however, as shown in section 5.3.1, in the case of high kinematic viscosity liquids, clear bubble bouncing was not observed. Further, their model describing bubble bouncing and coalescence in terms of *We*, as examined in section 5.3.1, was proved unsuccessful. On the other hand, remarkable differences, especially in the thin liquid film between the bubble and the free surface, were observed between the results in the cases of higher and lower kinematic viscosity liquids, as already shown in Figs. 5.3 and 5.6. In this section, the effects of kinematic viscosity on bubble bouncing are investigated.

Figure 5.15 shows the pressure and velocity distributions in the vicinity of the free surface in the case of a high kinematic viscosity liquid (ν = 5 mm^2/s), with *We* = 1.98. It has already been shown in Fig. 5.14 that the dimple was formed as *We* increased in the case of the low kinematic viscosity liquid (ν = 2 mm^2/s): however, the dimple was not observed in Fig. 5.15 although *We* was larger than that in the case of Fig. 5.13 (*We* = 1.56). The comparison of these results suggested that the liquid kinematic viscosity as well as the *We* number played an important role in dimple formation. The effects of the inertia force of the liquid were smaller in the case shown in Fig. 5.15 with *Re* = 80 than in the case shown in Fig. 5.13 with *Re* = 161. In the case of low kinematic viscosity liquids, it is remarkable that the large pressure reverse-gradient in the rising direction underneath the bubble, as shown in Fig. 5.13, was not observed when the bubble bounced off the free surface. This was the one of the main factors that prevented bubble bouncing.

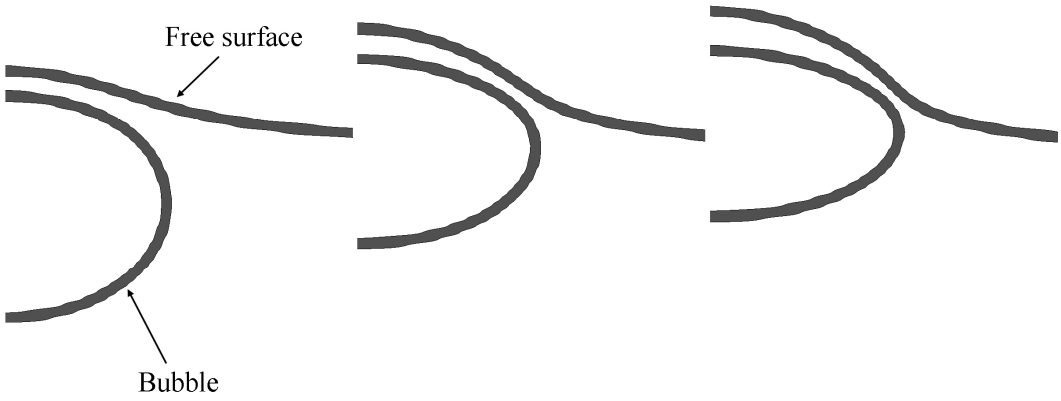

(1) *We* = 0.98 (2) *We* = 1.56 (3) *We* = 1.85

(a) Liquid film shape

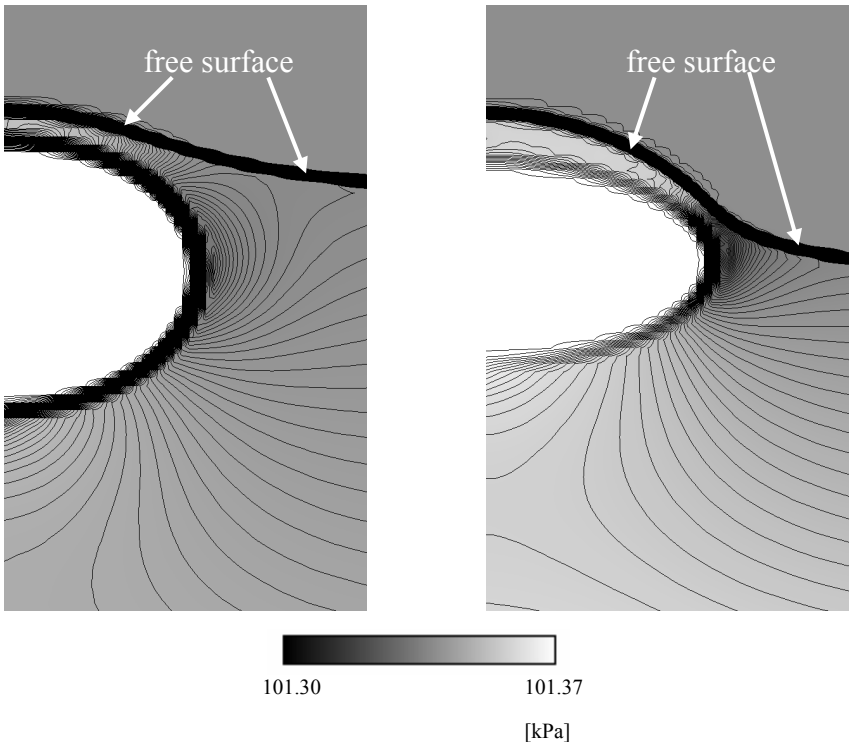

(1) *We* = 0.98 (2) *We* = 1.85

(b) Pressure distribution

Figure 5.14 Effect of Weber number on liquid film formation

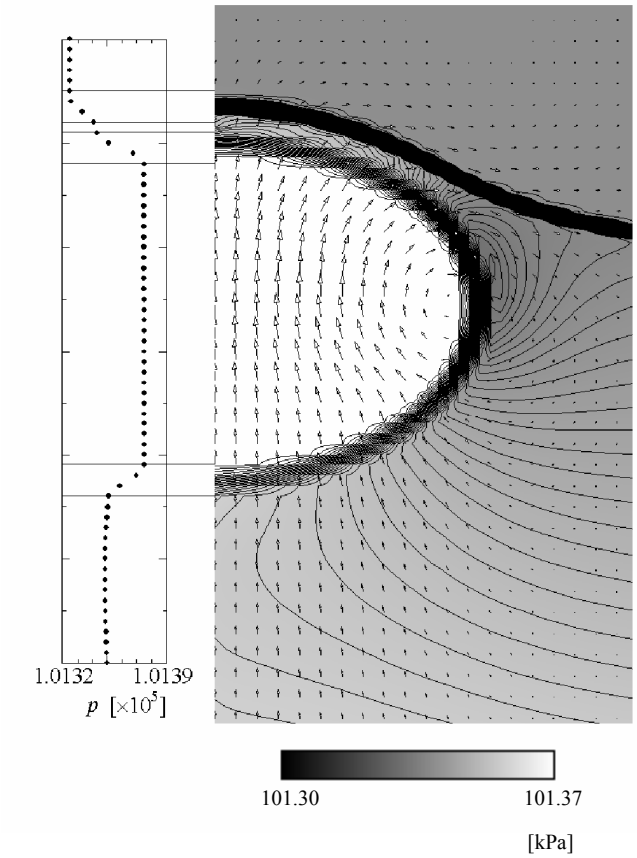

Figure 5.15 Velocity and pressure distribution of a high viscosity liquid ($\nu = 5$ mm^2/s, $We = 1.98$)

5.5 A pair of bubbles rising side by side

It was shown that as pair of bubbles either coalesced or bounced, depending on the *Re*, even with the same bubble generation distance l_i, in the section 4. It should be emphasized that the approaching velocity is one of the most important factors on bubble coalescence and bouncing (Kirkpatrick *et al*., 1974). Duineveld (1994) clarified the bubble coalescence and bouncing conditions by classifying *We* number of which the approaching velocity v was taken as the characteristic velocity, by using the superpurified water. The transient distances between bubbles are shown in Fig. 5.16 until they bounced or coalesced after generation. Figure 5.16 shows the distances between bubbles Δx as the function of time from the generation of a pair of bubbles to contact of them, where Δx was defined as the horizontal distance between the centers of a pair of bubbles and the diameters of bubbles were d = 1.2 ~ 1.6 mm with l_i = 3.1 mm. It should be noted that Δx at t = 0 corresponded to the initial distance between bubbles immediately after generation. The last point of the each segment represents the bubble contact. The bubbles with larger d moved to the horizontal repulsive directions after generation, which resulted in the larger initial distance between bubbles than l_i. Figures 5.16 (a) ~ (d) show the cases of K0.65, K1, K1.5 and K2, respectively. The clear distinctions between the cases of coalescence and bouncing were observed. A pair of bubbles always coalesced when the approach velocity was low, i.e., the low gradient of the segments as shown in Fig. 5.16 by filled circles. On the contrary, a pair of bubbles always bounced when the approach velocity was high. A quantitative comparison is to be performed in the future.

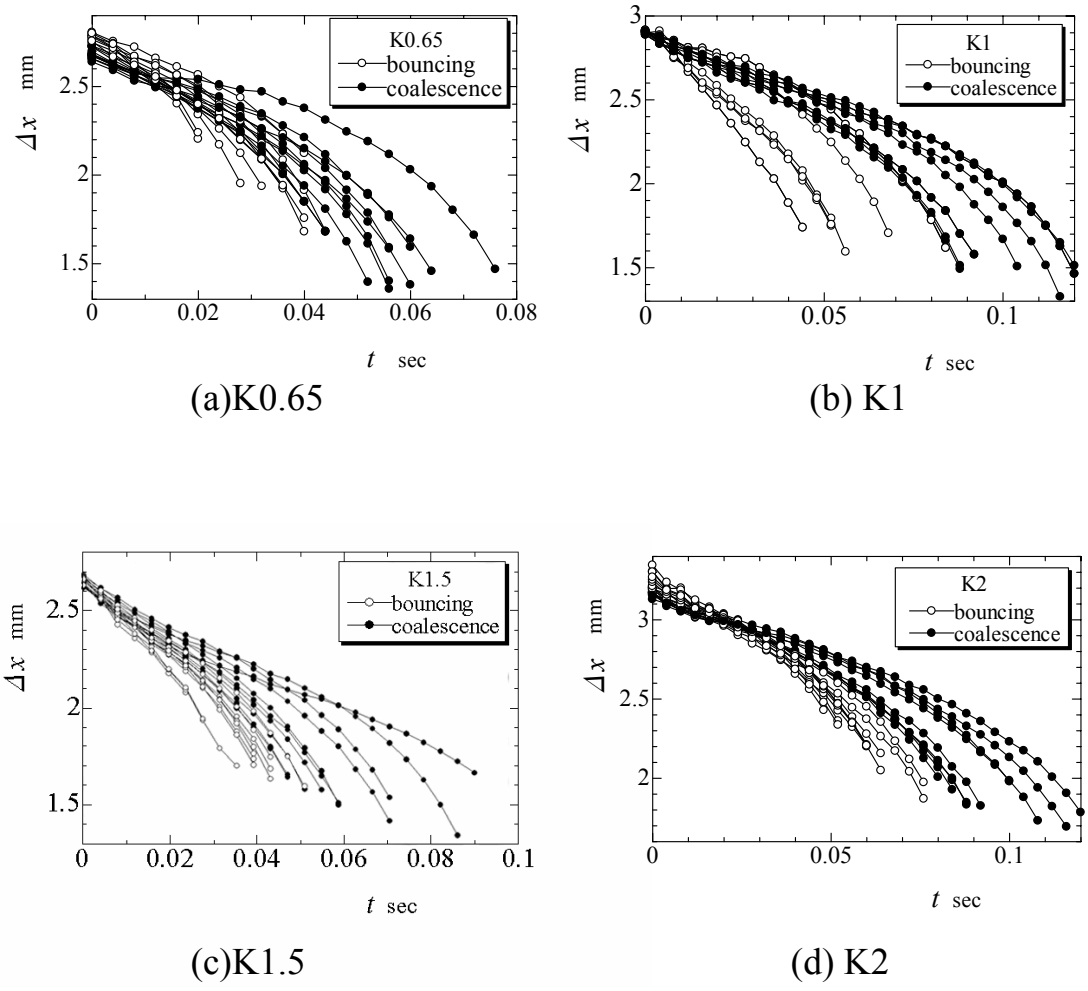

(a)K0.65 (b) K1

(c)K1.5 (d) K2

Figure 5.16 Relative distance of bubbles rising side by side versus time

5.6 Conclusion

The effects of liquid kinematic viscosity on coalescence were studied both experimentally and numerically. From the experimental study, the coalescence time, which was defined as the time from contact to coalescence, of a bubble with a free surface was successfully plotted as the single function of *We*. The coalescence time increased with the increase in *We* in a low kinematic viscosity liquid with $Mo = O(10^{-8})$ or less. It was understood that the coalescence time strongly depends on bubble bouncing.

When a rising bubble coalesced with a free surface in the range of $Mo = O(10^{-10})$~$O(10^{-9})$ and $Re > 40$, the critical *We* of bouncing were recognized as a constant, as predicted by Chesters *et al*. (1982),. However, critical *We* were dependent on the liquid kinematic viscosity in the $Mo = O(10^{-8})$ or more. For $Mo = O(10^{-7})$, the bubbles did not coalesce irrespective of *We* in the range of the experimental conditions of this study. It should be added that foam was formed on the free surface in the silicone oil pool with high viscosity liquids although silicone oil is non-polar and hence hardly susceptible to surfactants.

When the bubble bounced off the free surface, a pressure reverse-gradient was generated in the liquid just underneath the bubble by numerical analysis. The velocity field developed in the direction opposite to that in which the bubble travels. This flow field development promoted bubble bouncing at the free surface. The order of the pressure of the liquid film between the bubble and the free surface is equal.

The characteristic liquid film shape that is called the dimple was formed with increasing *We*. However, by investigating the distribution of the internal pressure of the liquid film, it was clarified that both the liquid film and the liquid flow field underneath the bubble significantly affected on bubble bouncing in the range of conditions of this study.

Chapter VI BEHAVIOR OF A BUBBLE CHAIN AND SURROUNDING LIQUID FLOW STRUCTURE

In this chapter, the bubble-bubble hydrodynamic interaction effects on bubbles rising in a chain are discussed. A chain of bubbles is considered to be one of the simplest fundamental elements in the meso-scale physical process where interactions between bubbles exist in bubbly flow. It is also considered the integration of multiple chains of bubbles results in the formation of bubbly flow. The motion of bubbles rising in a chain, in which bubbles are consecutively generated with accurate control of both the bubble diameter and the bubble generation frequenc is investigated. The relation between the bubble motions and the liquid flow structures in the vicinity of bubbles is also discussed.

6.1 Introduction

Dispersion of gas bubbles in a liquid phase is of special interest especially from the chemical engineering point of view, because of its importance in mass transfer operation, such as industrial fermentation, treatment of sewage by bio-oxidation, and so on. Zieminski & Raymond (1968) conducted a series of absorption tests with carbon dioxide bubbles in water under analogous operating conditions, and obtained the maximum mass transfer coefficient with bubbles in the diameter range from 2.8 to 3.3 mm, with corresponding Reynolds numbers in the range from 600 to 750. Therefore the modeling of behavior of bubbles of this range of Reynolds number in aqueous solutions is of most industrial importance, especially in homogeneous bubbly flow type standard bubble column. However, motion of a bubble with the existence of other bubbles in the near vicinity significantly differs from the one of an isolated bubble mainly because of the hydrodynamic interactions between bubbles.

There are several experimental studies focusing on bubble interaction. Katz & Meneveau (1996) studied the behavior of multiple bubbles in the diameter range from 0.05 to 1.0 mm, with corresponding Reynolds numbers in the rage from 0.2 to 35, rising in a line in tap water, and found that bubbles collided and repeatedly coalesced. Stewart (1995) studied how bubbles interacted with each other in swarms of freely rising bubbles in low-viscosity aqueous sugar solutions, with the maximum bubble equivalent diameter ranged from 6.5mm to 12.8 mm, with

Eotvos numbers and Reynolds numbers from 6 to 28 and from 100 to 400, respectively. His observation found some fundamental patterns that had been seen neither in dense continuous swarms nor with only a single bubble or a pair of bubbles. Brucker (1998) used Scanning-Particle-Image-Velocimetry to record the three-dimensional wake structure and bubble locations simultaneously in a bubbly two-phase flow by releasing bubbles with a mean diameter of 8.0 mm in counter water stream with Reynolds number of 250. His results demonstrated the important role of the wake-capture process in bubble interaction. It should be noticed that all above mentioned experiments were conducted in the range from low to intermediate Reynolds number. On the other hand, Marks (1973) measured the effect of frequency of formation on the velocity of air bubbles rising in a chain through distilled water, tap water, and sugar water with equivalent bubble diameter range from 1.4 mm to 18 mm, with Reynolds numbers from 400 to 8000. Although he found that the increase in the bubble generation frequency resulted in the increase in the rise velocity for a given bubble size, he provided information of neither the motion of bubbles, nor liquid flow field in the vicinity of bubbles. These information are essential for construction of bubbly flow model.

In this chapter, the motions of bubbles rising in a chain, in which bubbles are consecutively generated with accurate control of both the bubble diameter and the bubble generation frequency, are investigated. The experimental ranges of generation frequency and Reynolds number were from 1 Hz to 20 Hz and from 300 to 650, respectively. The relation between the bubble motions and the liquid flow structures in the vicinity of bubbles is also discussed.

6.2 Experimental apparatus and procedure

In this study, the motion of the bubbles in the diameter range from 1.0 mm to 2.5 mm released from a single nozzle in a distilled quiescent water pool (200 × 200 × 540 mm^3) was investigated. Duineveld (1995) experimentally studied the velocity and shape of rising bubbles, with an equivalent diameter from 0.66 to 2.00 mm in hyper clean water. He found that path instability occurred when the bubble diameter was equal to 1.82 mm. In other words, a bubble rose in a straight line even with Reynolds number of 660. On the other hand, Saffman (1956) found the onset of path instability to occur at diameter of 1.4 mm. Duineveld suggested that the difference of these results was due to impurities in the water used by Saffman (1956). Zhang & Finch (2001) addressed measurement of single bubble velocity in surfactant solutions and the physical model of surfactant concentration effects on the steady state velocity. Although the importance of the impurities on the motion of bubbles is widely acknowledged, commercially available distilled water was used in this study, partially because hyper pure water is not used in the real bubble columns, especially bio-reactors, but mainly because it is difficult to measure how impure the water is in bubble columns.

Both the motion of bubbles and the liquid-flow field were observed through a flat optical opaque acrylic wall of the water pool and recorded by a high-speed video camera and an analog single-lens-reflex camera. The pool was filled with commercially available distilled water, the level of which was kept at 300 mm above a nozzle tip.

The motion of rising bubbles was observed three dimensionally using the split mirror method with four mirrors (Fig. 6.1), developed by Murai *et al*. (1999). The motion of bubbles were captured using a single high-speed video camera with a shutter speed of 1/500s, 125 fps, and 512 × 480 pixels a frame. The frequencies of bubble production were measured by detecting the signal as bubbles transited through a line of light emitted by a photodiode.

The water flow field in the vicinity of the bubbles rising in a chain was visualized by dispersing orgasol particles, whose diameter and relative density were 50 ± 2 μm and 1.03, respectively, into water as tracers, and then slicing with a semi-conductor laser sheet, whose power, wavelength, and thickness were 30 mW, 650 nm, and 2.0 mm, respectively (Fig. 6.2). The particle image velocimetry (PIV) analysis with the cross correlation method (Raffel et al., 1998) was applied on the images taken by the high speed video camera, with 60 Hz in frame rate. The height of measurement view area was 50 mm above from the nozzle tip. The

velocity vector field was obtained by processing two consecutive images whose interval was 1/30 sec. Velocity vectors were calculated by averaging of fifty consecutive vector fields, which corresponded to averaging velocity data for 0.83 second. The spatial resolution of these images was 0.12 mm/pixel, using 480 x 420 pixels camera. This relatively low spatial resolution resulted from the requirement that measurement view area should be large enough for the simultaneous observation of both motion of both bubbles and liquid flow field in the vicinity of bubble chain. Consequently the magnitudes of error of velocities obtained by this PIV analysis were estimated as the order of 3.5 mm/s. The temporal resolution was optimized by using error analysis applied to PIV results.

In this study, the experiments were conducted with d ranging from 1.0 to 2.5 mm and f ranging from 1 to 20 Hz. It was assumed that the bubbles had rotational ellipsoidal shapes. The bubble diameter d was defined as the diameter of a sphere with the same volume as the equivalent rotational ellipsoid. Under these conditions, the bubble Reynolds numbers Re were between 300 and 650.

Although f was able to be controlled to be as large as 80 Hz, it was observed that bubbles formed multiple chains in the range of $d \geq 1$ mm when f exceeded 20 Hz. In this study, bubbles were generated with production frequency f ranging from 1 Hz to 20 Hz, since the motion of the bubbles in a single chain of bubbles were to be analyzed.

It was observed that the bubble rising velocities w in the vertical direction were hardly dependent on the bubble diameter and were approximately 300 mm/s (295 to 340 mm/s). Consequently, the distances of bubbles ls were approximately 300 mm, 150 mm, and 100 mm, for f of 1 Hz, 2 Hz, and 3 Hz, respectively. Roughly speaking, the trailing bubble was generated as the leading bubble reached the free surface, in the case when d and f were set as 1.0 mm and 1 Hz, respectively.

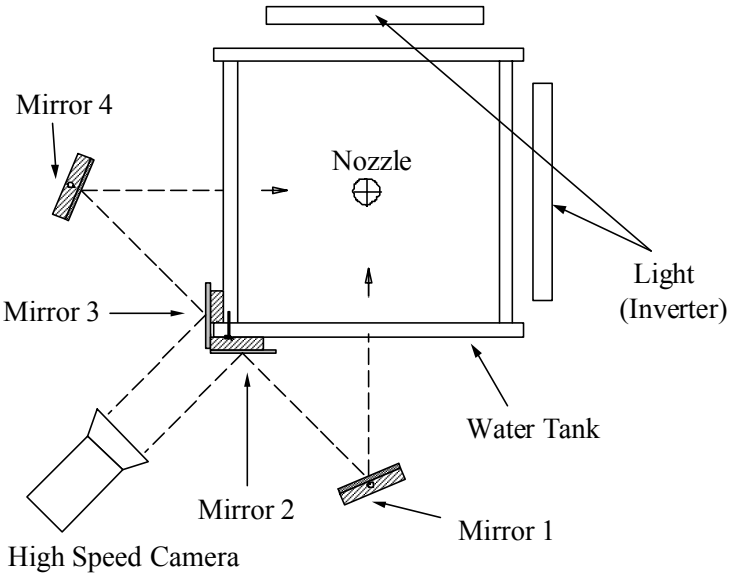

Figure 6.1 Schematic view of the split mirror method

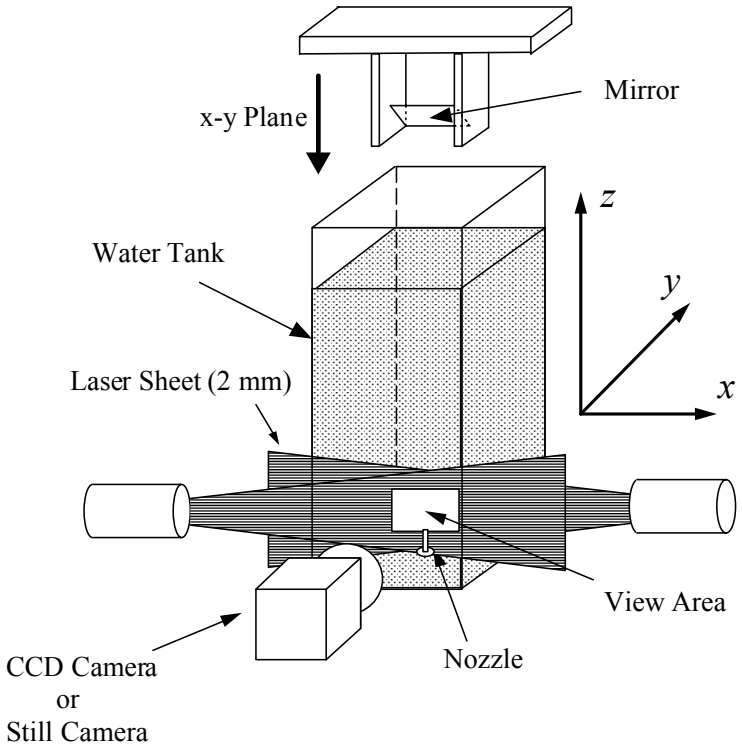

Figure 6.2 Flow visualization apparatus

6.3 Hydrodynamic interaction effects on bubbles rising in a chain

6.3.1 Evaluation of hydrodynamic interaction effects on bubbles

First, the motion of bubbles in a chain in the case of d between 1.0 mm and 2.5 mm are investigated. Bubbles in a chain with this range of diameters rose in either nearly straight or zigzag/helical trajectories in the present experimental conditions. Typical examples of trajectories of five bubbles consecutively produced in a chain are shown in Figs. 6.3 (a) and (b). These trajectories were projected on a horizontal plane, where Δx and Δy are the distances in the directions of x and y, respectively, from the vertical coordinate z-axis. The origin was set to be the nozzle tip. These figures correspond to the observation of the bubble motions from the top of the water pool. The trajectories of bubbles generated with f of 2 Hz and 5 Hz are shown in Figs. 6.3 (a) and (b), respectively.

It should be pointed out that the non-dimensional distances l/d were approximately 89 and 44 for the cases shown in Figs. 6.3 (a) and (b), respectively; hence, it is considered that hydrodynamic interaction effects on bubble motions in the latter are more prominent than those in the former. In the former case (f = 2 Hz), as shown in Fig. 6.3 (a), bubbles rose in indistinguishable trajectories. On the other hand, in the latter case (f = 5 Hz), the trajectories of bubbles were gradually scattered as they rose. It is strongly believed that the trailing bubbles followed the leading bubbles in the case of f = 2 Hz, not because the wake of the leading bubble captured the trailing bubbles but because the bubbles were generated with a high degree of accuracy and repeatability. Therefore, it is considered that the scattering in trajectories, as shown in Fig. 6.3 (b) (f = 5 Hz), can be attributed to the "strong" hydrodynamic interaction effects, namely to both the disturbances in the flow field induced by the leading bubbles and to the slight bubble shape modification due to the flow field modulation. On the contrary, it is considered that bubbles rose in indistinguishable trajectories, as shown in Fig. 6.3 (a) (f = 2 Hz), since the disturbances in the flow field induced by the leading bubbles was too weak to modulate both the flow field around the trailing bubble and the bubble shape and they simply followed the leading bubbles. In other words, the "weak" interaction effects on bubbles were insignificant in the motion of bubbles.

The hydrodynamic interaction effects on bubbles were evaluated as follows. It was regarded that the hydrodynamic interaction was "strong" when the trajectories of rising bubbles in a chain were significantly different from those of a single bubble, or when the scatters of the trajectories were prominent, and that the

hydrodynamic interaction was “weak” when the trajectories of rising bubbles in a chain were nearly identical to those of a single bubble, or when the bubbles rose following the trajectories of leading bubbles. In the present experimental conditions (1 Hz $\leq f \leq$ 20 Hz, 1.0 mm $\leq d \leq$ 2.5 mm), the bubbles always followed the leading bubbles up to a bifurcating point, the height of which depended on the frequency. When f was large enough, the bubbles ceased to follow the trajectories of the leading bubbles, as shown in Fig. 6.3 (b), due to the “strong” hydrodynamic interaction effects.

It should be added that the bubble trajectories just after the bubble production were also strongly affected by the frequency of bubbles production. Consequently, the horizontal components of bubble velocities became larger as the frequency increased. This change of the bubble trajectories was considered as the consequence of the strong interaction effects. This interaction effect is discussed in greater detail in the later section.

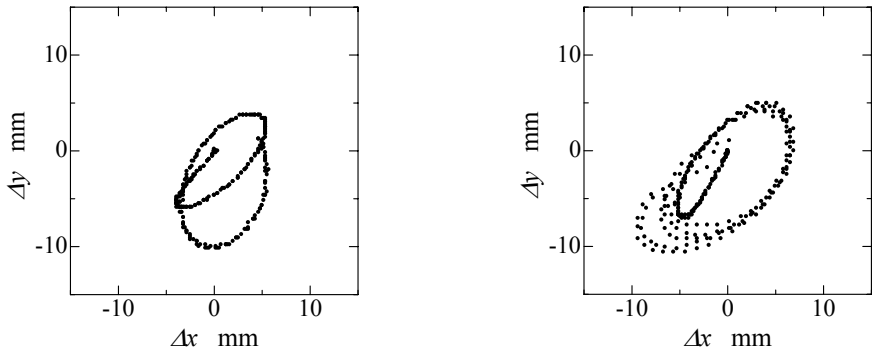

(a) f = 2 Hz, d = 1.8 mm (b) f = 5 Hz, d=1.5mm

Figure 6.3 Distinction of bubble interaction

6.3.2 Hydrodynamic interaction effects on bubble trajectory

As mentioned in the previous section, bubbles in a chain rose in either nearly straight or zigzag/helical trajectories in the present experimental conditions. The hydrodynamic interaction effects on bubbles in both the nearly straight chains as well as the zigzag/helical chains are discussed. In Figs. 6.4 (a) and (b), typical bubble trajectories in nearly straight chains, with d of 1.0 mm, are shown, and typical bubble trajectories in zigzag/helical chains, with d of 2.3 mm are shown in Figs. 6.5 (a) and (b). Figures 6.4 (a) and 6.5 (a) are the trajectories projected on z-Δr plane, where Δr is the deviation of the bubble location from the vertical axis z, and is defined as $\Delta r = \sqrt{\Delta x^2 + \Delta y^2}$, while Figs. 6.4 (b) and 6.5 (b) are those projected on Δy-Δx plane. These trajectories are the plots of the instantaneous locations of consecutively generated n bubbles, where n is specified in each figure. In order to investigate the effects of f, or the distances between bubbles, the results of four different f (1 Hz, 2 Hz, 3 Hz and 4 Hz) and five f (1 Hz, 3 Hz, 4 Hz, 10 Hz and 20 Hz) are plotted in Figs. 6.4 and 6.5, respectively.

As shown in Fig. 6.4, the bubbles generated with f of 1 Hz rose in nearly identical straight trajectories, while the scattering of the trajectories became prominent as f increased to be greater than 1.5 Hz. It should also be emphasized that the inclination of segments of bubble trajectories, from immediately near the nozzle tip and up to as high as approximately 50 mm from the nozzle tip, toward the Δr direction became substantial with the increase in the value of f. This modulation of the bubble trajectories was also the consequence of the strong interaction effects. It should be added that although bubbles initially deviated from the $\Delta r = 0$ line after they rose for a certain distance, their trajectories became nearly straight lines. It is considered from these results that the interaction between bubbles produced a strong effect on bubble behavior as f increased beyond 1.5 Hz.

With d of 2.3 mm, bubbles rose in a helical chain as shown in Fig. 6.5. The differences among the trajectories of each rising bubbles were negligible, with f of either 1 Hz or 3 Hz. In other words, the bubbles rose in nearly identical trajectories and followed the leading bubbles. However, the scatterings of trajectories became gradually remarkable as f increased over 4 Hz. Bubbles, generated with a frequency of 4 Hz or higher, rose in nearly identical trajectories up to a certain height, depending on f, after the production. They, then, stopped following the preceding bubbles; hence, the trajectories scattered, as similarly

observed in Fig. 6.4. It should be mentioned that when Δy was less than -15 shown in Figure 6.5 (b) - (5), the trajectories were out of the range of the measurement volume, where no data was acquired.

The comparison of results shown in Figs. 6.4 and 6.5 helps in understanding that the bubbles in either straight or helical chain follow leading bubbles in the cases of larger distances between bubbles; however, the trajectories of bubbles scattered in the cases of smaller distances between bubbles. In other words, the scatterings of bubble trajectories in a chain were caused by the "strong" interaction effects on bubbles. It should be noted that in the cases with smaller d, such as d of 1.0 mm, these "strong" interaction effects were observed with a smaller f.

The motion of bubbles in a chain with d of 0.5 mm was also investigatred. Bubbles rose in an identical straight line in the present experimental conditions (1 Hz $\leq f \leq$ 20 Hz); hence, the hydrodynamic interaction effects based on the scatterings of the trajectories were not evaluated. Therefore, it is required to focus on each single bubble in a chain and to analyze their motions as described by Katz & Menevau (1996).

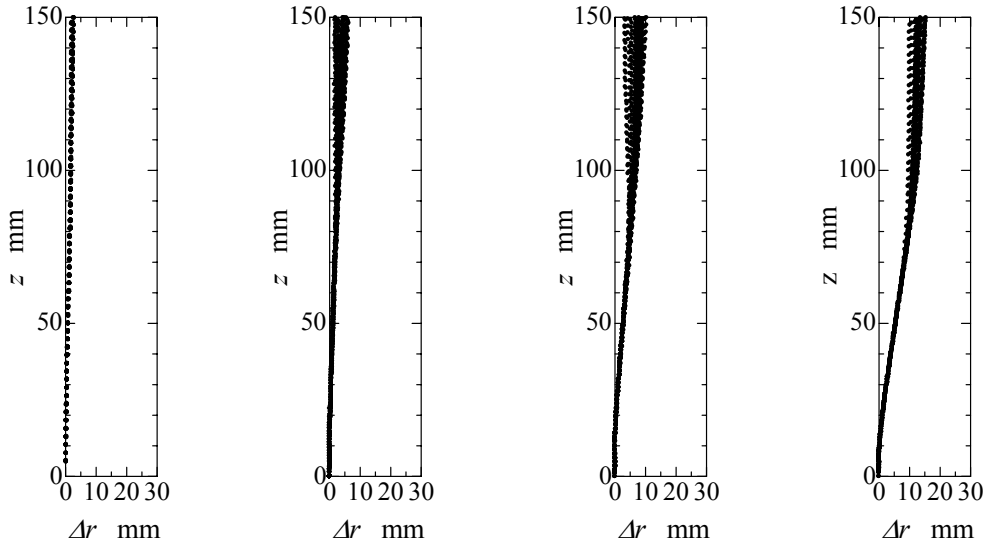

(1) f = 1 Hz (n = 16) (2) f = 1.5 Hz (n = 25) (3) f = 2Hz (n = 33) (4) f = 3Hz (n = 50)

(a) z-Δr

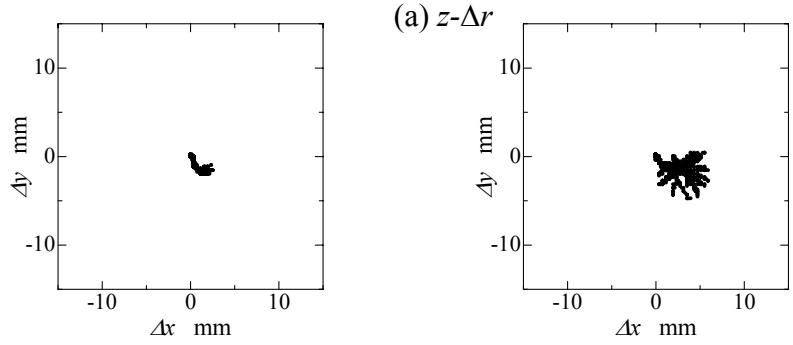

(1) f = 1 Hz (l/d = 300) (2) f = 1.5 Hz (l/d = 200)

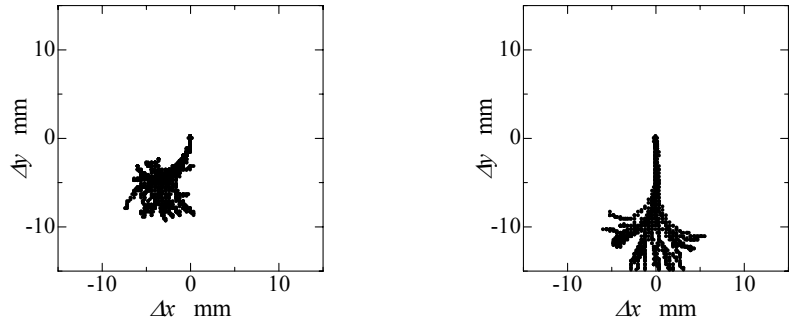

(3) f = 2 Hz (l/d = 150) (4) f = 3 Hz (l/d = 100)

(b) Δx-Δy

Figure 6.4 Bubble trajectory (d = 1.0 mm, Re = 300)

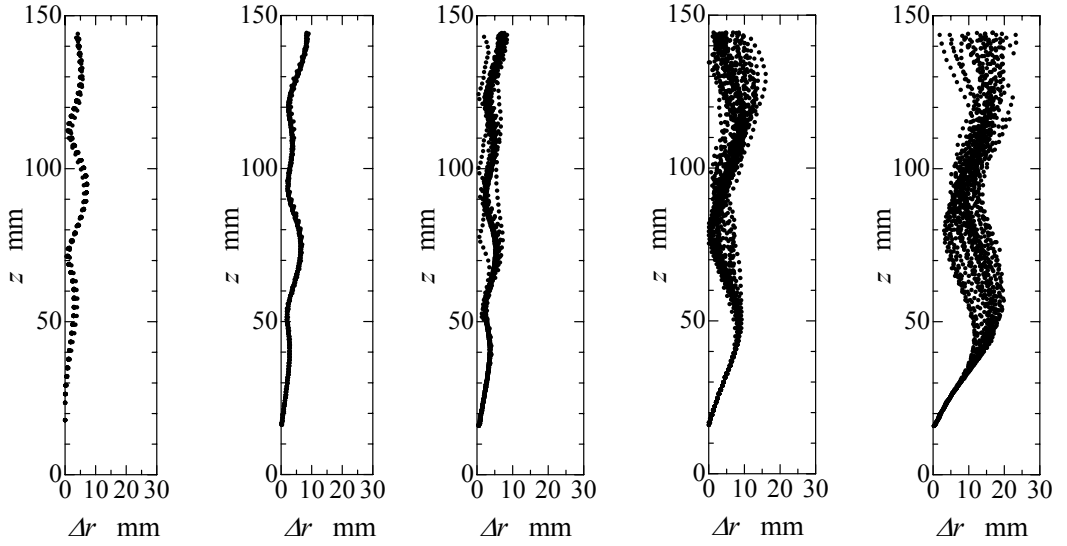

(1) f = 1 Hz (n = 16) (2) f = 3 Hz (n = 25) (3) f = 4 Hz (n = 50) (4) f = 10 Hz (n = 50) (5) f = 20 Hz (n = 50)

(a) z-Δr

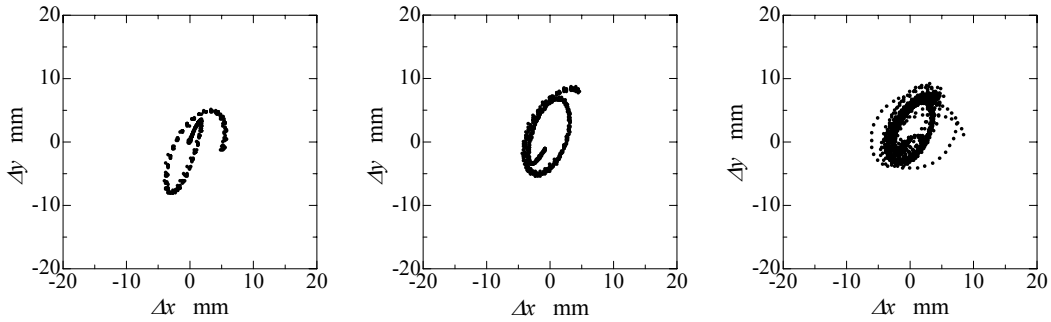

(1) f = 1 Hz (l/d = 134) (2) f = 3 Hz (l/d = 45) (3) f = 4 Hz (l/d = 34)

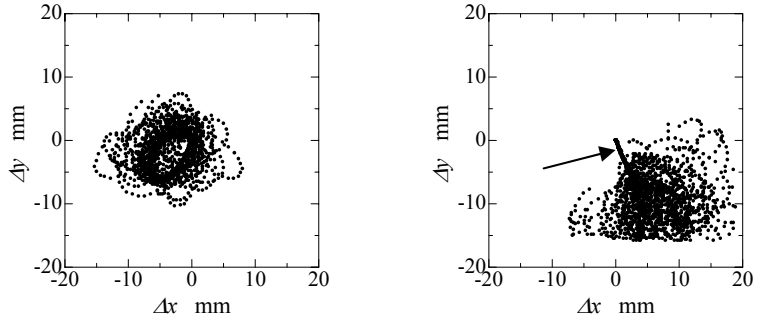

(4) f=10Hz (l/d=13) (5) f=20Hz (l/d=7)

(b) Δx-Δy

Figure 6.5 Bubble trajectory (d = 2.3mm, Re = 630)

6.3.3 Scatterings of bubble trajectories

In the previous section, it was concluded that the scatterings of bubble trajectories were caused by "strong" hydrodynamic interaction effects. In this section, these effects are discussed more quantitatively. The degree of the scatterings of bubble trajectories were evaluated by using the variance of Δr, σ^2, as defined in Equation 6.1:

$$\sigma^2 = \frac{1}{n}\sum_{i=1}^{n}\left(\Delta r_i - \overline{\Delta r}\right)^2 \qquad (6.1)$$

where n is the number of observed bubbles, $\overline{\Delta r}$ is the averaged value of Δr. Figure 6.6 (a) shows σ^2 of bubble rising trajectories in nearly straight chains, calculated using data in Fig. 6.4. Figure 6.6 (b) shows those in helical chains using data in Fig. 6.5. The large value of σ^2 indicates the significant deviation of trajectories of the consecutively produced bubbles at the given height z.

In the cases with d of 1.0 mm, as shown in Fig. 6.6 (a), the results obtained with f of 1 Hz and 1.25 Hz were clearly distinguishable from those with f greater than 1.5 Hz. As was discussed in the previous section, it is also clarified from Fig. 6.6 (a) that "strong" interaction effects on bubbles became prominent with f greater than 1.5 Hz in the cases with d of 1.0 mm, as shown in Fig. 6.4.

As already was mentioned in the previous section, in the cases with d of 2.3 mm, as shown in Fig. 6.6 (b), it was recognized that bubbles rose in nearly identical trajectories until a value of z of less than 40 mm after the production, since σ^2 were nearly zero for the height z less than 40 mm. These results are easily confirmed in Fig. 6.5 (a) as the bubble trajectories were plotted as a single line from the origin to a height of approximately 40 mm. When z was less than 40 mm, Δr increased as f increased, as shown in Fig. 6.5 (a). In other words, the bubble chain inclined more and moved further away from z-axis, with the increase in f.

Figure 6.7 shows the map, plotted with Re and l/d as axes, of "strong" and "weak" hydrodynamic interaction effects on bubbles in a chain. It was recognized that the interaction was "weak" when the bubbles followed the nearly identical trajectories and "strong" otherwise. The bubbles rose in nearly straight trajectories, similar to those of Fig. 6.4, with Re less than 400, and they rose in helical trajectories with Re between 400 and 750. It should be emphasized that, as Re decreased, strong interaction effects were observed with larger distances between bubbles.

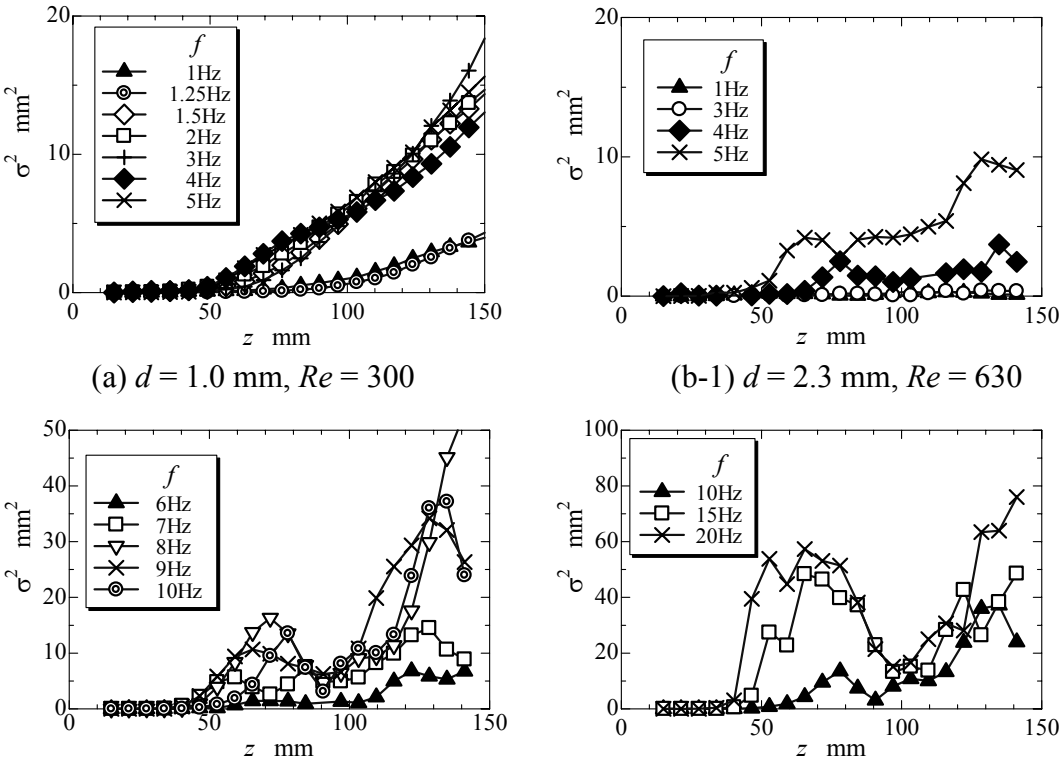

(a) d = 1.0 mm, Re = 300

(b-1) d = 2.3 mm, Re = 630

(b-2) d = 2.3 mm, Re = 630

(b-3) d = 2.3mm, Re = 630

Figure 6.6 Variance of Δr

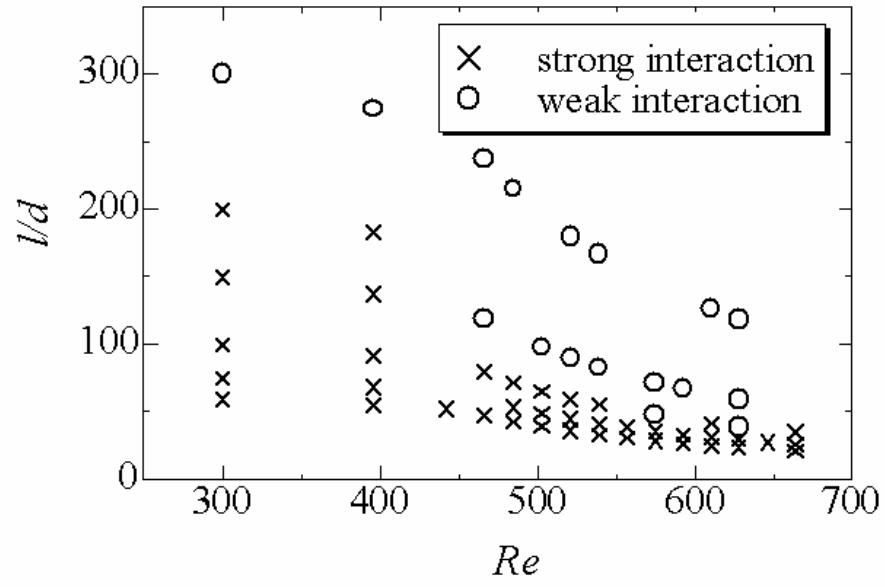

Figure 6.7 Classification of bubble-bubble interaction
(d = 1.0~2.5 mm, f = 1~5 Hz)

6.3.4 Flow field induced by bubble chain

In this section, the water flow field induced by bubble chains is examined. The water flow field, dispersed with orgasol particles, in the vicinity of bubbles rising in a chain was visualized using a laser sheet. The images of a water flow field induced by bubble chains with d of 2.3 mm, taken by using an analog single-lens-reflex camera with long shutter speeds from 2 to 8 s, are shown in Fig. 6.8. Figures 6.8 (a) and (b) are the results obtained with f of 1 Hz and 10 Hz, respectively.

In Fig. 6.8 (a), the bubbles rose in nearly identical straight trajectories as Δr of the segments of bubble trajectories, from the nozzle tip and up to as high as 40 mm from the nozzle tip, was approximately zero, as shown in Fig. 6.5 (a) (1). During the period of photography, the motions of 8 bubbles were captured in Fig. 6.8 (a). The water flow field was induced toward the bubbles, and then suddenly accelerated and turned sharply upward as it approached the bubble chain within approximately 15 mm, and it rose along the line of bubbles. It should be noted that the rise velocities of the water field in the vicinity of the bubbles were significantly smaller than those of the bubbles and its maximum possible value was 10 mm/s.

On the other hand, in Fig. 6.8 (b), two white curved lines represent both edges of bubbles rising in a chain. Under these experimental conditions and observation range, the trajectories of each bubble were nearly identical. Twenty bubbles passed in the frame during the period of photography in Fig. 6.8 (b). The bubbles rose straight in the vertical direction for approximately 10 mm after the release from nozzle and then inclined toward the left direction. As can be easily recognized in these pictures, the flow fields in the vicinity of the bubble chain have developed into very characteristic structures. At any height, as shown in Fig. 6.8 (b), the water in the vicinity of bubble chain flowed toward the bubble chain from its left side and then abruptly accelerated in the close vicinity of bubble trajectories. As a consequence, water flow fields were deflected in the right-upward direction. The water flow field induced in the right side of the vicinity of the bubble chain had a parallel and straight flow. The magnitude of the relatively fast liquid velocity in the right side of bubble chain was of the order of 30 mm/s, calculated from the length of flow path line. This flow field was completely different from those shown in Fig. 6.8 (a). This flow field is referred to as “liquid jet.”

It is considered that the "liquid jet" is induced due to the "strong" hydrodynamic interaction effects, since with the increase in *f*, the structure of flow field more developed. In the previous section, the bubble motions in helical chains, as shown in Fig. 6.5, were discussed. Their trajectories were similar to those shown in Fig. 6.8 (b). As the frequency of bubble production increased, the bubbles rose with greater inclination and in nearly identical trajectories up to approximately 40 mm and then their trajectories scattered. This liquid jet was observed in the vicinity of the bubble chain where the trajectories of the bubbles were nearly identical. It is considered that liquid jet was generated due to the balance of water flow field momentum and bubble lift. However, the detailed study of this liquid jet could be undertaken in the future.

It should be added that "liquid jet" was observed in the vicinity of bubble chains even without the use of bubble production control. Figure 6.9 shows the results in the case of bubble release with natural detachment, i.e. without control of bubble production. Figure 6.9 shows the results obtained with *d* of 1.5 mm and *f* of 13.1 Hz. It was confirmed that the liquid jet is not characteristic of the bubble production controller, but it is generally induced regardless of the choice of the methods of bubble generation as shown in Fig. 6.9.

In Fig. 6.10, it is shown that the visualization of liquid flow field on the horizontal plane 30 mm above the nozzle, under the same experimental conditions as Fig. 6.9, with shutter opening *s* of 8 s. The position of the horizontal plane was indicated by a white horizontal line in Fig. 6.10. It was confirmed, with the aid of the images taken by CCD video camera, that bubbles rose in the direction of arrow shown in Figure 6.10, and that a bubble chain crossed this plane at the root of the arrow, which corresponds to the point A shown in small picture of Fig. 6.10. The region of the existence of this characteristic liquid flow field was approximately a rectangle, whose length of the long side was specified as a line A-B (point B indicated in Fig. 6.10 corresponded to B in small picture of Fig. 6.10) shown in Fig.6.9, with superficially high density of tracers. This area corresponded to the horizontal cross sectional area of the liquid jet. It was found that the width of the liquid jet was considerably thin. Tracers in this area moved in the opposite direction of the arrow, i.e., bubble rising direction. It was also observed that the liquid in the vicinity of this liquid jet approached quite slowly toward the liquid jet, i.e. the oval area in Fig. 6.10, then joined the liquid jet to rise upward. It should be mentioned that path lines of tracers in Fig. 6.10 appeared points partially because of the small horizontal components of velocities of liquid, and also because of thin laser light sheet thickness

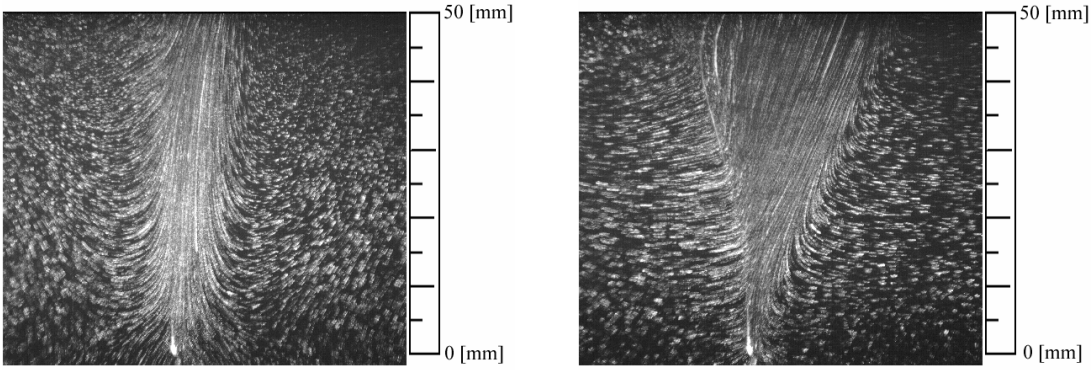

(a) d = 2.3 mm, f = 1 Hz, s = 8 s (b) d = 2.3 mm, f = 10 Hz, s=2 s

Figure 6.8 Visualization image of flow field (z-x)

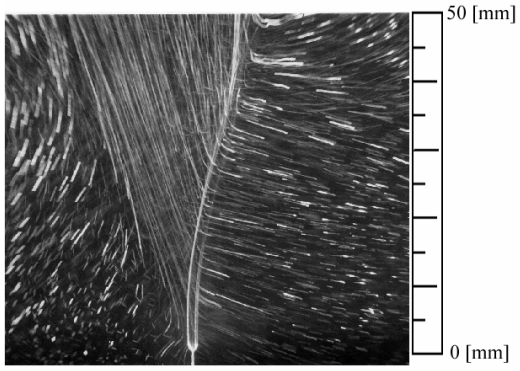

Figure 6.9 Visualization image of flow field of without control (z-x)
(d = 1.5 mm, f = 13.1 Hz, s = 4 s)

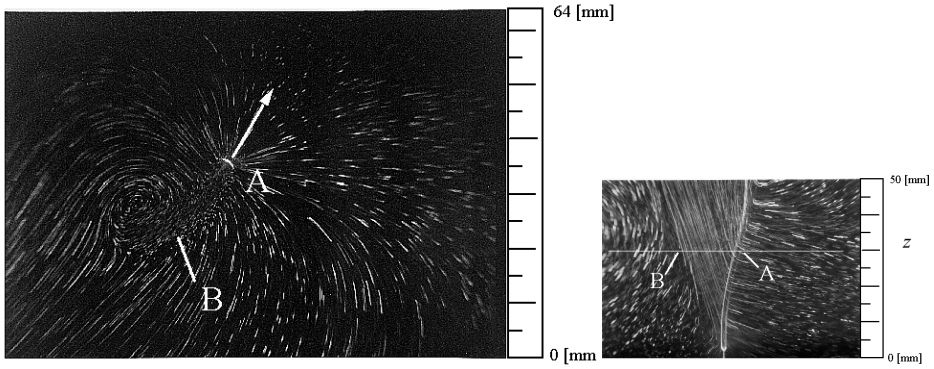

Figure 6.10 Visualization image of flow field of without control (x-y)
(d = 1.5 mm, f = 13.1 Hz, s = 8 s)

6.4 Behavior of a single coherent gas bubble chain and surrounding liquid jet flow structure

The most striking nature of the controlled bubble chains is that they possess the coherent structure. It was observed that bubbles rose in approximately identical trajectories up to z of less than 40 mm after departure from the nozzle with the specified frequency and bubble diameter. These results were verified by the results that σ^2 s were nearly zero for the height z of less than 40 mm, especially with higher f, as shown in Fig. 6.6, and also confirmed by the results that bubble trajectories were plotted as a single line from the origin, for example, as indicated by an arrow shown in Fig. 6.5 (b) (5).

These lower segments of controlled bubble chains, where bubbles rose in approximately identical trajectories with specified bubble diameter and generation frequency, were defined as the coherent bubble chains. The coherent bubble chains were observed in the region of z less than 40 mm in the present experimental conditions. In the coherent bubble chain, the distance of bubble trajectories from the z-axis, Δr, increased with the increase in f, as shown in Fig. 6.5 (a). This result implies that bubble chain inclined. In other words, bubbles were conveyed further from the z-axis, with the increase in f. This observation result suggested that the additional force in horizontal direction acted on the bubbles in the coherent bubble chain compared to the one on a single bubble. In the next section, The liquid flow field generated by a coherent bubble chain is discussed and this force is also discussed from the view of the momentum balance.

6.4.1 Bubble chain development process

The initial development process of coherent bubble chain is studied, by producing only four bubbles consecutively in the quiescent water, where no pre-produced bubbles, with the production frequency of f=5Hz. The bubble, which was produced just after the production controller activated, was referred to as the first bubble, and the second, the third, and fourth, in the order of the production. The whole water was quite quiescent before the first bubble was produced. Trajectories of these four bubbles are shown in Fig. 6.11, in the Δr- z coordinates, where n is the bubble order. For comparison, trajectories of bubbles in coherent bubble chain with different production frequencies in the vicinity of nozzle tip are also shown in Fig. 6.12.

It was observed in the controlled bubble chain development that the motion of

the first bubble (N=1) was significantly different from those of trailing bubbles, in the case of f=5 Hz as shown in Fig. 6.11. The first bubble rose in the nearly straight line up until about 40 mm above from the nozzle tip. The trajectory of this bubble was similar to the one observed in the case of f=1Hz, plotted in Fig. 6.12. On the contrary, the trajectories of the trailing bubbles inclined outwards from the vertical axis after bubbles reached about 20 mm height. Trajectories of the bubbles, except for the first bubble, as shown in Fig. 6.11 were approximately the same as those of the case of f=5Hz which is shown in Fig. 6.12, although the locations of the onset of inclination was shifted upward in the range of 10mm. It was confirmed that this motion of bubbles was quite reproducible. These results indicate that the additional force was exerted on bubbles in the coherent bubble chain other than the one on a single bubble, possibly due to the flow field formed by the leading bubble.

de Nervers & Wu (1971) reported that the effects of leading bubbles can be neglected in a bubble chain with l/d greater than about five in the case of d from10 to 20 mm. However results shown in Fig. 6.12 show that the leading bubbles had strong effects on the trajectories of trailing bubbles with l/d of greater than about twenty-five. These effects were also observed even in the case of l/d with 50 ~ 100 as observed in the case of f = 5 Hz. With the help of the theoretical results of Moore (1963), a spherical bubble is estimated to be accompanied with vorticity of $O(Re^{-1/4})$ in the wake with width of $O(Re^{-1/4})$ and length of $O(Re^{1/2})$. This theory leads to, for example, that vorticity resides in the region of l/d with O(25), in the case of Re of 600. This result and the present experimental results clarified that the wake of the leading bubble had a significant role in determining the trajectories of trailing bubbles. It is considered that the wake of leading bubble caused the instabilities of trailing bubble trajectories, which resulted in the inclined trajectories of bubbles.

Both this modification of trajectories from the one of a single bubble due to the coherency of bubble chain and the liquid flow structure in the vicinity of the bubble chain are discussed in detail by visualizing the liquid flow using PIV in the following sections. It should be noted that it is not to be discussed why the bubble trajectory should be inclined. In other words the mechanisms of the inclined trajectory development of rising bubbles are beyond the scope of the present study. It should also be mentioned that the mechanisms of zigzag / helical behavior of even a single bubble are still actively discussed (Ellingsen & Risso 2001; Mougin & Magnaudet 2002; Tomiyama *et al*. 2002; Yang *et al*. 2003; Wu & Gharib 2002).

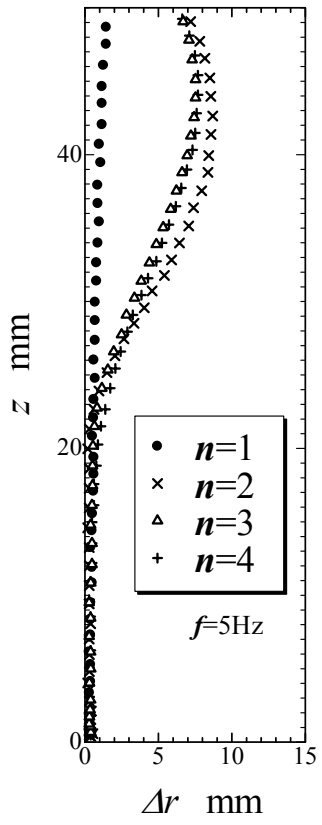

Figure 6.11 Bubble chain development in stagnant water (d=2.2mm)

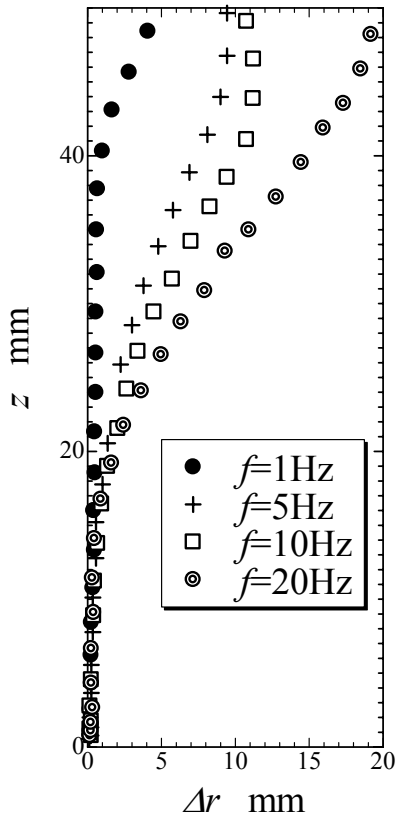

Figure 6.12 Comparison of bubble trajectories (d=2.2mm)

6.4.2 Liquid flow in the vicinity of a coherent bubble chain

The flow field in the vicinity of the coherent bubble chain was visualized by using laser light sheet with thickness of 2 mm. The experimental results with the bubble diameter d fixed as 2.2 mm are investigated in this section. Experiments were carried out with two cases of bubble generation frequencies, as 5Hz and 10 Hz. It was found that the order of velocity fluctuation was comparable with the one of the uncertainty of the present PIV analysis in the case of f less than 5 Hz, since the present PIV analysis contains the error of the order of 3.5 mm/s. The coherent bubble chains were not observed in the case of f larger than 20 Hz, due to the unsteady behavior of a bubble chain and consequently frequent escape of bubbles from the laser light sheet plane in the height of 30 mm or more.

Velocity vectors, obtained by PIV analysis, of liquid in the vicinity of a coherent bubble chain generated with the the production controller, are shown in Figs. 6.13 (a) and (b), with f of 5 and 10 Hz, respectively. The coherent bubble chains were observed in both cases. Liquid flow field was developed and steady, which were also confirmed by investigating images taken by high speed video camera. The solid lines in Figs. 6.13 (a) and (b) represent bubble trajectories obtained by superimposition of the traces of both edges of bubbles. The height, which was measured from the nozzle tip, of the measurement area was 50 mm as indicated by the scale shown at the right side in these figures. The time averaging duration was fixed as 0.83 sec, and eight and four bubbles passed through the measurement area during this time in the cases of f of both 10Hz and 5 Hz, respectively. The time series of the magnitude of liquid velocities v_j, taken at the points (1) and (2) indicated in Figs. 6.13 (a) and (b), are plotted in Figs. 6.14(a) and (b), respectively.

Figure 6.13(a) shows the result with f of 5 Hz. The “liquid jet” was observed. The time-averaged velocity at point (1), shown in Figure 6.13(a), was approximately 15 mm/s in the case of 5 Hz.

Figure 6.13(b) shows the result of higher bubble production frequency f of 10 Hz. The clear liquid jet formation due to the coherent bubble chain was observed than in the cases of 5 Hz. As the increase of bubble production frequency, it was observed that the averaged velocity increased to the order of 30 mm/s as shown in Fig. 6.14(b). They were considerably larger than those observed in the case of 5 Hz. Therefore it is considered that the liquid jet flow field in the vicinity of a coherent bubble chain was generated by the superposition of liquid flow field developed by the motion of each bubble. It should also be noted that a coherent

bubble chain rose more inclined in the case of higher generation frequency.

It also should be emphasized that liquid jet velocity field was recognized as steady rather than periodic, even in the case of low generation frequency as shown in Fig. 6.14 (a), although there were some fluctuations. It was considered that the fluctuations were rather random. Five bubbles, for example, passed through in one second in the case with f of 5 Hz. The effects of this intermittent motion of a single bubble on the liquid jet velocity fluctuations were hardly recognized.

It is assumed that the inverse of the characteristic time of dissipation of the liquid flow field due to a single bubble was much smaller than even low bubble production frequency; 5Hz: and hence the liquid jet seemed continuous in time even with low bubble production frequency f of 5 Hz due to the superposition of flow field developed by only a few bubbles. Here, the continuous liquid jet flow model is proposed that liquid jet in the vicinity of a coherent bubble chain is steady flow field within the accuracy of the present experimental conditions.

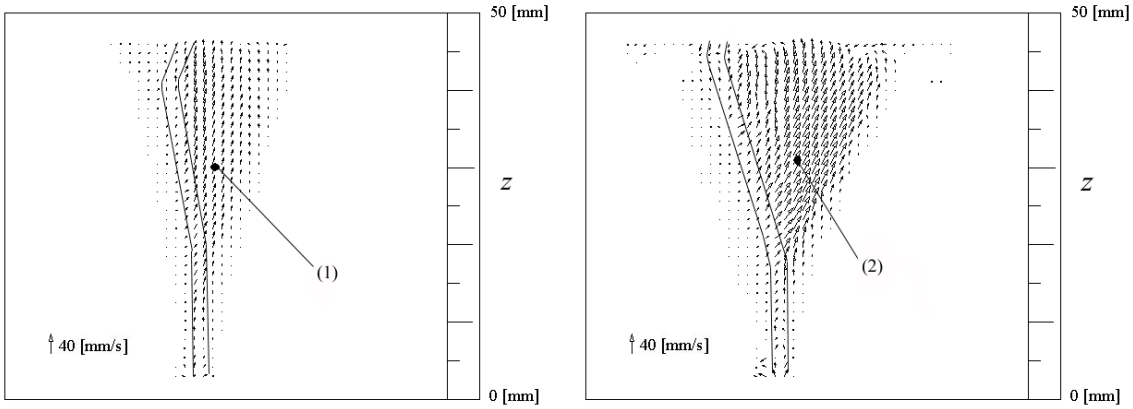

(a) f=5Hz (b) f=10Hz

Figure 6.13 Visualization of liquid flow field in the vicinity of a singe bubble chain by PIV (d=2.2mm)

(a) f=5Hz (b) f=10Hz

Figure 6.14 Time series of magnitude of velocity at specified location

6.4.3 Evaluation of force acting on bubbles in coherent bubble chain

In this section, the liquid jet, which was observed when bubbles rose in inclined trajectories as shown in the previous section, is discussed. The characteristic nature of the liquid jet is that the directions of characteristic velocity of the liquid jet deflect from that of a single bubble rising motion.

By examining the observation results that the liquid jet was clearly structured as bubbles rose in inclined trajectories, The following liquid flow model is introduced, as shown in Fig. 6.13, with the continuous liquid jet model as stated in section 6.4.2. The additional force acting on bubbles in bubble chain is referred to as bubble chain force, which drives bubbles into more inclined trajectories in a bubble chain. The liquid flow model is constructed based on the following assumptions.

1. Bubbles rise in a straight line, which is inclined from the vertical axis z by angle θ
2. The bubble chain force acting on bubbles, which rise in inclined trajectories, balances the component of the momentum flux of liquid jet in the vicinity of a bubble chain in the direction of this force
3. The bubble chain force acting on bubbles also balances the component of buoyancy force in the direction of this bubble chain force.

Both bubble chain force acting on bubble and liquid jet momentum flux are discussed in the followings.

The new ξ - ζ coordinate system is employed with ξ as the translational direction of bubble, and ζ as the normal to ξ. The control volume $\Delta\xi\,\Delta\zeta\Delta\eta$ is defined, where $\Delta\xi$ is small segment of bubble trajectory, $\Delta\zeta$ and $\Delta\eta$ are the width and the thickness of the volume, respectively. The order of magnitude of $\Delta\zeta$ is set to be the same as the bubble diameter. The momentum balance acting on this control volume in the ζ direction is discussed.

Bubbles pass through the control volume intermittently; however liquid jet velocity field is hardly affected by this intermittent motion of a single bubble and assumed to be continuous in time, as stated by the continuous liquid jet model. Therefore it is consider that the characteristic time, T, of the liquid jet behavior is much larger than the period of bubble generation, and also it is considered that the impulse balance which is obtained by integrating momentum equation in

sufficiently long time, T.

Momentum flux, $\dot{M}_{out}$, flowing out from control volume per unit time is exclusively advected by the liquid jet, which is shown in Figure 6.15. The component of $\dot{M}_{out}$ in the ζ direction is expressed by the following equation.

$$\dot{M}_{out} = \rho \cdot \Delta\xi \cdot \Delta\eta \cdot \left(V_j \sin\phi\right)^2 \tag{6.3}$$

where ρ is the liquid density, V_j is the magnitude of the averaged jet velocity. The ζ component of impulse, M_I, acting on liquid by a single bubble during time T is expressed as Eq. 6.4 by writing the bubble chain force acting on a single bubble as F_{BC},

$$M_I = \int_0^T F_{BC} \cdot P(t)\, dt = F_{BC} \frac{\Delta\xi \cos\theta}{l} T \tag{6.4}$$

where $P(t)$ is the function depending only on time, and defined as unity when bubble exists in the control volume, and zero otherwise. With the assumption that inflowing impulse into the control volume in the ζ direction per unit time is negligible compared to $\dot{M}_{out}$, as already discussed in Figs. 6.10 and 6.13, the following equation is derived by considering the conservation law of momentum during time T,

$$\boldsymbol{M_I = \int_0^T \dot{M}_{out}\, dt} \tag{6.5}$$

Therefore, the bubble chain force F_{BC} is obtained by Eqs. 6.3, 6.4, and 6.5 with the assumption of $\Delta\eta = \mathrm{O}(d)$.

$$F_{BC} = \rho \cdot d \cdot \frac{l}{\cos\theta} \cdot \left(V_j \sin\phi\right)^2 \tag{6.6}$$

On the other hand, $F_{BC\,exp}$, which is the ζ component of the bubble chain force acting on a bubble, balances the ζ direction component of F_{BC} which is the buoyancy force, since a bubble rises in the inclined straight line from the vertical axis by θ. The following equation is obtained with the aid of Fig. 6.15.

$$F_{BC\exp} = F_{BC} \sin\theta \tag{6.7}$$

The comparison of the results obtained by Eqs. 6.6 and 6.7 are shown in Table 1, where the magnitude of the averaged velocity of liquid obtained by PIV analysis and the bubble diameter were substituted in V_j and $\Delta\eta$, respectively. The order of magnitude of bubble chain force obtained by the analysis agrees well with the one obtained by the experiment. This result leads to the hypothesis that liquid jet is the liquid flow field activated by the bubble chain force as a bubble chain rising in the inclined straight line from the vertical axis.

It should be added that there are no report so far on the liquid jet with regard to the study of bubble behavior, although subjects of bubble rising behavior in inclined trajectory has been actively studied from the view point of both lift force acting on bubble and in the past decades. Lift force acting on a single bubble, especially in the vicinity of solid wall (Takemura *et al*. 2002), or in the shear stress field (Fujiwara *et al*. 2004; Kariyasaki 1987), has been studied. On the subject of rising bubble, extensive studies have been reported in the literatures, such that bubbles rise in zigzag / helical trajectories, even without vortex shedding in the wake (Lunde & Perkins, 1997; de Vries et al. 2002), and that the development of zigzag / helical motions are closely related to the bubble shapes (Ellingsen & Risso 2001; Mougin & Magnaudet 2002). However, there are neither studies nor even suggestions of the existence of the liquid jet as in this study. Therefore it is possible for significant difference between a single bubble and a bubble chain, to exist in mechanism of rising in inclined trajectories. In order to clarify this difference, further detailed study of liquid jet in much smaller length scale will be required, and is our future subject of study.

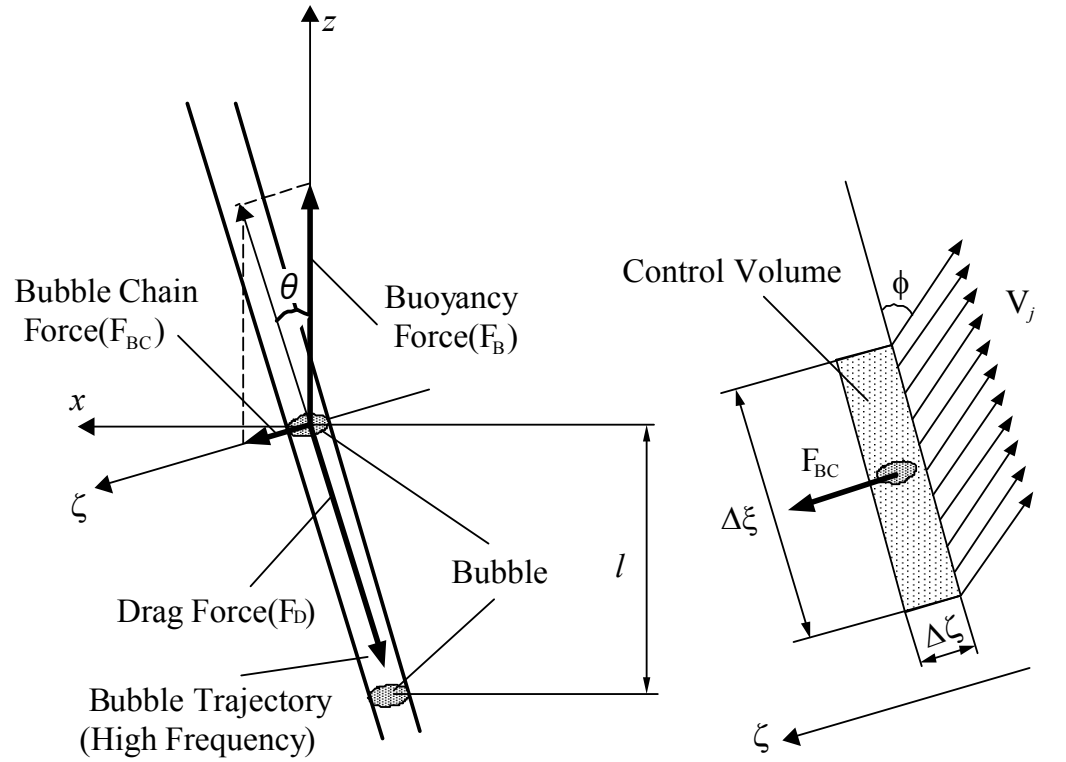

(a) Force balance (b) Control volume

Figure 6.15 Forces acting on a bubble in a single bubble chain

Table 1 Comparison of force acting on bubble chain

f Hz	θ°	ϕ°	V_j m/s	l m	ρ kg/m^3	$F_{BC\,exp}$ N	F_{BC} N
5Hz	9	25	0.15	0.0605	998	1.11×10^{-5}	5.40×10^{-6}
10Hz	20	41	0.30	0.0285	998	2.42×10^{-5}	2.58×10^{-5}

6.5 Conclusions

The motions of bubbles rising in a chain were experimentally studied in the case of *Re* from 25 to 650. Bubbles were generated by controlling both bubble production frequency and bubble diameter independently and accurately. In the cases of low frequencies (large bubble distances), it was observed that the trajectories of the bubbles were nearly identical. It is considered that the bubbles followed the leading bubbles simply because of the high degree of accuracy and repeatability of bubble production and that the hydrodynamic interaction effects were "weak" in these cases. On the contrary, with the increase in bubble production frequency, the trajectories of bubbles scattered after the bubbles rose at a certain point, depending on the frequency. It is considered that the bubbles ceased to follow the leading bubbles due to the disturbances induced by leading bubbles, and that the hydrodynamic interaction effects were "strong" in these cases. Furthermore, in cases of much higher frequency, the bubbles rose in nearly identical inclined trajectories immediately after production to a certain point. The variance of the trajectories was approximately zero. Then, the trajectories of the bubbles scattered.

The existence of a characteristic flow field structure was confirmed. This flow field, "liquid jet," was observed in the vicinity of the nearly identical inclined trajectories of bubbles when the hydrodynamic interaction effects were "strong."

Chapter VII CONCLUSION

The construction of bubbly flow model with a high degree of accuracy is strongly demanded by industries. However, the modeling of bubbly flow is difficult due to the multi-scale structure. For the bridge of the macro-scale and the micro-scale, the meso-scale physical processes of bubbly flow were experimentally and numerically investigated in this study. Especially the effect of interaction on the bubble motion and consequently induced coalescence were carefully studied. The knowledge obtained through this research summarized as followed.

The experiments with various spatial configurations of bubbles were enabled by implementing a bubble production controller which was developed by Kariyasaki *et al*. (1999). In chapter 3, the mechanism of bubble production control was investigated. When bubbles were produced from an orifice, the bubble detached itself from the orifice due to the effects of displacement of the bubble center, as pointed out by Sirota *et al*. (2004). On the other hand, when bubbles were produced from a nozzle, two types of bubble release processes were observed. In the first type of release, the bubble was produced as it was cut during the growth. In the second type of release, the bubble was produced with Fritz volume due to the slow growing rate of the bubble. In the study to investigate the motion of a pair of bubble, the latter type of bubble production was used due to the much less bubble shape oscillation at the production.

In chapter 4, the motions of bubbles rising in line and rising side by side were investigated experimentally. In the case of bubbles rising in line, a numerical analysis was also conducted. Bubble diameter and liquid kinematic viscosity were taken as the parameters. Reynolds number *Re* significantly affected the motion of a pair of bubbles rising in line, as well as rising side by side. When a pair of bubbles rose in line, the trailing bubble was attracted by the wake of the leading bubble, and then it collided with the leading bubble, in the case of low *Re*. On the other hand, in the case of intermediate *Re,* a pair of bubbles kept a mutual equilibrium distance. As *Re* further increased, the trailing bubble deformed and then escaped from the vertical line. When a pair of bubbles rose side by side, they separated from each other as they rose in the case of low *Re*. On the contrary, in the case of high *Re,* they attracted each other and then collided when the initial bubble horizontal distance was smaller than a critical value. At the moment of the

collision of a pair of bubbles, no significant deceleration of the bubble rising velocity was observed, unlike the motion of bubble rising with wall bouncing.

In chapter 5, the coalescence of a pair of bubbles was investigated experimentally and numerically. The two types of coalescence of bubbles were observed, i.e., those between a rising bubble and a free surface, and between a pair of bubbles rising side by side. Especially the effect of liquid viscosity was investigated. From experimental results, when a bubble coalesced with a free surface, Weber number was the most important parameter since it ruled the coalescence time in low viscosity liquids. In contrast, the coalescence time in a high viscosity liquid was much greater than that of a low viscosity liquid with the same Weber number. In addition, the thresholding Weber number between bubble coalescence and bouncing was affected by liquid viscosity. Due to the increase in the coalescence time in liquid with higher viscosity, foam was observed to form on the free surface even in the non-polar liquid. By examining the pressure distribution of both the liquid film between the bubble and the free surface and the downward liquid flow, it was concluded that not only the liquid film but also the liquid flow field underneath the bubble played an important role in bubble coalescence or bouncing from numerical study. In the case of coalescence of bubbles rising side by side, it was clarified that the approach velocity was important factor on coalescence of a pair of bubbles. However, a quantitative comparison is to be done in the future.

In chapter 6, as the extension of chapter 4, the motion of bubbles rising in a chain was studied. In the cases of low bubble production frequencies (large bubble distances), it was observed that the trajectories of the bubbles were nearly identical. It is considered that the bubbles followed the leading bubbles simply because of the high degree of accuracy and repeatability of bubble production and that the hydrodynamic interaction effects were “weak” in these cases. On the contrary, with the increase in the bubble production frequencies, the trajectories of bubbles scattered after the bubbles rose at a certain point, depending on the frequency. It is considered that the bubbles ceased to follow the leading bubbles due to the disturbances induced by leading bubbles, and that the hydrodynamic interaction effects were “strong” in these cases. Furthermore, with further increase in the bubble production frequencies, bubbles rose in nearly identical inclined trajectories immediately after the production until a certain point. The variances of the trajectories were approximately zero, Thereafter the trajectories of the bubbles began to scatter. It was confirmed that a characteristic flow field structure of the surrounding water, “liquid jet” was observed in the vicinity of the nearly identical inclined trajectories of bubbles when the hydrodynamic interaction effects were

"strong."

Finally, a pair of theories derived in the course of this study is proposed.

The first theory is on the bubble motion and the path instability. The motions of bubbles under the influence of other bubbles are much more unstable than the motion of single bubble. The path instability of bubbles are investigated with respect to the critical condition expressed by either *Re*, *We*, *Ga*, χ or combination of these. Whichever the expression of the critical condition are chosen, the critical values of the path instability of interacting bubble are smaller than those of single bubble because of the wake instability due to the disturbance of the wake of other bubbles.

The second theory is on the role of wake on coalescence. It is not only the liquid film between bubbles but also the bubble wake that rules whether bubble coalesces or bounces. In short, bubble wake is essential in bubble coalescence/bounding because the most of the momentum transported with bubble exists in the wake of bubble.

Although large amount of new findings and knowledge obtained in the course of this study contribute the society, it is considered that the meso-scale physical processes in bubbly flow, such as bubble-bubble interaction, and coalescence of bubbles are, unfortunately, not yet fully understood to satisfy both academic curiosity and industrial requirement. It is greatly aspired that this study shall be the cornerstone of the prosperity of studies in bubble-bubble interactions and coalescence of bubbles.

REFERENCES

Allan, R. S., Charles, G. E., Mason, S. G., (1961)
"**The approach of gas bubble to a gas/liquid interface**"
J. Colloid Sci., **16**, 150-165.

Auton, T. R., (1987)
"**The lift force on a spherical body in a rotational flow**"
J. Fluid Mech., **183**, 199-218.

Batchelor, G. K., (1972)
"**Sedimentation in a dilute dispersion of spheres**"
J. Fluid Mech., **52**, 245-268.

Batchelor, G. K., Green, J. T., (1972)
"**The determination of the bulk stress in a suspension of spherical particles to order c^2**"
J. Fluid Mech., **56**, 401-427.

Bhaga, D., Weber, M. E., (1981)
"**Bubbles in viscous liquids; shape, wakes and velocities**"
J. Fluid Mech., **105**, 61-85.

Biesheuvel, A., van Wijngaarden, L., (1982)
"**The motion of pairs of gas bubbles in a perfect liquid**"
J. Engng. Maths, **16**, 349-365.

Bowonder, B., Kumar, R., (1970)
"**Studies in bubble formation IV: bubble formation at porous discs**"
Chem. Eng. Sci., **25**, 25-32.

Brackbill, J. U., Kothe, D. B., Zemach, C., (1992)
"**A continuum method for modeling surface tension**"
J. Comput. Phys., **100**, 335-354.

Brady, J. F., Bossis, G., (1988)
"**Stokesian dynamics**"
Annu. Rev. Fluid Mech., **20**, 111-157.

Brucker, C., (1999)
"**Structure and dynamics of the wake of bubbles and relevance for bubble interaction**"
Phys. Fluids, **11**-7, 1781-1796.

Buner, B., Tryggvason, G., (1999)
"**Direct numerical simulations of three-dimensional bubbly flows**"
Phys. Fluids, **11**-8, 1967-1969.

Buner, B., Tryggvason, G., (2002)
"**Dynamics of homogeneous bubbly flows: Part 1 rise velocity and microstructure of the bubbles**"
J. Fluid Mech., **466**, 17-52.

Buner, B., Tryggvason, G., (2002)
"**Dynamics of homogeneous bubbly flows: Part 2 velocity fluctuations**"
J. Fluid Mech., **466**, 53-84.

Buner, B., Tryggvason, G., (2003)
"**Effect of bubble deformation on the properties of bubbly flows**"
J. Fluid Mech., **495**, 77-118.

Chang, Y. C., Hou, T. Y., Merriman, B., Osher, S., (1996)
"**A level set formulation of eulerian interface capturing methods for incompressible fluid flows**"
J. Comput. Phys., **124**, 449-464.

Chen, J. L. S., (1974)
"**Growth of the boundary layer on a spherical gas bubble**"
J. Appl. Mech., **41**, 873-878.

Chesters, A. K., (1975)
"**The applicability of dynamic-similarity criteria to isothermal, liquid-gas, two-phase flows without mass transfer**"
Int. J. Multiphase Flow, **2**, 191-212.

Chesters, A. K., (1991)
"**The modeling of coalescence processes in fluid-liquid dispersions**"
Trans IChemE, **69** A, 259-270.

Chesters, A. K., Hofman, G., (1982)
"**Bubble coalescence in pure liquid**"
Appl. Sci. Res., **38**, 353-361.

Chi, B. K., Leal, L. G., (1989)
"**A theoretical study of the motion of a viscous drop toward a fluid interface at low Reynolds number**"
J. Fluid Mech., **201**, 123-146.

Clift, R, Grace, J. R., Weber, M. E., (1978)
"**Bubbles, Drops and Particles**"
Academic Press

Cuenot, B., Magnaudet, J., Spennato, B., (1997)
"**The effects of slightly soluble surfactants on the flow around a spherical bubble**"
J. Fluid Mech., **339**, 25-53.

Das, R. K., Pattanayak, S., (1994)
"**Bubble to slug flow transition in vertical upward two-phase flow through narrow tube**"
Chem. Eng. Sci., **49-**13, 2163-2172.

de Nevers, N., Wu, J. L., (1971)
"**Bubble coalescence in viscous fluids**"
AIChE J., **17**-1, 182-186.

de Vries, A. W. K., Biesheuvel A., van Wijngaarden, L., (2002)
"**Note on the path and wake of a gas bubble rising in pure water**"
Int. J. Multiphase Flow, **28**, 1823-1835.

de Vries, J., Luther, S., Lohse, D., (2002)
"**Induced bubble shape oscillations and their impact on the rise velocity**"
Eur. Phys. J. B, **29**, 503-509.

Doubliez, L., (1991)
"**The drainage and rupture of a non-foaming liquid film formed upon bubble impact with a free surface**"
Int. J. Multiphase Flow, **17**-6, 783-803.

Drogaris, G., Weiland, P., (1983)
"**Coalescence behavior of gas bubbles in aqueous solutions of *n*-alcohols and fatty acids**"
Chem. Eng. Sci., **38**-9, 1501-1506.

Duineveld, P. C., (1994)
"**Bouncing and coalescence of two bubbles in water**"
Ph. D. thesis, University of Twente.

Duineveld, P. C., (1995)
"**The rise velocity and shape of bubbles in pure water at high Reynolds number**"
J. Fluid Mech., **292**, 325-332.

Duineveld, P. C., (1996)
"**The influence of an applied sound field on bubble coalescence**"
J. Acoust. Soc. Am., **99**-1, 622-624

Ellingsen, K., Risso, F., (2001)
"**On the rise of an ellipsoidal bubble in water**"
J. Fluid Mech., **440**, 235-268.

Esmaeeli, A., Tryggvason, G., (1996)
"**An inverse energy cascade in two-dimensional, low Reynolds number bubbly flows**"
J. Fluid Mech., **314**, 315-330.

Esmaeeli, A., Tryggvason, G., (1998)
"**Direct numerical simulation of bubby flows: Part 1 Low Reynolds number arrays**"
J. Fluid Mech., **377**, 313-345.

Esmaeeli, A., Tryggvason, G., (1999)
"**Direct numerical simulation of bubby flows: Part 2 Moderate Reynolds number arrays**"

J. Fluid Mech., **385**, 325-358.

Fan, L. S., Tsuchiya, K., (1999)
"**Bubble wake dynamics in liquid and liquid-solid suspensions**"
Butterworth-Heinemann
Fdhila, R. B., Duineveld, P. C., (1996)
"**The effect of surfactant on the rise of a spherical bubble at high Reynolds numbers**"
Phys. Fluids, **8**-2, 310-321.

Fujiwara, A., Takagi, S., Watanabe, K., Matsumoto, Y., (2003)
"**Experimental study on the new micro-bubble generator and its application to water purification system**"
Proc. 4th ASME/JSME Joint Fluids Eng. Conf., FEDSM2003-45162, Hawaii, USA.

Fujiwara, A., Danmoto, Y., Hishida, K., Maeda, M., (2004)
"**Bubble deformation and flow structure measured by double shadow image and PIV/LIF**"
Exp. Fluids, **36**, 157-165.

Furukawa, T., Fukano, T., (2001)
"**Effects of liquid viscosity on flow patterns in vertical upward gas-liquid two-phase flow**"
Int. J. Multiphase Flow, **27**, 1109-1126.

Haberman, W. L., Morton, R. K., (1954)
"**An experimental study of bubbles moving in liquids**"
Trans. ASCE, **387**, 227-252

Harper, J. F., (1997)
"**Bubbles rising in line: why is the first approximation so bad?**"
J. Fluid Mech., **351**, 289-300.

Hartunian, R. A., Sears, W. R., (1957)
"**On the instability of small gas bubbles moving uniformly in various liquid**"
J. Fluid Mech., **3**, 27-47.

Hewitt, G. F., (2002)
"**Multiphase Flow: surprise, surprise, surprise!**"
Proc. 21st Multiphase flow symposium, Nagoya, Japan.

Himeno, T., Watanabe, T., (1999)
"**Numerical analysis of two-phase flow under microgravity condition**"
J. Jpn. Soc. Mech. Eng., **B 65-635**, 2333-2340. (Japanese)

Ichiki, K., (2002)
"**Improvement of the stokesian dynamics method for systems with a finite number of particles**"
J. Fluid Mech., **452**, 231-262.

Johnson, T. A., Patel, V. C., (1999)
"**Flow past a sphere up to a Reynolds number of 300**"

J. Fluid Mech., **378**, 19-70.

Kamp, A. M., Chesters, A. K., Colin, C., Fabre, J., (2001)
"**Bubble coalescence in turbulent flows**"
Int. J. Multiphase Flow, **27**, 1363-1396.
Kariyasaki, A., (1987)
"**Behavior of single gas bubble in a liquid flow with a liner velocity profile**"
Proc. of the 1987 ASME/JSME Thermal Eng. Conf., 261-267.

Kariyasaki, A., Ousaka, A., Kagawa, M., (1999)
"**Effect of pressure oscillation on the bubble generation from a nozzle**"
Proc. of the 3rd ASME/JSME Joint Fluids Eng. Conf., FEDSM99-7846, San Francisco, USA.

Kariyasaki, A., Ousaka, A., (2001)
"**Control of bubble size and detaching frequency from a submerged nozzle by means of pressure oscillation induced in the gas flow**"
Proc. of 5th Int. Conf. on GAS-LIQUID and GAS-LIQUID-SOLID Reactor Eng., Melbourne, Australia.

Kariyasaki, A., Ousaka, A., (2002)
"**Control of bubble formation (effect of additional oscillation to gas velocity on bubble formation)**"
J. Jpn. Soc. Mech. Eng., **B 68-674**, 2712-2718. (Japanese)

Katz, J., Meneveau, C., (1996)
"**Wake-induced relative motion of bubbles rising in line**"
Int. J. Multiphase Flow, **22**, 239-258.

Khurana, A. K., Kumar, R., (1969)
"**Studies in bubble formation III**"
Chem. Eng. Sci., **24**, 1711-1723.

Kirkpatrick, R. D., Lockett, M., J., (1974)
"**The influence of approach velocity on bubble coalescence**"
Chem. Eng. Sci., **29**, 2363-2373.

Kodama, Y., Kakugawa, A., Takahashi, T., Kawashima H., (2000)
"**Experimental study on microbubbles and their applicability to ships for skin friction reduction**"
Int. J. Heat Fluid Flow, **21**, 582-588.

Kok, J. B. W., (1989)
"**Dynamics of gas bubbles moving through liquid**"
Ph.D. thesis, University of Twente

Kok, J. B. W., (1993)
"**Dynamics of a pair of bubbles moving through liquid: Part 1 theory**"
Eur. J. Mech., B/Fluids, **12**, 515-540.

Kok, J. B. W., (1993)
"**Dynamics of a pair of bubbles moving through liquid: Part 2 experiment**"

Eur. J. Mech., B/Fluids, **12**, 541-560.

Kumar, R., Kuloor, N. R., (1970)
"**The formation of bubbles and drops**"
Adv. Chem Engng., **8**, 256-368.

Legendre, D., Magnaudet, J., (1997)
"**A note on the lift force on a spherical bubble or drop in a low-Reynolds-number shear flow**"
Phys. Fluids, **9**-11, 3572-3574.

Legendre, D., Magnaudet, J., (1998)
"**The lift force on a spherical bubble in a viscous linear shear flow**"
J. Fluid Mech., **368**, 81-126.

Legendre, D., Magnaudet, J., Mougin, G., (2003)
"**Hydrodynamic interactions between two spherical bubbles rising side by side in a viscous liquid**"
J. Fluid Mech., **497**, 133-166.

Lessard, R. R., Zieminski, S. A., (1971)
"**Bubble coalescence and gas transfer in aqueous electrolytic solutions**"
Ind. Eng. Chem. Fundam, **10**-2, 260-269

Levich, V. G., (1962)
"**Physicochemical hydrodynamics**"
Prentice-Hall.

Lohse, D., Prosperetti, A., (2003)
"**Controlling bubbles**"
J. Phys. Condens. Matter, **15**, s415-s420

Loose, D., (2003)
"**Bubble puzzles**"
Physics Today, **56**-2, 36-41.

Lunde, K., Perkins, R. J., (1995)
"**A method for the detailed study of bubble motion and deformation**"
Advances in Multiphase flow 1995 (Serizawa, A., Fukano, T., and Bataille J. editors), Elsevier, 395-405.

Lunde, K., Perkins, R. J., (1997)
"**Observations on wakes behind spheroidal bubbles and particles**"
Proc. of 1997 ASME Fluids Eng. Div. Summer Meeting, FEDSM97-3530, CD-ROM.

Magnaudet, J., (2004)
"**Migrating, zigzagging, spiraling: fascinating bubbles**"
Proc. of 5th Int. Conf. on Multiphase Flow, Yokohama, Japan.

Magnaudet, J., Eames, I., (2000)
"**The motion of high-Reynolds-number bubbles in inhomogeneous flows**"

Annu. Rev. Fluid. Mech., **32**, 659-708.

Marks, C. H., (1973)
"**Measurements of the terminal velocity of bubbles rising in a chain**"
J. Fluids Eng., **2**, 17-22.

Marrucci, G., (1969)
"**A theory of coalescence**"
Chem. Eng. Sci., **24**, 975-985.

Marrucci, G., Nicodemo, L., (1967)
"Coalescence of gas bubbles in aqueous solutions of inorganic electrolytes"
Chem. Eng. Sci., **22**, 1257-1265.

Matsumoto, Y., Allen, J. S., Yoshizawa, S., Ikeda, T., Kaneko, Y., (2005)
"**Medical ultrasound with microbubbles**"
Exp. Therm. Fluid Sci., **29**, 255-265.

Maxworthy, T., Gnann, C., Kurten, M., Durst, F., (1996)
"**Experiments on the rise of air bubbles in clean viscous liquids**"
J. Fluid Mech., **321**, 421-441.

Mclaughlin, J. B., (1996)
"**Numerical Simulation of bubble motion in water**"
J. Colloid Interface Sci., **184**, 614-625.

Mei, R., Klausner, J. F., (1992)
"**Unsteady force on a spherical bubble at finite Reynolds number with small fluctuations in the free-stream velocity**"
Phys. Fliuds, **4**-1, 63-70.

Mei, R., Klausner, J. F., Christopher J. L., (1994)
"**A note on the history force on a spherical bubble at finite Reynolds number**"
Phys. Fliuds, **6**-1, 418-420.

Miyagi, O., (1925)
"**The motion of an air bubble rising in water**"
Technol. Rep. Tohoku Imperial University, **5**, 135-172.

Moore, D. W., (1963)
"**The boundary layer on a spherical gas bubble**"
J. Fluid Mech., **16**, 161-176.

Moore, D. W., (1965)
"**The velocity of rise of distorted gas bubble in a liquid of small viscosity**"
J. Fluid Mech., **23**, 749-766.

Mougin, G., Magnaudet, J., (2002)

"**Path instability of a rising bubble**"
Phys. Rev. Let., **88**-1, 041502.

Mougin, G., Magnaudet, J., (2002)
"**The generalized Kirchhoff equations and their application to the interaction between a rigid body and an arbitrary time-dependent viscous flow**"
Int. J. Multiphase Flow, **28**, 1837-1851.

Murai, Y., Watanabe, S., Yamamoto, F., Matsumoto, Y., (1997)
"**Three-dimensional measurement of bubble motion in bubble plume using stereo image processing**"
Proc. of Int. Workshop on PIV'97-Fukui, 13-18.

Oguz, H. N., Prosperetti, A., (1993)
"**Dynamics of bubble growth and detachment from a needle**"
J. Fluid Mech., **257**, 111-145.

Ohl, C. D., (2001)
"**Generator for single bubbles of controllable size**"
Rev. Sci. Instrum., **72-1**, 252-254.

Ohl, C. D., Tijink, A., Prosperetti, A., (2003)
"**The added mass of an expanding bubble**"
J. Fluid Mech., **482**, 271-290.

Onari, H., (2001)
"**Fisheries experiments of cultivated shells using micro-bubbles techniques**"
J. Heat Transfer Soc. Japan, **40**-160, 2-7. (Japanese)

Osher, S., Fedkiw, R. P., (2001)
"**Level set methods: an overview and some recent results**"
J. Comput. Phys., **169**, 463-502.

Osher, S., Fedkiw, R., (2003)
"**Level set methods and dynamic implicit surfaces**"
Springer, NewYork.

Osher, S., Paragios, N. editors, (2003)
"**Geometric level set methods**"
Springer, NewYork.

Osher, S., Sethian, J., (1988)
"**Fronts propagating with curvature-dependent speed; algorithms based on hamilton-jacobi formulations**"
J. Comput. Phys., **79**, 12-49.

Otsu, H., (1980)
"**An automatic threshold selection method based on discriminant and least squares criteria**"
Trans. Electro. Commun. Eng. Jpn D, J63, 349-356. (Japanese)

Pinczewski, W. V., (1981)
"**The formation and growth of bubbles at a submerged orifice**"
Chem. Eng. Sci., **36**, 405-411.

Prewitt, J. M. S., (1970)
"**Object enhancement and extraction**"
Picture Processing and Psychopictorics (edited by Lipkin, B. S. and Rosenfeld, A.), Academic Press, 75-149.

Prince, M. J., Blanch, H. W., (1990)
"**Bubble coalescence and break-up in air-sparged bubble columns**"
AIChE J., **36**-10, 1485-1499

Prosperetti, A., (2004)
"**Bubbles**"
Phys. Fliuds, **16**-6, 1852-1865.

Raffel, M., Willert, C. H., Kompenhas, J., (1998)
"**Particle Image Velocimetry**"
Springer-Verlag.

Ramakrishnan, S., Kumar, R., Kuloor, N. R., (1969)
"**Studies in bubble formation I bubble formation under constant flow conditions**"
Chem. Eng. Sci., **24**, 731-747.

Rensen, J., Bosman, D., Magnaudet, J., Ohl, C. D., Prosperetti, A., Togel, R., Versluis, M., Lohse D., (2001)
"**Spiraling bubbles: How acoustic and hydrodynamic force compete**"
Phys. Rev. Let., **86**-21, 4819-4822.

Saffman, P. G., (1956)
"**On the rise of small air bubbles in water**"
J. Fluid Mech., **1**, 249-275.

Saffman, P. G., (1965)
"**The lift on a small sphere in a slow shear flow**"
J. Fluid Mech., **22**, 385-400.

Sangani, A. S., Didwania, A. K., (1993)
"**Dynamic simulations of flows of bubbly liquids at large Reynolds numbers**"
J. Fluid Mech., **250**, 307-337.

Satyanarayan, A., Kumar, R., Kuloor, N. R., (1969)
"**Studies in bubble formation II bubble formation under constant pressure conditions**"
Chem. Eng. Sci., **24**, 749-761.

Sethian, J. A., (1999)
"**Level set methods and fast marching methods: evolving interfaces in computational geometry, fluid mechanics, computer vision and materials sciences**"

Cambridge Univ. Press. 2ed, Cambridge.

Sethian, J. A., Smereka, P., (2003)
"**Level set methods for fluid interfaces**"
Annu. Rev. Fluid. Mech., **35**, 341-372.

Sirignano, W. A., (1993)
"**Fluid dynamics of sprays -1992 Freeman scholar lecture**"
J Fluids Eng., **115**, 345-378

Sirota, M., Imamura, T., Kameda, M., (2004)
"**Acoustic force-enhanced production of a sub-millimeter gas bubble from an orifice**"
Proc. of 5th Int. Conf. on Multiphase Flow, Yokohama, Japan.

Sirota, M., Kameda, M., (2001)
"**The bubble generator to produce 0.1mm-diameter gas bubbles**"
Proc. of 4th Int. Conf. on Multiphase Flow, New Orleans, USA.

Smereka, P., (1993)
"**On the motion of bubbles in a periodic box**"
J. Fluid Mech., **254**, 79-112.

So, S., Morikita, H., Takagi, S., Matsumoto, Y., (2002)
"**Laser Doppler velocimetry measurement of turbulent bubbly channel flow**"
Exp. Fliuds, **33,** 135-142.

Sridhar, G., Katz, J., (1995)
"**Drag and lift forces on microscopic bubbles entrained by vortex**"
Phys. Fliuds, **7**-2, 389-399

Stewart, C. W., (1995)
"**Bubble interaction in low-viscosity liquids**"
Int. J. Multiphase Flow, **21**, 1037-1046.

Sugiyama, K., Takagi, S., Matsumoto, Y., (2001)
"**Multi-scale analysis of bubbly flow**"
Comut. Methods Appl. Mech. Engrg., **191**, 689-704.

Sussman, M, Fatemi, E., Smereka, P., Osher, S., (1998)
"**An improved level set method for incompressible two-phase flow**"
Computers & Fluids, **27**, 663-680.

Sussman, M., Smereka, P., Osher, S., (1994)
"**A level set approach for computing solutions to incompressible two-phase flow**"
J. Comput. Phys., **114**, 146-159.

Takagi, S., (1994)
Doctor thesis, The University of Tokyo. (Japanese)

Takagi, S., Matsumoto, Y., (1995)
"**Three dimensional calculation of a rising bubble**"
Proc. of 2nd Int. Conf. on Multiphase Flow, Kyoto, Japan.

Takagi, S., Matsumoto, Y., (1996)
"**Force acting on a spherical bubble rising through a quiescent liquid**"
Japanese J. Multiphase Flow, **10**-3, 264-273. (Japanese)

Takagi, S., Uda, T., Watanabe, Y., Matsumoto, Y., (2003)
"**Behavior of a rising bubble in water with surfactant dissolution**"
J. Jpn. Soc. Mech. Eng., **B 69-686**, 2192-2199. (Japanese)

Takahira, H., Horiuchi, T., Banerjee, S., (2004)
"**An improved three-dimensional level set method for gas-liquid two phase flows**"
J. Fluids Eng., **126**, 578-585.

Takemura, F., Magnaudet, J., (2003)
"**The transverse force on clean and contaminated bubbles rising near a vertical wall at moderate Reynolds number**"
J. Fluid Mech., **495**, 235-253.

Takemura, F., Takagi. S., Magnaudet, J., Matsumoto, Y., (2002)
"**Drag and lift force on a bubble rising near a vertical wall in a viscous liquid**"
J. Fluid Mech., **461**, 277-300.

Takemura, F., Yabe, A., (1997)
"**Terminal velocity of spherical gas bubbles below Reynolds number of 100**"
J. Jpn. Soc. Mech. Eng., **B 63-613**, 2909-2914. (Japanese)

Terasaka, K., Tsuge, H., (1993)
"**Bubble formation under constant-flow conditions**"
Chem. Eng. Sci., **48**-19, 3417-3422.

Tezduyar, T. E., Behr, M., Liou, J., (1992)
"**A new strategy for finite element computations involving moving boundaries and interfaces –The deforming-spatial-domain / space-time procedure: 1 The concept and the preliminary numerical tests**"
Comput. Methods Appl. Mech. Eng., **94**, 339-351.

Tezduyar, T. E., Behr, M., Liou, J., (1992)
"**A new strategy for finite element computations involving moving boundaries and interfaces –The deforming-spatial-domain / space-time procedure: 2 Computation of free-surface flows, two-liquid flows, and flows with drifting cylinders**"
Comput. Methods Appl. Mech. Eng., **94**, 353-371.

Tomiyama, A., Celata, G. P., Hosokawa, S., Yoshida, S., (2002)
"**Terminal velocity of single bubbles in surface tension force dominant regime**"
Int. J. Multiphase Flow, **28**, 1497-1519.

Tsao, H. K., Koch, D. L, (1994)
"**Collisions of slightly deformable, high Reynolds number bubbles with short-range repulsive forces**"
Phys. Fluids, **6**-8, 2591-2605.

Tse, K., Martin, T., Mcfarlane, C. M., Nienow, A W., (1998)
"**Visualization of bubble coalescence in a coalescence cell, a stirred tank and a bubble column**"
Chem. Eng. Sci., **53**-23, 4031-4036.

Tsuge, H., Hibino, S., (1977)
"**The onset conditions of oscillatory motion of single gas bubbles rising in various liquids**"
J. Chem. Eng. Japan, **10**-1, 66-68.

Tsuji, Y., Morikawa, Y., Terashima, K., (1981)
"**Fluid-dynamic interaction between two spheres**"
Int. J. Multiphase Flow, **8**, 71-82.

van der Vorst, H. A., (1992)
"**BI-CGSTAB: a fast and smoothly converging variant of BI-CG for the solution of nonsymmetric linear systems**"
SIAM J. Sci. Stat. Comput., **13**-2, 631-644.

van Wijngaarden, L., (1976)
"**Hydrodynamic interaction between gas bubbles in liquid**"
J. Fluid Mech., **77**, 27-44.

van Wijngaarden, L., (1982)
"**Bubble interaction in liquid/gas flows**"
Appl. Sci. Res., **38**, 331-339.

van Wijngaarden, L., (1993)
"**The mean rise velocity of pairwise-interacting bubbles in liquid**"
J. Fluid Mech., **251**, 55-78.

Wraith, A. E., (1971)
"**Two stage bubble growth at a submerged plate orifice**"
Chem. Eng. Sci., **26**-10, 1659-1671.

Wu, M., Gharib, M., (2002)
"**Experimental studies on the shape and path of small air bubbles rising in clean water**"
Phys. Fluids, **14**-7, 2033-2036.

Yang, B., Prosperetti, A., Takagi, S., (2003)
"**The transient rise of a bubble subject to shape or volume changes**"
Phys. Fluids, **15**, 2640-2648.

Yang, S. M., Leal, L. G., (1991)
"**A note on memory-integral contributions to the force an accelerating spherical drop at low Reynolds**

number"
Phys. Fluids, **3**, 1822-1824.

Yuan, H., Prosperetti, A., (1994)
"**On the in-line motion of two spherical bubbles in a viscous fluid**"
J. Fluid Mech., **278**, 325-349.

Zhang, Y., Finch, J. A., (2001)
"**A note on single bubble motion in surfactant solutions**"
J. Fluid Mech., **429**, 63-66.

Zieminsky, S. A., Raymond, D. R., (1968)
"**Experimental study of the behavior of single bubbles**"
Chem. Eng. Sci., **23**, 17-28.

Acknowledgement

This thesis is the summary that I have been studied in the Thermo-Fluid Mechanics Laboratory in Kyushu University. A lot of people always supported to me. I would like to thank everybody.

I would first like to express my gratitude to Prof. Fukano Tohru of Kurume Institute of Technology. He always gave me valuable suggestions. I am really happy to be a last doctor student of his teaching in Kyushu University.

I would also like to thank Prof. Takata Yasuyuki, Prof. Furukawa Akinori, and Dr. Watanabe Masao of Kyushu University. They gave me valuable comments as the member of the chair of this thesis. Especially Dr. Watanabe gave not only the suggestions of this research but also the basics of fluid mechanics.

I would like to thank Prof. Kariyasaki Akira of Fukuoka University. He gave me the all of the controller of bubble production.

I also thank the entire laboratory member. I would like to thank Prof. Matsumiya Hikaru, Dr. Watanabe Satoshi, Dr. Hara Yoshinori, and Mr. Matsushita Daisuke of Kyushu University. They gave me a lot of supports as the staff of the laboratory. As the senior, Dr. Inatomi Takanari of Toshiba, and Dr. Mori Shoji of Yokohama National University gave me many advices. As the group member, Mr. Narikiyo Takahisa, Mr. Noda Hitomi, Mr. Yuda Tomohiro, Mr. Ishida Dijiro, Ms. Sato Ayaka, Mr. Sato Shinsuke, and Mr. Sugihara Keiji of students of Kyushu University help me many experiments.

At the conference, Dr. Takagi Shu, Dr. Fujiwara Akiko of University of Tokyo, Dr. Kameda Masaharu, and Mr. Shirota Minori of Tokyo University of Agriculture and Technology, gave me many comments. Especially Dr. Takagi gave me many impressive advices.

During the stay of the Johns Hopkins University, Prof. Andrea Prosperetti, Dr. Matsukuma Yosuke of Kyushu University, and Dr. Ichiki Kenogo of University of Western Ontario gave me great experiences. In the visit to the Prague, I enjoyed the fruitful discussion with Dr. Marek Ruzicka of Academy of Science of the Czech Republic.

I would like to express my thank of the financial support by Harada Kinen Zaidan, 21st COE program, and Research Fellowships of the Japan Society of the Promotion of Science for Young Scientists.

Finally, I would like to show my gratitude to my family. They always supported me, and loved me. I would like to repeat my appreciation to my father, Mr. Sanada Takashi, my mother, Ms. Sanada Setsuko, my sister, Ms. Akihiro Hiromi, and my wife Ms. Sanada Yuka.

Sanada Toshiyuki
December 2004

Outline of this thesis

1. 研究背景と目的

気泡を利用した工業操作は，構造が簡単なため多くの化学装置（気泡塔，バイオリアクタなど）で利用されている．また原子炉冷却系統やボイラなどの運転は，気泡流の状態で行われていることが多い. さらに気泡流は, 湖沼, 浄水場および養殖場等での水質改善や, 船舶における摩擦抵抗低減など様々な分野での応用が期待されている. その簡単な装置構造とは逆に，その内部で起こっている現象（流動，物質・熱移動，反応等）は，気泡流が本質的に多重スケール構造を有しているため, そのそれぞれのスケールにおける現象が複雑に干渉し合い，予測が困難である．そのため，産業界からの研究要請の強い気泡流の数値予測は，未だ設計で応用可能なレベルには達していない.

ミクロおよびマクロスケールにおける現象は，多くの研究者により研究されているが, それらのスケール間を結ぶメゾスケールの現象に着目した研究は少ない．本研究では，メゾスケールの現象である気泡間の相互作用および合体現象に着目し, 実験および数値解析の双方から現象の調査を行う. この素過程は, 気泡流の流動構造を支配するにも関わらず, その実験的研究が非常に少ない．その理由として，気泡の発生制御が非常に困難であり, 再現性の高い実験を行えないことが挙げられる.

本研究では，高精度に気泡の発生を制御できる装置の開発を行い，その装置を用いることにより, 気泡の空間配置および気泡径を変えることによる気泡間相互干渉現象について調査を行う．特に鉛直線上および横に並んで上昇する2気泡の挙動，また単一のノズルから発生する気泡列に着目する. さらに相互干渉により気泡が接触した際の合体条件を明らかにする.

2. 実験装置および数値解析の概略

実験では，プール中に単一のノズルから窒素ガスを放出し，制御された気泡を発生させた．図 1 に実験装置の概要を示す．窒素ガスはボンベより発生制御装置上流に設けられた圧力タンク(ステンレス製圧力容器)に導かれる．圧力タンク内の圧力は，ニードルバルブの開度により調整した．発生制御部により圧力振動を与えられたガスを，タンク内部に設置されたノズルよりプール中へと放出し気泡を生成した．発生制御部では，オーディオスピーカーを用いてノズルへの導管内に圧力変動を加えた．プール中の気泡の挙動を観測するため，透明なアクリル樹脂で容器を製作した．液体としてシリコンオイルを使用した．ノズルとして，ガラス毛細管もしくはチューブに穴を開けたオリフィスを使用した．気泡の挙動は，高速度ビデオカメラで撮影された．3 次元挙動が必要な場合には，ステレオ撮影を行った．撮影された画像に，背景処理, ノイズ除去もしくはエッジ強調フィルタ，2 値化，ラベリング処理を施し，気泡の重心位置を決定した. より高精度な重心位置が必要な場合には, フーリエ記述子を用いて気泡形状を再構築し, 重心を求めた．また高速度ビデオカメラは，必要に応じてトラバース装置を用い，気泡に追従させ撮影を行った．また気泡周囲液体の流れ場については相互相関法による PIV 解析を行った.

数値解析においては，Level Set 法および DSD/ST 有限要素法を使用した．いずれも軸対象の仮定で，Navier-Stokes 方程式を直接解いた．反発現象の調査には Level Set 法を，鉛直線上を上昇する 2 気泡の挙動に関して DSD/ST 有限要素法を用いた．いずれも変形でき

る気泡を取り扱っているが特徴である．実験結果との比較のために，計算はすべて有次元計算を行った．

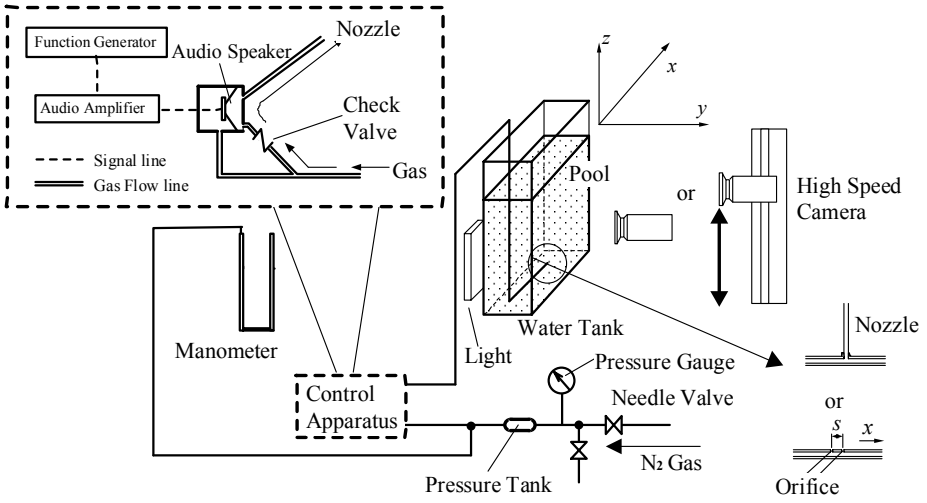

Fig.1 Schematic of experimental setup

3. 結果および考察

3.1 2 気泡間の相互干渉

鉛直線上を上昇する 2 気泡，および水平に並んで上昇する 2 気泡の 2 種類の気泡配置において挙動の調査をした．まず鉛直線上を上昇する場合の結果について述べる．図 2 (a)に本実験で得られた K20 での 2 気泡挙動の一例(*Re*=5)について示す．図に示すように，後続気泡は前方気泡と衝突している．これは，Katz らの実験と同様に気泡後流によるものだと考えられる．K20 で行った全ての実験において後続気泡は発生後前方気泡に接近し，衝突を生じた．次に中間 *Re* 数について議論を行う．図 2 (b)に K5 での 2 気泡の挙動の一例（*Re*=25）を示す．図 2 (b)に示すように，後続気泡はある距離まで接近するが，それ以上接近せず，ある一定距離すなわち平衡距離を保ち上昇する．この結果は，Yuan らが予測した “potential repelling force”と気泡後流による引力がつりあったためと考える．しかし本実験での無次元平衡距離は 10~25 程度と Yuan らの予測および本数値解析より大きな値となり，さらに初期の気泡間隔 *Li* を変更することにより，平衡距離が異なるとの結果が得られた．より高い *Re* 数においては，後方気泡は発生後少し接近するが，すぐに鉛直線上から逸脱し，また逸脱する際に大きな形状変化生じた．図 3 に示すように，DSD/ST 有限要素法を用いた解析においても同様な傾向が見られた．高い *Re* 数においては，非軸対称運動は形状振動となり現れた．

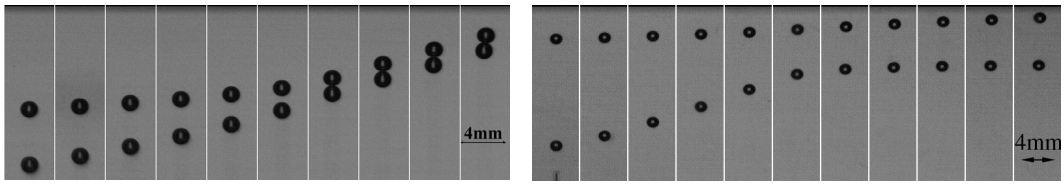

(a) *Re* = 5 , Δ*t*=0.048 s　　(b) *Re* = 25, Δ*t*=0.112 s

Fig.2 Motion of a pair of bubbles rising in line

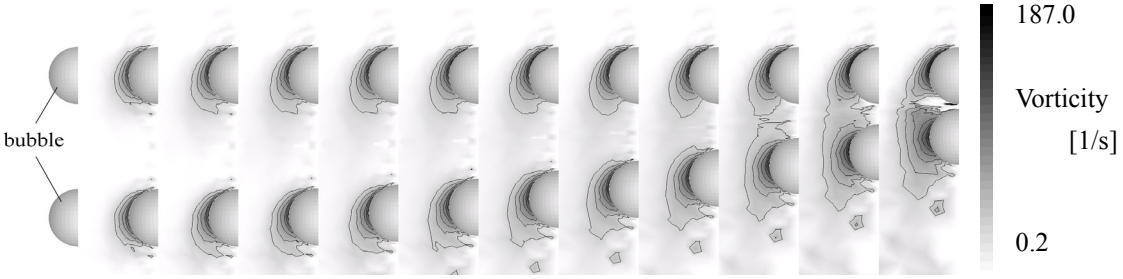

(a) *Re*=27, Δ*t*=0.01 s

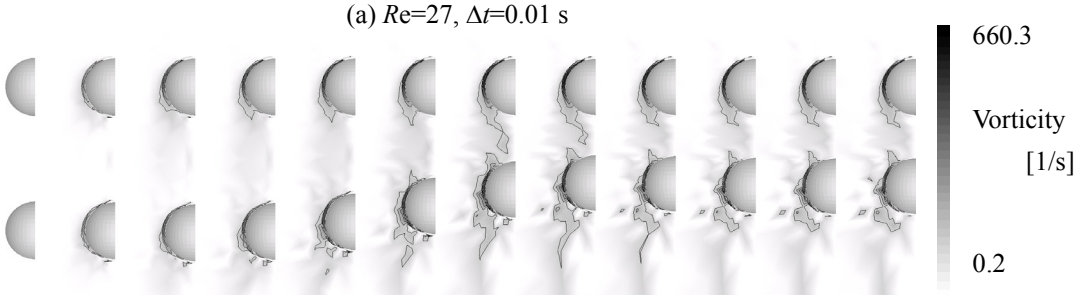

(b) *Re*=72, Δ*t*=0.01 s

Fig. 3 Vorticity distribution

次に，横に並んで上昇する 2 気泡の挙動について検討する．図 4 に *Re* 数を変えた場合の気泡挙動について示す．図 4(a)および(b)が高動粘度液体を用いた低 *Re* 数の場合で，(c)~(f)は低動粘度液体を用いた高 *Re* 数の場合である．まず，低 *Re* 数の結果について述べる．図 4(a)に示す *Re*=6 の場合，2 気泡は離れながら上昇する．これは Legendre らが数値解析より予測したように，気泡表面での渦度の影響によるものと考えられる．*Re* 数が大きくなるにつれてこの効果は小さくなり，図 4(b)に示す *Re*=49 の場合，気泡はほぼまっすぐ上昇している．それに対し，図 4 (c)~(f) に示す高 *Re* 数のすべての場合において，2 気泡は発生後接近した．これも Legendre らが数値解析で示したように，渦度の影響は薄い境界層と後流に閉じ込められるため，コアンダ効果により接近したものと考えられる．こ

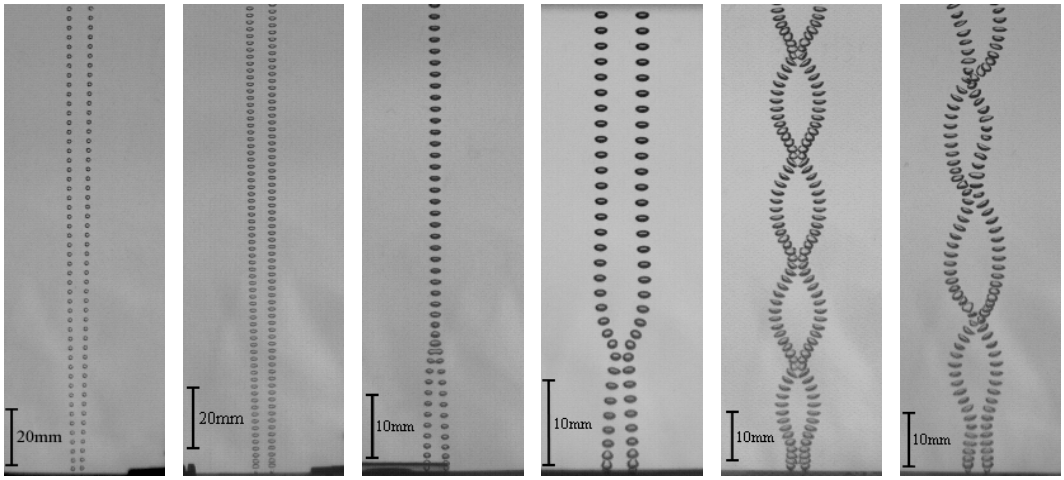

(a) *Re*=6, l_i=2.2mm　(b) *Re*=49, l_i=4.5mm　(c) *Re*=109, l_i=3.0mm　(d) *Re*=160, l_i=2.2mm　(e) *Re*=341, l_i=2.5mm　(f) *Re*=304, l_i=3.0mm

Fig.4 Motion of a pair of bubbles rising side by side

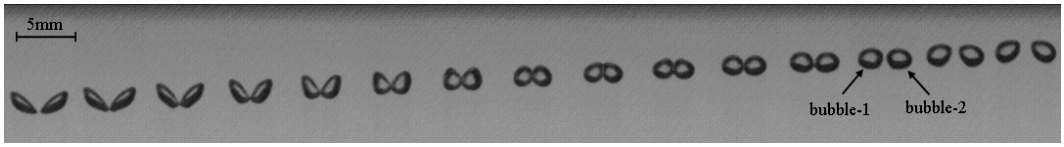

(a) Bubble motion (Δt=2ms)

の高 *Re* 数の場合には，接近した後に，合体する場合もしくは反発する場合が観察された．気泡が反発を繰り返す際に，とても特徴的な反発が見られた. その詳細を図 5 に示す．壁面で反発を行う気泡は，その運動量のほとんどを失い, 速度が大きく低下することが知られているが, 図 5 より反発する 2 気泡では速度低下がほとんどないことがわかった. またこの現象は接触する際の気泡エッジがずれると観察されず, 気泡の反発には気泡後流が大きく関係しているということが示唆される.

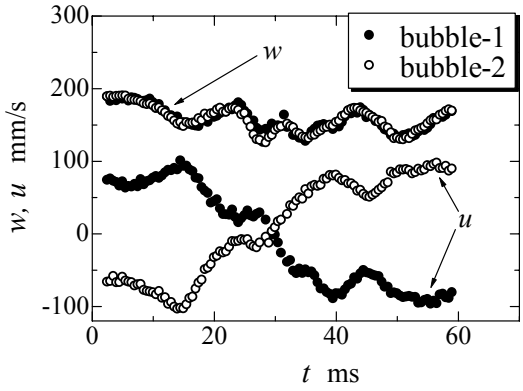

(b) velocity

Fig.5 Bouncing of bubbles

3.2 気泡の合体および反発現象

3.1 で述べたように気泡が相互干渉により接近すると，合体もしくは反発を行う．本節ではそのメカニズムについて検討を行った．大きく 2 つの合体現象を取り扱った．自由界面と単一上昇気泡の合体，および横に並んで上昇する 2 気泡の合体および反発である．まず，自由界面との合体について述べる．図 6 は自由界面に接した気泡が，合体するまでの時間を調べたものである．図からわかるように，低動粘度液体中での合体時間は *We* 数によって整理できるが, 高動粘度液体中では合体時間は低動粘度液体中と比較して非常に大きくなることわかる．このとき，自由界面近傍での気泡挙動の液体動粘度による違いを図 7 に示す. 図 7(a)に示す低動粘度の場合の結果では, 気泡は自由界面で明確な反発を生じている. それと比較して図 7(b)に示す高動粘度液体中の結果では, 気泡は明確な反発を示さない. 低動粘度の場合, 非常に低い *We* 数になると，合体時間はゼロ，すなわち瞬時に合体をする．しかし高動粘度液体中では, この気泡の合体と反発の境界値にも液体動粘度の影響が現れ, 従来影響が無いと予測されていた合体に及ぼす液体粘度の影響が, 実際には非常に大きく現れることが明らかになった.

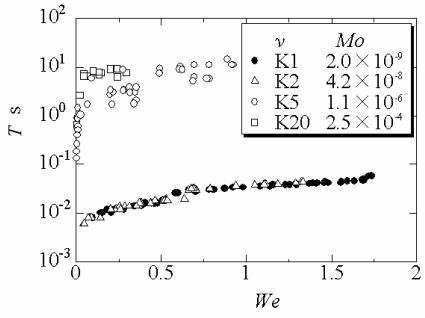

Fig.6 Coalescence time

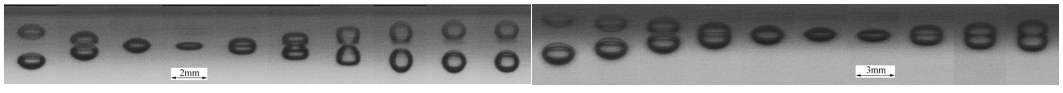

(a) low viscosity liquid (We=1.7, ν=1.16mm^2/s)(b) high viscosity liquid (We=1.1, ν=5.91mm^2/s)

Fig.7 Bubble motion near free surface (Δt=2ms)

次に，液体動粘度の違いによる，自由界面での気泡挙動の違いについて数値解析より比較を行う．図 7 は気泡が自由界面に接近した場合における，液体動粘度の違いによる流れ場の様子を示す．従来の研究においては，2 気泡間の薄い液膜の圧力上昇により気泡が反発すると予測されていたが，本数値解析結果では，気泡に凹みを生じるほどの圧力上昇は見られない．また，明確な反発を示した低粘度の結果である図 7(a) と明確な反発を生じない図 7(b) の大きな違いは，気泡後流部に見られる．明確な反発した場合，反発前に気泡下部において大きな逆圧力勾配が生じ，その結果後流は逆流して，それに伴うように気泡は反発したが，高動粘度液体中の気泡下部にはそのような逆圧力勾配は観察されなかった．以上のことより，気泡の反発現象には気泡間の薄い液膜だけでなく，気泡後流部も重要であることが明らかになった．

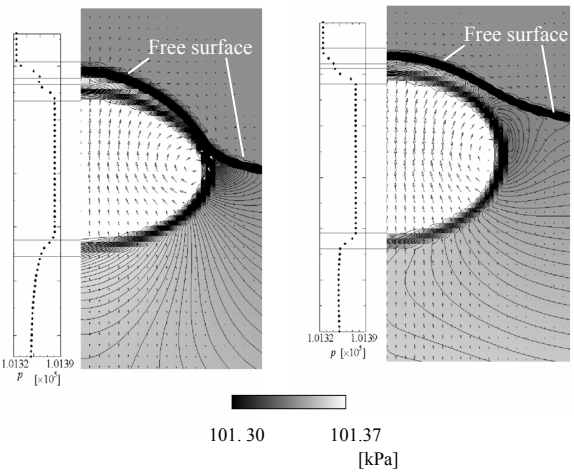

(a)ν=2 mm^2/s, *We*=1.56　(b)ν=5mm^2/s, *We*=1.98

Fig.7 Velocity and pressure distribution of low viscosity

次に図 4(c)および(d)で観察されたような，横に並んで上昇しながら接近して合体や反発を示す 2 気泡の合体および反発について検討を行う．2 気泡を発生させて接触するまでの相対的気泡間距離Δ*x* の時間変化を図 8 に示す．(a)は液体動粘度が 1 mm^2/s のもの，(b)は 2 mm^2/s の場合の結果である．*t*=0 におけるΔ*x* が発生直後の気泡間距離に相当し，最後の点は気泡が接触した点である．*d* が大きな気泡は発生直後にそれぞれ水平で反発する向きに移動し，*s* より大きな初期気泡間隔となった．図 8 に示すように，気泡の接近速度が遅い（気泡軌跡の曲線のこう配が小）場合，全ての気泡は合体し，逆に早い場合は全て反発するという明確な境界が観察された．この結果はすべての粘度の場合で同じで，いずれの場合も接近速度が早ければ反発，遅い場合合体が見られるという明確な境界が観察された．

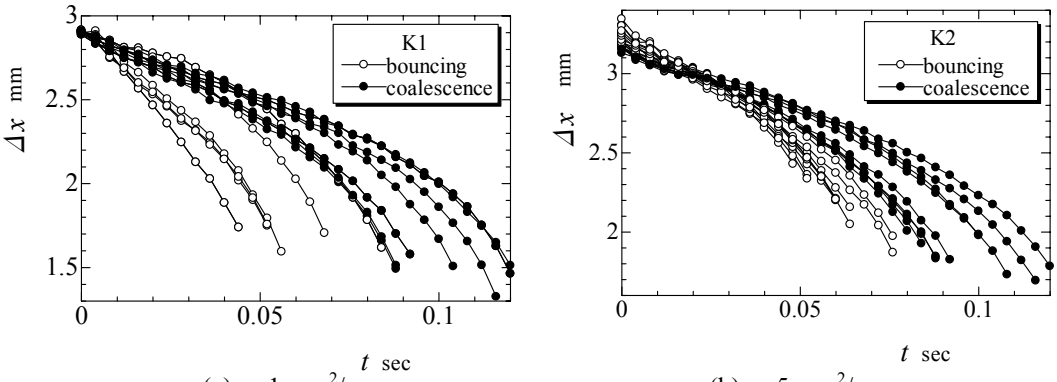

(a) ν=1 mm^2/s　(b) ν=5 mm^2/s

Fig.8 Relative distance of bubbles rising side by side versus time

3.3 単一の気泡列挙動

最後に，単一のノズルから制御して発生させた気泡列の挙動および周囲液体構造について示す．ステレオ撮影を行い，気泡挙動の 3 次元位置変化を調査した．図 9 はその一例で，気泡径を同じ 2.3mm で固定しておき，気泡発生周波数を変えた場合の気泡挙動を，タンクの上から見たのに相当するΔx-Δy 平面で整理したものである．図は 50 個の気泡通過全てを示している．気泡発生周波数 f が低い場合，つまり気泡間距離が大きな場合には，気泡はほぼ同じ軌跡を通る．それに対し気泡発生周波数 f が大きくなるにつれて気泡挙動がばらつくようになる．高 Re 数の気泡では，前方気泡の後流によってひきつけられず，逆にばらつくようになることが明らかになった．さらに気泡の発生周波数 f をあげた場合でも，ノズル近傍（ノズルはΔx=Δy=0 に相当）では，気泡は一本の線で示され，ほぼ同じ軌跡を通過していることがわかる．次にこのことに着目し，ノズル近傍での気泡挙動について調査を行う．図 10 にノズル近傍での気泡の鉛直方向位置 z とノズルを含む鉛直線上からのずれΔr（Δr=$(\Delta x^2+\Delta y^2)^{1/2}$ で定義）を示す．図より気泡発生周波数が増加するに従い，ノズル近傍において気泡列はより傾きながら，すなわちノズルを含む鉛直線上からより遠くまで運ばれながら上昇することが観察される．このことは，気泡列中の気泡が，単一の気泡に比較してより大きな揚力を受けることを示す．次に気泡の発生していない静止した水プール中に，発生周波数 f=5Hz で制御し連続して気泡を生成させた．初めて生成された気泡を第一気泡とし，以下発生順に第四気泡までの気泡の軌跡を z-Δr で示したものを図 11 に示す．図中の n は気泡番号である．図 11 において，第一気泡(n=1)は，図 10 の f=1Hz の場合と同じように，40mm程度の高さまではほぼ直線的な軌跡を通過する．一方，第二気泡以後は 20mm の高さを通過した後曲がり，曲がり始めの点は 10mm 程度異なるが図 10 の f=5Hz の場合とほぼ同じ軌跡を通るようになる．このことより，気泡列中の気泡がより大きな揚力を受けるのは，先行気泡によって形成された流れ場の影響であると理解される．

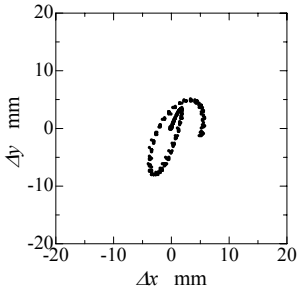

(1) f = 1 Hz (l/d = 134)

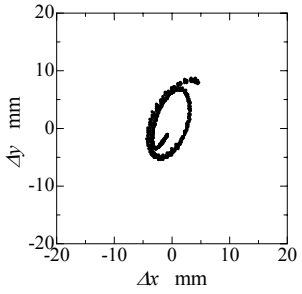

(2) f = 3 Hz (l/d = 45)

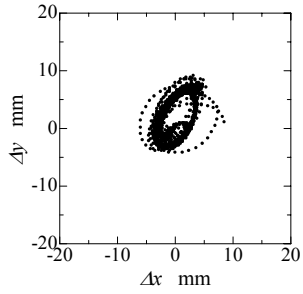

(3) f = 4 Hz (l/d = 34)

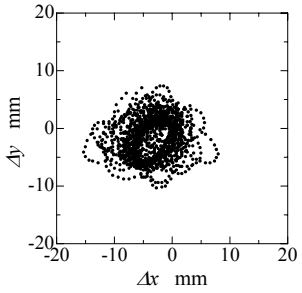

(4) f=10Hz (l/d=13)

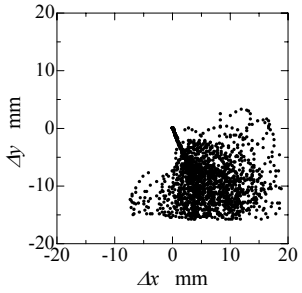

(5) f=20Hz (l/d=7)

Fig. 9 Bubble trajectory (Δx-Δy, d = 2.3mm, Re = 630)

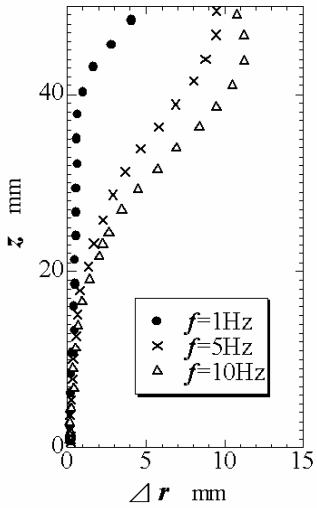

Fig.10 Comparison of bubble trajectory

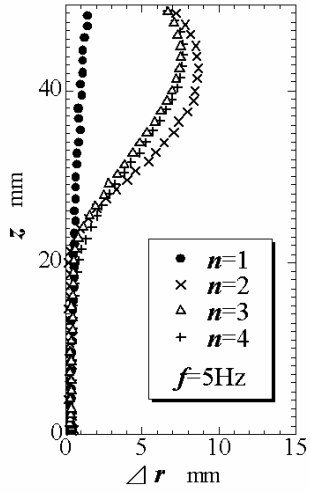

Fig.11 Bubble chains generation in stagnant water

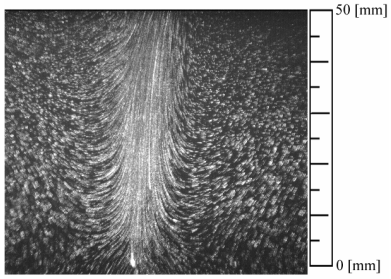

(a) d = 2.3 mm, f = 1 Hz, s = 8 s

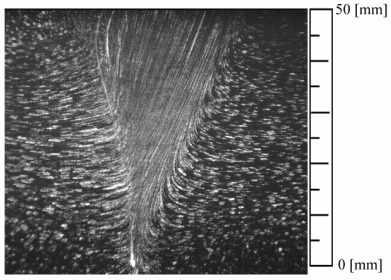

(b) d = 2.3 mm, f = 10 Hz, s=2 s

Fig. 12 Visualization image of flow field

次に，ノズル近傍における気泡列の周囲液体挙動について，可視化を行った．結果を図 12 に示す．図 12(a)はf=1Hz の場合，(b)は曲がりながら気泡列が上昇したf=10Hz の場合である．図 12(a)の場合，周囲液体は気泡の上昇方向に沿って上昇するが，図 12(b)の場合，周囲液体は気泡の上昇方向とは異なる流れ場が観察された．本研究において，この図 12(b)の際に観察された流れ場を液ジェットと呼ぶ．PIV 解析を行い，運動量理論を適用することで，この液ジェットは気泡列に働く揚力に対する反力であることが明らかになった．

4. まとめ

プール中に制御させた気泡を発生させ，気泡間の相互干渉および合体現象について実験的および数値的に調査し，以下の結論を得た．

(1) 鉛直線上を上昇する 2 気泡は，始めいずれの場合も前方気泡の後流の影響を受け接近する．その後，低 *Re* 数ではさらに接近し衝突するが，中間 *Re* 数では平衡距離に達する．さらに高 *Re* 数では，後方気泡は大きく形状が変化し鉛直線上から逸脱した．一方，横に並んで上昇する 2 気泡は，低 *Re* 数では反発し，高 *Re* 数では接近した．

(2) 気泡の合体および反発現象には，液体粘度が大きな影響を与える．気泡の反発は，2 気泡間の薄い液膜での圧力上昇によって起こると予測されていたが，本研究では，気泡後流も反発する際の重要なパラメータであることを示した．

(3) ノズル近傍において高 *Re* 数で上昇する気泡列は，単一の気泡と比べて，より曲がりながら上昇する．その際，周囲液体に液ジェットが発生することを明らかにした．